Suppressing Discretization Error in Langevin Simulations of (2+1)-dimensional Field Theories

A thesis

submitted in partial fulfilment

of the requirements for the Degree

of

Master of Science in Physics

in the

University of Canterbury

by

David H. Wojtas

University of Canterbury

2006

Abstract

Lattice simulations are a popular tool for studying the non-perturbative physics of nonlinear field theories. To perform accurate lattice simulations, a careful account of the discretization error is necessary. Spatial discretization error as a result of lattice spacing dependence in Langevin simulations of anisotropic $(2+1)$-dimensional classical scalar field theories is studied. A transfer integral operator (TIO) method and a one-loop renormalization (1LR) procedure are used to formulate effective potentials. The effective potentials contain counterterms which are intended to suppress the lattice spacing dependence. The two effective potentials were tested numerically in the case of a ϕ^4 model. A high accuracy modified Euler method was used to evolve a phenomenological Langevin equation. Large scale Langevin simulations were performed in parameter ranges determined to be appropriate. Attempts at extracting correlation lengths as a means of determining effectiveness of each method were not successful. Lattice sizes used in this study were not of a sufficient size to obtain an accurate representation of thermal equilibrium. As an alternative, the initial behaviour of the ensemble field average was observed. Results for the TIO method showed that it was successful at suppressing lattice spacing dependence in a mean field limit. Results for the 1LR method showed that it performed poorly.

Acknowledgements

Firstly, I thank my parents for their unconditional love and for encouraging me to continue studying. I thank my supervisor, Dr. Surujhdeo Seunarine. Without his expertise and intuitive input, this study would not have been possible. I thank Dr. Steve Churchwell for his help with computational problems. I thank Associate Prof. Mike Reid and Prof. Phil Butler for their encouragement to undertake this study. I also thank Dr. Surujhdeo Seunarine and Prof. Phil Butler for allowing me to attend QFTfest at the University of Tasmania, last December. The conference provided an opportunity to discuss this work with experts in the field. Lastly, I thank my friends for their supportive attitudes during the latter stages of this study.

Contents

Chapter 1

Introduction

Lattice simulations such as the Monte Carlo method and Langevin simulations are often the only tools available to explore the physics of complicated nonlinear field theories. The nonlinear character of such systems generally exhibit non-perturbative behaviour. Due to its complex nature, non-perturbative behaviour is difficult, if not impossible, to study analytically. The usual tool, perturbation theory, in which approximate solutions are found by adding small terms to a related exactly solvable problem fails (hence the term "non-perturbative"). The nonlinear behaviour is usually not present in the exactly solvable model to begin with.

Extensive efforts have been made to find exact analytic solutions of scalar, one-dimensional "toy" models with nonlinear degenerate double-well potentials. Notable success has been achieved with ϕ^4, double-quadratic and double-Gaussian models [1]. The ϕ^4 and double-quadratic models admit solitary-wave solutions to the equation of motion, with which, low-temperature semiclassical methods can be used to approximate the ground state eigenfunction. The double sinh-Gordon model, as well as having solitary-wave solutions, has a quasi-exactly solvable eigenspectrum [2]. Quasi-exact in that while the static Schrodinger equation of the nonlinear, nonintegrable Hamiltonian is not solvable in general, low-lying states of the eigenspectrum can be found exactly. With the exception of the double sinh-Gordon model, lattice simulations are usually required to probe the

non-perturbative dynamics of this simple class of models.

The toy models described above are popular objects of study because their non-perturbative properties are representative of those found in many physical theories. Such properties include topological soliton formation, structural phase transitions and symmetry breaking phase transitions.

Topological solitons (or less formally "kink/antikink" pairs, as they will be referred to) are spatially dependent solutions to the static equation of motion. These solutions depend, not so much on the nature of the static equaton of motion, but the boundary conditions imposed [3]. Examples of topological solitons [4] include vortices in liquid crystals, magnetic flux tubes in superconductors and domain walls in ferromagnets. Various soliton-type defects [5] such as magnetic monopoles, cosmic strings, domain walls and Skyrmions are believed to have formed as a result symmetry breaking in the early universe. Soliton models of hadron structure have also been considered as a mechanism for quark confinement [6].

Common structural phase transitions are the changes between solid, liquid, and gaseous phases. The distinguishing characteristic of such processes is a sudden change in one or more of the physical properties of the system (often the free energy), with a small change in a thermodynamic variable such as temperature. More exotic examples [7] are the Bose-Einstein condensation of Rb^{87} and the transition of He^3 into a superfluid.

Symmetry breaking phase transitions occur in ferromagnetic materials at the Curie temperature, above which the order parameter (magnetization) is zero. Analogously, for the electroweak model [8] the Higgs field acts as the order parameter breaking the electroweak gauge symmetry to the electromagnetic gauge symmetry. According to most models of inflation [9], the universe decayed from an initial hot, metastable state triggering a series of symmetry breaking phase transitions.

Recent advancements in large-scale computation have made it possible to perform high resolution Langevin simulations of nonlinear field theories. Quantities such as the probability distribution function, in which all thermodynamic information resides, have been calculated to a high level of accuracy [2]. With rapid developments in computing technology, computational methods are being used more frequently in areas where direct experimentation is not feasible.

For example, analytic and perturbative solutions in Quantum Chromodynamics (QCD) are complicated, if not impossible. Lattice QCD is a growing field concerned with formulating theories of quarks and gluons on a space-time lattice [6]. A lattice formulation of QCD provides a framework for the investigation of important non-perturbative phenomena such as quark confinement and quark-gluon plasma formation.

With obvious difficulties in performing experiments in the cosmological context, lattice simulations prove a useful tool in the study of cosmic phase transitions [10]. Flatness and horizon problems as well as mechanisms for primordial fluctuations are now being studied on the lattice[11].

However, there are obvious limitations with such lattice studies. Using discrete computational schemes for solving continuous field theories introduces errors in several ways. Round-off errors arise because it is impossible to represent all real-numbers exactly on a digital computer. Truncation errors occur when an iterative method is terminated and the approximate solution differs from the exact solution. Discretization errors arise when the solution of the discrete problem is dependent on the lattice spacing and time-step used in the simulation.

A careful treatment of these errors is necessary if one wishes to perform accurate lattice studies of continuous field theories. Round-off error can be avoided by simply using more data-intensive classes for the array that represents the field on a lattice (such as double and long double in the language of C/C++). Truncation error is eliminated by using higher order time-stepping schemes. Error due to

spatial discretization is certainly the more difficult type of error to suppress. One needs to consider the nature of the lattice spacing dependence that arises in the discrete field system. Such dependence is the primary concern of this study.

It arises because field theories are continuous (they have an infinite number of degrees of freedom) and usually formulated in an infinite volume, lattice simulations are discrete and finite, imposing both a maximum (size of the box L) and a minimum (lattice spacing Δx) wavelength that can be probed by the simulation. When one considers a system coupled to an external thermal bath, fluctuations will be constrained within the allowed range of wavelengths, leading to discrepancies between the continuum formulation of the theory and its lattice simulations.

In linear systems, lattice discretizaton effects are usually not an issue of concern. Minimum length scales often occur naturally in such systems, making the choice of Δx simple. It is possible to show that results are independent of Δx provided the choice is small enough.

For nonlinear fields, the case is more complicated as the effect of nonlinearities is to couple different wavelength modes. Thus, short wavelength modes set by the lattice spacing influence the long wavelength modes. This illustrates a general problem with the Langevin simulation of nonlinear field theories. The evolution of the physically important, long-wavelength modes are severely influenced by short wavelengths. The true dynamics of the long-wavelength modes are only obtained in the limit where the $\Delta x \to 0$.

Currently there exist two contending methods for controlling the effects of spatial discretization. Namely, a transfer integral operator (TIO) method and a one-loop renormalization (1LR) method. In the context of $(1 + 1)$-dimensional scalar field theories, the transfer integral operator method proved very successful [12], whereas a one-loop renormalization method gave results worse than one would get if no control method had been used. Studies [13][14] have shown

considerable success for a one-loop renormalization method applied to an isotropic (2+1)-dimensional scalar field theory. The study presented in this work is focused on discretization effects in lattice simulations of anisotropic $(2+1)$-dimensional classical scalar field theories. It parallels the study of [12]. As far as we know, this is the first study of its type for a classical field theory with two spatial dimensions.

The outline of this work is as follows: Chapter 2 introduces the continuous and discrete formulations of the classical $(2+1)$-dimensional scalar field theory. Certain specializations made in this work, such as the introduction of anisotropy and the ϕ^4 model, are discussed also this chapter. In chapters 3 and 4, the two methods for controlling discretization error mentioned above are applied to the anisotropic system introduced in chapter 2. Results for the general class of theories are presented first, then are applied specifically to the ϕ^4 model. In chapter 5, an introduction to Langevin simulations is given. The effects of time discretization error, time-stepping methods and round-off error are then studied. A second-order Runge-Kutta method constructed for the accurate time-stepping of the Langevin simulations is presented. As an illustration of the effect of time-stepping error, decay times of metastable states are briefly investigated using two different time-stepping methods. Finally, to validate the time-stepping method, the one-dimensional results of [12] were reproduced. In chapter 6, results from testing the control methods derived in chapters 3 and 4 are presented and discussed. A detailed discussion of some of the limitations encountered in the numerical studies is given. Finally, in chapter 7 the results of this study are summarized and conclusions made. Ways in which this study could be improved on, and future work that could be carried out are discussed.

Chapter 2

The System

In this chapter preliminary details of the system used in this study are introduced. Firstly, the continuum formulation of the general class of classical thermal (2+1)-dimensional scalar field theories is presented. The "ϕ^4" model is introduced as a means of testing the results derived in chapters 3 and 4. A rescaling procedure specific to this model is also outlined. In the second section, the discretized theory is introduced. Anisotropy conditions used in this study are also discussed. The specialization of this study to anisotropic models came about when a mean field approximation was necessary during the implementation of the transfer integral operator method (see the next chapter). Definitions and notation presented here will be referenced throughout this work.

2.1 Continuum Formulation

The scalar field is the simplest type of field, and as such, was the obvious choice for this basic study. Despite their simplicity, scalar fields have many important uses[9]. In theoretical physics, a scalar field is associated with spin 0 particles such as mesons and the Higgs boson. There is still no experimental evidence of a fundamental, point-like scalar field. Other scalar fields of current interest are dilaton fields in Kaluza-Klein and superstring theories and massless scalar fields known as inflatons thought to have caused the accelerated expansion of the universe. Only classical scalar fields are considered in this study.

The Hamiltonian functional describing a classical (2+1)-dimensional scalar field theory is,

$$H(\phi) = \int \mathrm{d}\mathbf{x} \left\{ \frac{1}{2}\pi^2 + \frac{1}{2}(\nabla\phi)^2 + V(\phi) \right\}, \tag{2.1}$$

where $\phi \equiv \phi(\mathbf{x}, t)$ and

$$(\nabla\phi)^2 = \left(\frac{\partial\phi}{\partial x}\right)^2 + \left(\frac{\partial\phi}{\partial y}\right)^2. \tag{2.2}$$

The function $V(\phi)$ is the local potential particular to the model of interest. With the Lagrangian density of the form,

$$\mathcal{L} = \frac{1}{2}\left[\left(\frac{\partial\phi}{\partial t}\right)^2 - \left(\frac{\partial\phi}{\partial \mathbf{x}}\right)^2\right] + V(\phi) \equiv \frac{1}{2}\left(\dot{\phi}^2 - \phi'^2\right) + V(\phi), \tag{2.3}$$

the conjugate momentum field is simply, $\pi = \frac{\partial\mathcal{L}}{\partial\dot{\phi}} = \dot{\phi}$.

The correction methods presented in this study are intended to be applicable in the most general case possible. However, to test the results presented in chapters 3 and 4, a degenerate "ϕ^4" model was utilized. The classical (tree-level) ϕ^4 potential is,

$$V(\phi) = -\frac{m^2}{2}\phi^2 + \frac{\lambda}{4}\phi^4, \tag{2.4}$$

where m is and λ are constants that take on physical significance in applications. The critical points ϕ_1, ϕ_2 and ϕ_m of eq.(2.4) are illustrated in fig.(2.1). As mentioned earlier, the dynamical processes of this model are intrinsically non-perturbative leading to the formation of kink/antikink pairs. Kink/antikink pairs are discussed further in chapter 6.

For practicality, the Hamiltonian was rescaled into a dimensionless form as follows. The Hamiltonian,

$$H = \int \mathrm{d}\mathbf{x}\mathcal{H}, \tag{2.5}$$

has units of energy, E. So each term in the 2-dimensional Hamiltonian density,

$$\mathcal{H} = \frac{1}{2}\pi^2 + \frac{1}{2}(\nabla\phi)^2 + V(\phi), \tag{2.6}$$

must have the units EL^{-2}. With the spatial gradient squared term, $(\nabla\phi)^2 = (\partial\phi/\partial\mathbf{x})^2$, having these dimensions, the field, ϕ, has units $E^{1/2}$. With this, and the

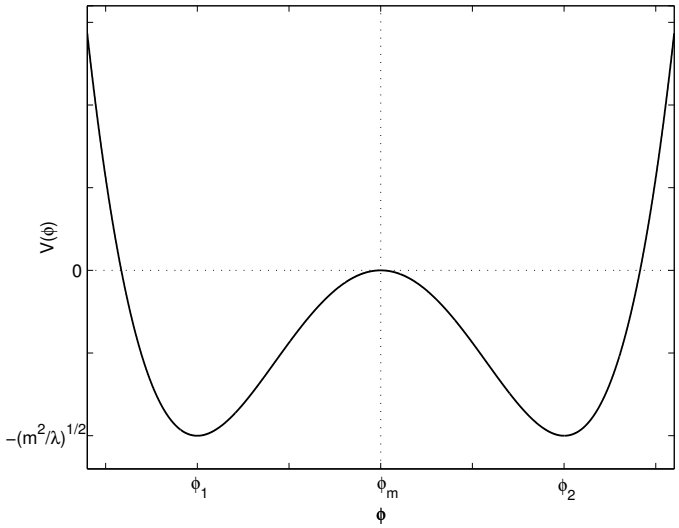

Figure 2.1: The degenerate "ϕ^4" potential of eq.(2.4). ϕ_1 and ϕ_2 are the locations of local minima. ϕ_m is the position of the barrier seperating each minimum.

form of $V(\phi)$ in eq.(2.4), it follows that the parameters m and λ have respective units of L^{-1} and $E^{-1}L^{-2}$. With the definitions $\tilde{x} = mx$, $\tilde{y} = my$, $\tilde{t} = mt$, $\tilde{\phi} = \phi/a$ where $a^2 = m^2/\lambda$ each term in $\mathcal{H}$ becomes dimensionless.

$$\begin{aligned} H &= \int \mathrm{d}\mathbf{x} \left[\frac{1}{2}\pi^2 + \frac{1}{2}(\nabla\phi)^2 - \frac{m^2}{2}\phi^2 + \frac{\lambda}{4}\phi^4\right] \\ &= \int \frac{\mathrm{d}\tilde{\mathbf{x}}}{m^2} \left[\frac{1}{2}(m^2a^2)\left(\frac{\partial\tilde{\phi}}{\partial\tilde{t}}\right)^2 + \frac{1}{2}(m^2a^2)\left(\frac{\partial\tilde{\phi}}{\partial\tilde{\mathbf{x}}}\right)^2 - \frac{m^2a^2}{2}\tilde{\phi}^2 + \frac{m^2a^2}{4}\tilde{\phi}^4\right]. \end{aligned} \tag{2.7}$$

With these redefinitions, the Hamiltonian becomes $\tilde{H} = H/a^2$ where $\tilde{H}$ is of the original form except that the ϕ^4 potential is now of the form

$$V(\phi) = -\frac{1}{2}\phi^2 + \frac{1}{4}\phi^4. \tag{2.8}$$

2.2 Lattice Formulation

Lattice simulations of classical field theories use an equivalent lattice field theory which regulates the number of degrees of freedom. The fields of continuous space-

time are replaced by aggregate, or "block" fields, on the sites of a lattice. Since the lattice has a finite volume, the lattice field theory is a classical thermal system with a large but finite number of degrees of freedom. It is a fixed volume or "canonical" ensemble of systems (in this case lattice points), all of which are allowed to exchange heat with an external bath of fixed temperature, T. Energy is not conserved.

The field, ϕ, must represented by a finite amount of data, in this instance by its value at a finite number of points as its domain, even though in reality this domain is a continuum. On a lattice, ϕ is a one-component scalar quantity defined on a plane of $M \times N$ lattice points labelled by the indices i, j. The spacings between lattice points, are denoted by Δx and Δy for $\hat{x}$ and $\hat{y}$ directions, respectively. The 2-dimensional lattice has a physical size of $(\Delta x M) \times (\Delta y N)$. The corresponding discretized Hamiltonian is given by,

$$H_{lat}(\phi_{i,j}) = \Delta x \Delta y \sum_{i}^{M} \sum_{j}^{N} \left[\frac{1}{2} \pi_{i,j}^2 + (\nabla_{lat} \phi_{i,j})^2 + V(\phi_{i,j}) \right] \tag{2.9}$$

The discrete form of the spatial gradient squared term is,

$$(\nabla_{lat} \phi_{i,j})^2 = \frac{1}{2} \frac{(\phi_{i+1,j} - \phi_{i,j})^2}{\Delta x^2} + \frac{1}{2} \frac{(\phi_{i,j+1} - \phi_{i,j})^2}{\Delta y^2}. \tag{2.10}$$

which acts as an elastic energy between nearest-neighbour lattice sites. The momentum, $\pi_{i,j}$, becomes a function of two lattice field configurations separated by a "time step" Δt in time. The behaviour of the local potential, $V(\phi)$, remains unchanged, except that now it is a function of $\phi_{i,j}$.

Anisotropy has the effect of introducing directionally dependence into the system. To implement this in the discrete system, different values for the lattice spacings, Δx and Δy, were used. The "effective" lattice spacing of the system was taken to be the lower value of Δx and Δy (set as Δx later). The larger lattice spacing defines the weakly coupled direction, the smaller lattice spacing defines the strongly coupled direction. With Δx as the effective lattice spacing, the strong coupling strength is unity and the weak coupling strength is $(\Delta y / \Delta x)^2$.

The discrete anisotropic model described above is found extensively in condensed matter physics [15]. Quasi one-dimensional materials have molecular arrangements in which coupling is strong along linear chains and weak between linear chains. Such materials are usually half-integer spin Heisenberg antiferromagnets which exhibit a wide range of electronic behaviour from localized spin magnetism to short-range order at low temperatures [16]. Anisotropy in scalar field theories could be attributed to space-time curvature or the presence of other external fields. While the applications of this particular model are interesting in themselves, they are not discussed further in this study.

Chapter 3

The Transfer Integral Operator Method

The transfer operator integral (TIO) method reduces the calculation of the canonical partition function describing a discrete system to an equivalent problem of finding the eigenvalues of a certain integral operator. With some continuity assumptions regarding the eigenfunctions, the problem can be further reduced to a problem of finding the energy eigenvalues of an equivalent quantum-mechanical problem. The formalism applied to (1+1)-dimensional scalar field theories [1][17] proved extremely successful in predicting lowest order lattice-spacing artifacts that arise in the Langevin simulation of such theories[12].

The result arrived at in section 3.1 of this chapter is applicable to the general class of (2+1)-dimensional scalar field theories. In order to obtain a correction suitable for comparison to other methods, it was necessary to specialize our study to the case of anisotropic lattice in section 3.2. With a suitable level of anisotropy, a mean-field aproximation can be made. This simplifies the problem in such a way that an effective local potential to control lattice effects in numerical simulations can be derived. The derivation of this effective potential is oultined in section 3.3.

3.1 Calculation of the Partition Function

The partition function, Z, encodes the statistical properties of a system in thermodynamic equilibrium. To realise its important statistical meaning, consider

the probability, P_n, a system occupies a particular microstate, n,

$$P_n = Ce^{-\beta E_n} \tag{3.1}$$

where $\beta = \frac{1}{k_b T}$, T is the temperature and k_B is the Boltzmann constant. The sum over all probabilites must equal unity. It must be the case then, that

$$\sum_n P_n = \sum_n Ce^{-\beta E_n} = C \sum_n e^{-\beta E_n} = 1 \tag{3.2}$$

if, and only if, the normalisation constant,

$$C = \frac{1}{\sum_n e^{-\beta E_n}} \equiv \frac{1}{Z} \tag{3.3}$$

where,

$$Z = \sum_n e^{-\beta E_n}. \tag{3.4}$$

This is the "first principles" definition of the canonical partition function. It is the sum over states. The origin of its name can also be inferred from eq.(3.2). Z encodes how the probabilties are partitioned among different microstates.

Many thermodynamic quantities such as the total energy, free energy, entropy and pressure can be expressed as a function of the partition function. In this study, the calcuation of such quantities was not a concern. However, the calculation of the partition function of the discretized system, eq.(2.9), using a transfer integral operator (TIO) method yields insight into the effect of spatial discretization in numerical studies.

The canonical partition function describing the canonical ensemble introduced in the previous chapter is the functional integral of the equilibrium density of configurations over the field, ϕ,

$$Z = \int_{-\infty}^{\infty} \mathcal{D}[\pi]\mathcal{D}[\phi] \exp\left(-\beta H[\phi]\right). \tag{3.5}$$

It is clear that the solvability of Z is governed by form of the Hamiltonian, $H(\phi)$. Because of this, there are only few nonlinear field theories where exact solutions

to the partition function exist. Indeed, it was necessary to restrict this study, as will be seen, to parameter ranges in which certain approximations could be made.

Following the usual procedure, the canonical partition function was seperated into functions of kinetic and configurational variables,

$$Z = Z_\pi Z_\phi. \tag{3.6}$$

The first factor is the kinetic contribution

$$Z_\pi = \int_{-\infty}^{\infty} \mathcal{D}[\pi] \exp\left(-\beta \int \mathrm{d}\mathbf{x} \frac{1}{2}\pi^2\right) \tag{3.7}$$

After discretization of the Hamiltonian, eq.(3.7) can be evaluted by simple Gaussian integration,

$$\begin{aligned} Z_\pi &= \int_{-\infty}^{\infty} \prod_i^M \prod_j^N \mathrm{d}\pi_{i,j} \exp\left(-\frac{\beta \Delta x \Delta y}{2} \sum_i^M \sum_j^N \pi_{ij}^2\right) \\ &= \left(\sqrt{\frac{\beta}{2\pi \Delta x \Delta y}}\right)^{\frac{MN}{2}}. \end{aligned} \tag{3.8}$$

Gaussian integration is discussed in appendix B.

The rest of this section will be devoted to the evaluation of the configurational contribution, Z_ϕ. Difficulty arises with the gradient squared term, $(\nabla\phi)^2$, as the discrete version, eq.(2.10), is dependent on field values $\phi_{i+1,j}$ and $\phi_{i,j+1}$. As a result, there is a coupling of the integrals in eq.(3.5) at different space points. Thus, functional integration over ϕ is not an option. To explicitly calculate Z_ϕ, the integrals need to be "localized". This was achieved by the use of a transfer integral operator (TIO) method.

To apply a TIO method, it was necessary to define the vectors,

$$\varphi_i = \{\phi_{i,1}, \phi_{i,2}, \ldots, \phi_{i,N}\}, \tag{3.9}$$

which describe the ith column of field values with $1 \leq i \leq M+1$. φ are illustrated in fig.(3.3) below. The configurational partition function, Z_ϕ, is then a functional

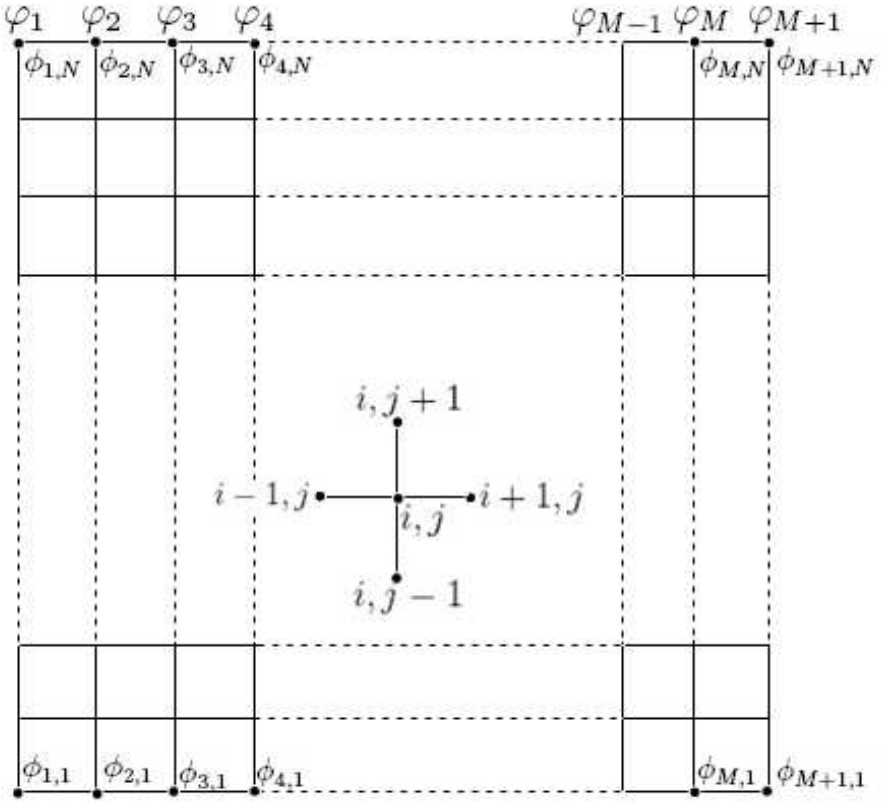

Figure 3.1: The $M \times N$ lattice consisting of the columnar vectors of field values, φ_i.

integral over all φ_i fields,

$$Z_\phi = \int_{-\infty}^{\infty} \mathcal{D}[\varphi] e^{-\beta S[\varphi]}. \tag{3.10}$$

In its discrete form, the integration over all scalar field configurations is the discrete product

$$\mathcal{D}[\phi] = \prod_{i=1}^{M} \prod_{j=1}^{N} \mathrm{d}\phi_{i,j} \tag{3.11}$$

or equivalently,

$$\mathcal{D}[\varphi] = \prod_{i=1}^{M} \mathrm{d}\varphi_i \tag{3.12}$$

The configurational part of the lattice Hamiltonian, eq.(2.9), in φ notation is

$$\begin{aligned} S[\varphi] &= \Delta x \sum_{i}^{M} \left[\frac{1}{2} \frac{(\varphi_{i+1} - \varphi_i)^2}{\Delta x^2} + \Delta y \sum_{j}^{N} \left[\frac{1}{2} \frac{(\phi_{i,j+1} - \phi_{i,j})^2}{\Delta y^2} + V(\phi_{i,j}) \right] \right] \\ &= \Delta x \sum_{i}^{M} \left[\frac{1}{2} \frac{(\varphi_{i+1} - \varphi_i)^2}{\Delta x^2} + U(\varphi_i) \right], \end{aligned} \tag{3.13}$$

where,

$$U(\varphi_i) = \Delta y \sum_{j}^{N} \left[\frac{1}{2} \frac{(\phi_{i,j+1} - \phi_{i,j})^2}{\Delta y^2} + V(\phi_{i,j}) \right], \tag{3.14}$$

Eq.(3.10) is now of the form,

$$Z_\phi = \int_{-\infty}^{\infty} \mathrm{d}\varphi_1 \ldots \mathrm{d}\varphi_M \exp\left(-\beta \Delta x \sum_{i}^{M} \left[\frac{1}{2} \frac{(\varphi_{i+1} - \varphi_i)^2}{\Delta x^2} + U(\varphi_i) \right] \right). \tag{3.15}$$

Cyclic boundary conditions were imposed in the $\hat{x}$-direction such that,

$$\varphi_{M+1} = \varphi_1. \tag{3.16}$$

This is achieved by the introduction of a delta function, $\delta(\varphi_{M+1} - \varphi_1)$, into eq.(3.15) and the additional variable, φ_{M+1}, such that

$$\begin{aligned} Z_\phi = \int_{-\infty}^{\infty} & \mathrm{d}\varphi_1 \ldots \mathrm{d}\varphi_{M+1} \delta(\varphi_{M+1} - \varphi_1) \\ & \exp\left(-\beta \Delta x \sum_{i}^{M} \left[\frac{1}{2} \frac{(\varphi_{i+1} - \varphi_i)^2}{\Delta x^2} + U(\varphi_i) \right] \right). \end{aligned} \tag{3.17}$$

The delta function can be represented as a bilinear expansion in a set of complete orthonormal eigenstates, $\{\Psi_n(\varphi)\}$ [18]. Consider the sum

$$K(\varphi_1, \varphi_{N+1}) \equiv K(\varphi_{M+1}, \varphi_1) = \sum_{n}^{\infty} \Psi_n^*(\varphi_1) \Psi_n(\varphi_{M+1}). \tag{3.18}$$

The uniform convergence of the series in eq.(3.18) is not assured. However, with its use in the configurational partition function, subsequent integration will make it convergent. This is evident from a corollary to Abel's test for uniform convergence [19]. If the individual terms, $u_n(x)$, of a series sum

$$f(x) = \sum_{n}^{\infty} u_n(x), \tag{3.19}$$

are continuous, the series may be integrated term-by-term. In simple words, the integral of the sum is equal to the sum of the integrals,

$$\int_a^b f(x)\mathrm{d}x = \sum_n^\infty \int_a^b u_n(x)\mathrm{d}x. \tag{3.20}$$

Continuity of the indiviual terms is almost always satisfied in physical applications, and so, it is assumed to be the case for $\Psi_n(\phi)$.

Now consider the integral

$$\int F(\varphi_{M+1})K(\varphi_1, \varphi_{M+1})\mathrm{d}\varphi_{M+1}, \tag{3.21}$$

where $F(\varphi_1)$ can be expanded in a series of eigenfunctions and coefficients, a_n,

$$F(\varphi_{M+1}) = \sum_p^\infty a_p \Psi_p^*(\varphi_{M+1}). \tag{3.22}$$

Substituting eq.(3.18) and eq.(3.22) into eq.(3.21) gives

$$\begin{aligned}
&\int F(\varphi_{M+1})K(\varphi_1, \varphi_{M+1})\mathrm{d}\varphi_{M+1} \\
&= \int \sum_p^\infty a_p \Psi_p(\varphi_{M+1}) \sum_n^\infty \Psi_n^*(\varphi_1)\Psi_n(\varphi_{M+1})\mathrm{d}\varphi_{M+1} \\
&= a_0\Psi_0(\varphi_{M+1})\Psi_0^*(\varphi_1)\Psi_0(\varphi_{M+1}) + a_0\Psi_0(\varphi_{M+1})\Psi_1^*(\varphi_1)\Psi_1(\varphi_{M+1}) + \cdots \\
&\quad + a_1\Psi_1(\varphi_{M+1})\Psi_0^*(\varphi_1)\Psi_0(\varphi_{M+1}) + a_1\Psi_1(\varphi_{M+1})\Psi_1^*(\varphi_1)\Psi_1(\varphi_{M+1}) + \cdots \\
&= \sum_p^\infty a_p \Psi_p^*(\varphi_1) \\
&= F(\varphi_1),
\end{aligned} \tag{3.23}$$

where, by orthonormality, the cross products $\Psi_n\Psi_p$ vanish for $n \neq p$ and equal unity for $n = p$. By setting $F(\varphi_{M+1}) = \varphi_o$ in eq.(3.23), where φ_o is a constant, it easy to show

$$\int K(\varphi_1, \varphi_{M+1})\mathrm{d}\varphi_{M+1} = 1. \tag{3.24}$$

Lastly, let $\varphi_1 = \varphi_{M+1}$ such that

$$K(\varphi_{M+1}, \varphi_{M+1}) = \sum_n^\infty [\Psi_n(\varphi_{M+1})]^2. \tag{3.25}$$

Using Bessel's inequality [19], which states that the sum of the squares of the expansion coefficients, a_n, is less than or equal to the integral of the square of the function being expanded,

$$\begin{aligned}\int [K(\varphi_{M+1}, \varphi_{M+1})]^2 &\geq \sum_n^\infty a_n^2 \\ &= \sum_n^\infty 1 \\ &= \infty. \end{aligned} \tag{3.26}$$

Note that equality holds if, and only if, the eigenfunction expansion is exact, that is, if the eigenfunctions form a complete set. Thus, it has been shown that $K(\varphi_1, \varphi_{M+1})$ satisfies the defining properties of the Dirac delta function and therefore is a representation of it. This representation,

$$\delta(\varphi_{M+1} - \varphi_1) = \sum_n \Psi_n^*(\varphi_{M+1})\Psi_n(\varphi_1), \tag{3.27}$$

is known as the closure relation.

With use of the closure relation, the configurational partition function has the form,

$$\begin{aligned} Z_\phi = \sum_n^\infty \int_{-\infty}^\infty \mathrm{d}\varphi_1 \ldots \mathrm{d}\varphi_{M+1} \Psi_n^*(\varphi_{M+1}) \times \\ \exp\left(-\beta\Delta x \sum_i^M \left[\frac{1}{2}\frac{(\varphi_{i+1} - \varphi_i)^2}{\Delta x^2} + U(\varphi_i)\right]\right) \Psi_n(\varphi_1). \end{aligned} \tag{3.28}$$

Expansion of the sum in the exponent gives

$$\begin{aligned} &\frac{1}{2}\frac{(\varphi_2 - \varphi_1)^2}{\Delta x^2} + U(\varphi_1) + \frac{1}{2}\frac{(\varphi_3 - \varphi_2)^2}{\Delta x^2} + U(\varphi_2) + \frac{1}{2}\frac{(\varphi_4 - \varphi_3)^2}{\Delta x^2} + U(\varphi_3) \\ &\quad + \cdots + \frac{1}{2}\frac{(\varphi_M - \varphi_{M-1})^2}{\Delta x^2} + U(\varphi_{M-1}) + \frac{1}{2}\frac{(\varphi_1 - \varphi_M)^2}{\Delta x^2} + U(\varphi_M), \end{aligned}$$

which can be written in the symmetric form

$$\begin{aligned} &\left[\frac{1}{2}\frac{(\varphi_2 - \varphi_1)^2}{\Delta x^2} + \frac{1}{2}\left\{U(\varphi_1) + U(\varphi_2)\right\}\right] + \left[\frac{1}{2}\frac{(\varphi_3 - \varphi_2)^2}{\Delta x^2} + \frac{1}{2}\left\{U(\varphi_2) + U(\varphi_3)\right\}\right] \\ &+ \cdots + \left[\frac{1}{2}\frac{(\varphi_M - \varphi_{M-1})^2}{\Delta x^2} + \frac{1}{2}\left\{U(\varphi_{M-1}) + U(\varphi_M)\right\}\right] \\ &+ \left[\frac{1}{2}\frac{(\varphi_1 - \varphi_M)^2}{\Delta x^2} + \frac{1}{2}\left\{U(\varphi_M) + U(\varphi_1)\right\}\right]. \end{aligned} \tag{3.29}$$

The configurational partition function is now of the form,

$$\begin{aligned} Z_\phi &= \sum_n^\infty \int_{-\infty}^\infty \mathrm{d}\varphi_1 \ldots \mathrm{d}\varphi_{M+1} \Psi_n^*(\varphi_{M+1}) \times \\ &\quad \exp\left(-\beta\Delta x \sum_i^M \left[\frac{1}{2}\frac{(\varphi_{i+1}-\varphi_i)^2}{\Delta x^2} + \frac{1}{2}\left\{U(\varphi_i)+U(\varphi_{i+1})\right\}\right]\right)\Psi_n(\varphi_1) \\ &= \sum_n^\infty \int_{-\infty}^\infty \mathrm{d}\varphi_1 \ldots \mathrm{d}\varphi_{M+1} \Psi_n^*(\varphi_{M+1}) \times \\ &\quad \prod_i^M \exp\left(-\beta\Delta x \left[\frac{1}{2}\frac{(\varphi_{i+1}-\varphi_i)^2}{\Delta x^2} + \frac{1}{2}\left\{U(\varphi_i)+U(\varphi_{i+1})\right\}\right]\right)\Psi_n(\varphi_1). \end{aligned} \tag{3.30}$$

Now, it is important to recognize the symmetric kernel

$$T(\varphi_{i+1},\varphi_i) = \exp\left\{-\beta\Delta x \left[\frac{1}{2}\frac{(\varphi_{i+1}-\varphi_i)^2}{\Delta x^2} + \frac{1}{2}\left\{U(\varphi_i)+U(\varphi_{i+1})\right\}\right]\right\}, \tag{3.31}$$

such that if φ_{i+1} and φ_i were interchanged the kernal will remain the same. The kernal, $T(\varphi_{i+1},\varphi_i)$, resembles a component of an infinite matrix, $\mathbb{T}$. This matrix $\mathbb{T}$, in effect, transfers us from the i^{th} column of the lattice to the $(i+1)^{th}$ column as depicted in fig.(3.2). Hence, it can be classified as a transfer matrix. Formulating a transfer matrix in order to simplify the partition function was an idea conceived by Kramers and Wannier [20]. It in fact, later formed the basis for Onsager's famous solution [21] for the free-energy of the two-dimensional Ising model. It has since, proved to be a useful tool in the analysis of many systems in statistical mechanics. As will become clear, it acts as a bridge between two apparently unrelated fields; probabilty theory and linear operators on Hilbert spaces. Consequently, it opens up the use of some powerful tools from analysis.

By the introducing the transfer matrix, the configurational partition function is of the compact form,

$$Z_\phi = \sum_n^\infty \int_{-\infty}^\infty \mathrm{d}\varphi_1 \ldots \mathrm{d}\varphi_{M+1} \Psi_n^*(\varphi_{M+1}) \prod_i^M T(\varphi_{i+1},\varphi_i)\Psi_n(\varphi_1). \tag{3.32}$$

A transfer integral operator, $\widehat{T}$, is defined by the integral equation,

$$\widehat{T}\Psi_n^*(\varphi_{i+1}) = \int_{-\infty}^\infty \mathrm{d}\varphi_i T(\varphi_{i+1},\varphi_i)\Psi_n(\varphi_i). \tag{3.33}$$

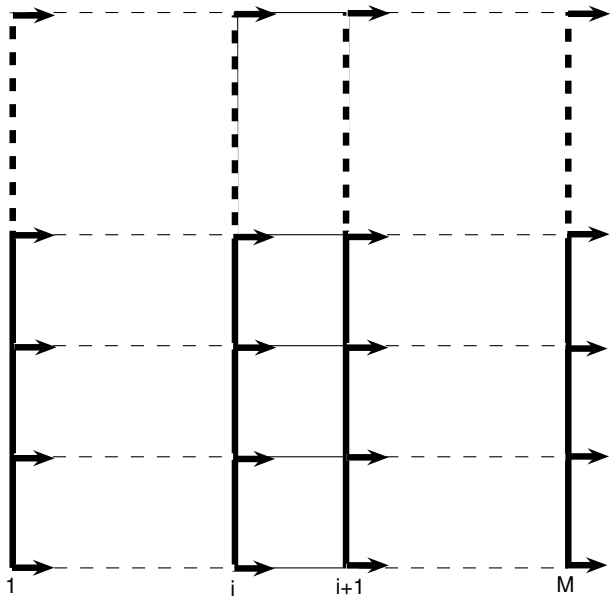

Figure 3.2: The transfer matrix, $\mathbb{T}$, acts to transfer from ith column to the $(i+1)^{th}$ column.

The operator $\widehat{T}$ is a Hilbert-Schmidt operator, such that

$$\mathrm{Tr}\widehat{T}^2 = \int_{-\infty}^{\infty} \mathrm{d}\varphi_i \mathrm{d}\varphi_{i+1} |T(\varphi_{i+1}, \varphi_i)|^2 < \infty \tag{3.34}$$

The orthonormal eigenbasis, $\{\Psi_n(\varphi)\}$, has the property

$$\{\Psi_n(\varphi)\} \in \mathrm{L}^2(-\infty, \infty) \tag{3.35}$$

where $\mathrm{L}^2(-\infty, \infty)$ is the completion of the set of continuous functions on $[-\infty, \infty]$, $\mathrm{C}[-\infty, \infty]$, with respect to the $\|\cdot\|_2$-norm. Corresponding eigenvalues and eigenvectors of $\widehat{T}$ are defined as follows,

$$\widehat{T}\Psi_n(\varphi_i) = t_n \Psi_n(\varphi_i) \qquad (t_n \geq t_{n+1}) \tag{3.36}$$

$$\mathrm{Tr}\widehat{T}^2 = \sum_n^{\infty} t_n^2 \tag{3.37}$$

$$T(\varphi_{i+1}, \varphi_i) = \sum_n^{\infty} t_n \Psi_n(\varphi_{i+1}) \Psi_n(\varphi_i). \tag{3.38}$$

The spectrum is discrete and the t_n have 0 as the only accumulation point.

A symmetric Fredholm integral equation of the first kind [22] can be written as

$$\int_{-\infty}^{\infty} \mathrm{d}\varphi_i T(\varphi_{i+1}, \varphi_i)\Psi_n(\varphi_i) = t_n \Psi_n(\varphi_{i+1}). \tag{3.39}$$

After repeated applications of eq.(3.38), the configurational partition function reduces to

$$\begin{aligned} Z_\phi &= \mathrm{Tr}(\widehat{T}\cdot\widehat{T}\cdot\widehat{T}\ldots\widehat{T})_{Mtimes} \\ &= \sum_n^{\infty} t_n^M \end{aligned} \tag{3.40}$$

The original problem of finding the configurational partition function for a system has been transformed to the equivalent problem of finding the eigenvalues of a transfer integral operator.

The point of concern now is to determine the eigenvalues, t_n. It was found useful to perform the functional transform

$$\chi_n(\varphi) = \exp\left(-\frac{1}{2}\beta\Delta x U(\varphi)\right)\Psi_n(\varphi). \tag{3.41}$$

With this and the form of $T(\varphi_i, \varphi_{i+1})$ given in eq.(3.31), the left hand side of eq.(3.39) becomes

$$\int_{-\infty}^{\infty} \mathrm{d}\varphi_i \exp\left(-\beta\Delta x\left(\frac{\varphi_{i+1}-\varphi_i}{\Delta x}\right)^2\right)\exp\left(\frac{1}{2}\beta\Delta x U(\varphi_{i+1})\right)\chi_n(\varphi_i), \tag{3.42}$$

where the $U(\varphi_i)$ terms have cancelled. In the strong-coupling (displacive) limit, $\frac{\Delta x}{M} \to 0$, satisfied in the $\hat{x}$-direction a Taylor series expansion of $\chi_n(\varphi_i)$ about $\chi_n(\varphi_{i+1})$ is possible,

$$\begin{aligned} \chi_n(\varphi_i) &= \sum_{s=0}^{\infty} \frac{(\varphi_i-\varphi_{i+1})^s}{s!}\frac{\partial^s\chi(\varphi)}{\partial\varphi^s}\bigg|_{\varphi=\varphi_{i+1}} \\ &= \exp\left((\varphi_i-\varphi_{i+1})\frac{\partial}{\partial\varphi}\bigg|_{\varphi=\varphi_{i+1}}\right)\chi_n(\varphi_{i+1}). \end{aligned} \tag{3.43}$$

With this, eq.(3.42) becomes

$$\begin{aligned} \exp\left(-\frac{1}{2}\beta\Delta x U(\varphi_{i+1})\right)\int_{-\infty}^{\infty}\mathrm{d}\varphi_i \exp\left(-\frac{\beta}{2\Delta x}(\varphi_{i+1}-\varphi_i)^2\right)\times \\ \exp\left((\varphi_i-\varphi_{i+1})\frac{\partial}{\partial\varphi}\bigg|_{\varphi=\varphi_{i+1}}\right)\chi_n(\varphi_{i+1}). \end{aligned} \tag{3.44}$$

Noting that $(\varphi_{i+1}-\varphi_i)^2 = (\varphi_i-\varphi_{i+1})^2$, Gaussian integration was carried out (see appendix B). Eq.(3.42) reduces to

$$\exp\left(-\frac{1}{2}\beta\Delta x U(\varphi_{i+1})\right)\exp\left(\frac{1}{2}\frac{\Delta x}{\beta}\frac{\partial^2}{\partial\varphi^2}\bigg|_{\varphi=\varphi_{i+1}}\right)\times \exp\left(-\frac{1}{2}\beta\Delta x U(\varphi_{i+1})\right)\Psi_n(\varphi_{i+1}). \tag{3.45}$$

where the reverse tranform from $\chi(\varphi)$ back to $\Psi(\varphi)$ has been performed. The lattice indices are not required since eq.(3.45) is now in terms of one lattice site, and so will be omitted for brevity. To combine the three exponent product in eq.(3.45), a Campbell-Baker-Hausdorff (CBH) expansion of the form,

$$e^B e^A e^B = e^{A+2B+\frac{1}{3!}[A+B,[A,B]]+\ldots}, \tag{3.46}$$

was performed. To zeroth order in Δx^2, eq.(3.39) reads

$$\exp\left(\frac{\Delta x}{2\beta}\frac{\partial^2}{\partial\varphi^2}-\beta\Delta x U(\varphi)\right)\Psi_n(\varphi) = \exp\left(-\beta\Delta x\epsilon_n\right)\Psi_n(\varphi), \tag{3.47}$$

where the convenient form for t_n has been introduced,

$$t_n = e^{-\beta\Delta x\epsilon_n}, \tag{3.48}$$

and the ϵ_n are defined by eq.(3.48). Equivalently

$$\exp\left(-\beta\Delta x H\right)\Psi_n(\varphi) = \exp\left(-\beta\Delta x\epsilon_n\right)\Psi_n(\varphi), \tag{3.49}$$

where H is the effective Hamiltonian,

$$H = -\frac{1}{2\beta^2}\frac{\partial^2}{\partial\varphi^2}+U(\varphi). \tag{3.50}$$

Eq.(3.49) can then be written as an equivalent Schrödinger-type equation

$$\left[-\frac{1}{2\beta^2}\frac{\partial^2}{\partial\varphi^2}+U(\varphi)\right]\Psi_n(\varphi) = \epsilon_n\Psi_n(\varphi). \tag{3.51}$$

Thus, the problem of solving the partition function has reduced to finding energy eigenvalues, ϵ_n, of a related quantum-mechanical problem. In the thermodynamic

limit $L \to \infty$, where $L = M\Delta x$, the problem simplifies even further. The sum in eq.(3.40) is dominated by the largest eigenvalue,

$$\sum_{n}^{\infty} t_n^M \to t_0^M. \tag{3.52}$$

Once the partition function is known in the thermodynamic limit, other important thermodynamic quantities follow in a simple manner.

3.2 The Mean Field Approximation

The result, eq.(3.51), of the previous section is applicable to the general class of (2+1)-dimensional scalar field theories eq.(2.1). When specific conditions on the coupling strengths $1/\Delta x^2$, $1/\Delta y^2$ are satisfied, certain approximations can be made. By requiring

$$\frac{1}{\Delta x^2} > \frac{1}{\Delta y^2}, \tag{3.53}$$

mean field approximations could be made in a certain anisotropic limit. Enforcing this condition specialises this study to anisotropic (2+1)-dimensional scalar field theories. The intended purpose of using a mean field approximation was to simplify $U(\varphi)$ so that it is dependent on only one field value. This was a necessary step for subsequent development towards lowest order lattice corrections presented in the next section.

The main idea of mean field theory is to replace all interactions to any one body with an average interaction. The interaction term present in $U(\varphi_i)$ is the $\hat{y}$-directional elastic energy between nearest neighbour lattice sites. This can be represented by the use of the coupling matrix,

$$D_{jj'} = \begin{bmatrix} 0 & \Delta y^{-2} & 0 & \dots & 0 \\ \Delta y^{-2} & 0 & \Delta y^{-2} & \ddots & \vdots \\ 0 & \ddots & \ddots & \ddots & 0 \\ \vdots & \ddots & \Delta y^{-2} & 0 & \Delta y^{-2} \\ 0 & \dots & 0 & \Delta y^{-2} & 0 \end{bmatrix} \tag{3.54}$$

The $\hat{y}$-directional interaction term becomes

$$\frac{1}{2}\sum_{j\neq j'}^{N} D_{jj'}(\phi_{i,j'}-\phi_{i,j})^2 = \frac{1}{2}\sum_{j\neq j'}^{N} D_{jj'}(\phi_{i,j'}\phi_{i,j'}-\phi_{i,j'}\phi_{i,j}-\phi_{i,j}\phi_{i,j'}+\phi_{i,j}\phi_{i,j})$$
$$= -\frac{1}{\Delta y^2}\sum_{j}^{N}\phi_{i,j+1}\phi_{i,j}. \tag{3.55}$$

The field, ϕ, was then decomposed as follows

$$\phi_{i,j} = \langle\phi\rangle + \Delta\phi_{i,j}, \tag{3.56}$$

where $\Delta\phi_{i,j}$ is the fluctuation size about the mean field value $\langle\phi\rangle$. The decomposition is valid in, what is called, the mean-field limit. A detailed discussion of parameter values involved to approach this limit is discussed in [23]. Essentially, they found that the different couplings ($\hat{x}$ and $\hat{y}$-directional) had to satisfy certain characteristics. In the strongly coupled direction ($\hat{x}$-direction in our case) one looks for coherant "displacive" patterns. The displacive regime in the ϕ^4 case corresponds to the field being allowed to vary smoothly from ϕ_1 to ϕ_2 and not via first-order phase transitions. This behaviour occurs when the intersite elastic energy is large in comparison to the well-depth. In contrast, "order-disorder" patterns are required in the weakly coupled direction. The order-disorder regime occurs when the intersite elastic energy is small in comparison to the well-depth. Here, regions of the field situate randomly in either well. First order phase transitions over the barrier at ϕ_m take place only by thermal activation. The onset of the mean field limit can be easily identified by tuning the level of anisotropy and observing the field configuration near thermal equilibrium. This is discussed further in chapter 6.

With ϕ in its decomposed form, eq.(3.55) becomes

$$-\frac{1}{\Delta y^2}\sum_{j}^{N}(\langle\phi\rangle+\Delta\phi_{i,j+1})(\langle\phi\rangle+\Delta\phi_{i,j}) = -\frac{1}{\Delta y^2}\sum_{j}^{N}(\langle\phi\rangle^2+\Delta\phi_{i,j+1}\langle\phi\rangle+$$
$$\langle\phi\rangle\Delta\phi_{i,j}+\Delta\phi_{i,j+1}\Delta\phi_{i,j}). \tag{3.57}$$

In the parameter range where mean field approximations are applicable, fluctuations about the mean field value are small. Accordingly, $\mathcal{O}(\Delta\phi)^2$ terms were safely omitted from eq.(3.57). Using the decomposition eq.(3.56), and substituting for $\Delta\phi_{i,j+1}$ and $\Delta\phi_{i,j}$ gives,

$$\begin{aligned}
-\frac{1}{\Delta y^2}\sum_j^N\langle\phi\rangle^2 - \frac{1}{\Delta y^2}\sum_j^N\{(\phi_{i,j+1}-\langle\phi\rangle)\langle\phi\rangle + (\varphi_i-\langle\phi\rangle)\langle\phi\rangle\} \\
&= \frac{1}{\Delta y^2}\sum_j^N\langle\phi\rangle^2 - \frac{1}{\Delta y^2}\sum_j^N\langle\phi\rangle(\phi_{i,j}+\phi_{i,j+1}) \\
&= \frac{1}{\Delta y^2}N\langle\phi\rangle^2 - \frac{2\langle\phi\rangle}{\Delta y^2}\sum_j^N\phi_{i,j}. \qquad (3.58)
\end{aligned}$$

With a mean field approximation of the $\hat{y}$-directional interaction term, the potential, $U(\varphi_i)$, becomes

$$U(\varphi_i) = \frac{1}{\Delta y}N\langle\phi\rangle^2 + \Delta y\sum_j^N\left[V(\phi_{i,j}) - \frac{2\langle\phi\rangle}{\Delta y^2}\phi_{i,j}\right]. \qquad (3.59)$$

The constant term, $\frac{1}{\Delta y}N\langle\phi\rangle^2$, may be factored out of the configurational partition function, amounting to a constant factor outside the functional integral. This gives

$$\begin{aligned}
Z_\phi = \exp\left(-\frac{\beta MN\Delta x}{\Delta y}\langle\phi\rangle^2\right)\int_{-\infty}^{\infty}\mathrm{d}\varphi_1\ldots\mathrm{d}\varphi_M\times \\
\exp\left(-\beta\Delta x\sum_i^M\left(\frac{1}{2}\frac{(\varphi_{i+1}-\varphi_i)^2}{\Delta x^2} + \Delta y\sum_j^N\left[V(\phi_{i,j}) - \frac{2\langle\phi\rangle}{\Delta y^2}\phi_{i,j}\right]\right)\right) \qquad (3.60)
\end{aligned}$$

Performing the change of variable,

$$u = \exp\left(-\frac{\beta MN\Delta x}{\Delta y}\langle\phi\rangle^2\right)\varphi \qquad (3.61)$$

such that

$$Z_u = \int_{-\infty}^{\infty}\mathrm{d}u_1\ldots\mathrm{d}u_M\exp\left(-\beta\Delta x\sum_i^M\left[\frac{1}{2}\frac{(u_{i+1}-u_i)^2}{\Delta x^2} + U(u_i)\right]\right). \qquad (3.62)$$

resets our configurational partition function to the form of eq.(3.15). Proceeding with the TIO method presented in the previous section, the Schrödinger-type

equation of eq.(3.51) is obtained where, $U(\varphi)$, is now of the form

$$U(\varphi_i) = \Delta y \sum_j^N \left[V(\phi_{i,j}) - \frac{2\langle\phi\rangle}{\Delta y^2}\phi_{i,j} \right]. \tag{3.63}$$

Notice that the desired dependence on just one field value has been achieved.

3.3 Lattice Discreteness Corrections

In this section, the derivation of lowest order discreteness corrections is presented. This correction consists of higher-order derivative operators which are generated by considering higher order commutator terms in the CBH expansion of eq.(3.46). Instead of truncating the expansion to include terms only of zeroth order in Δx, $\mathcal{O}(\Delta x^2)$ terms are also considered. Reverting back to eq.(3.46), the CBH expansion to order $\mathcal{O}(\Delta x^2)$ gives

$$\exp\left(\frac{\Delta x}{2\beta}\frac{\partial^2}{\partial\varphi^2} - \beta\Delta x U - \frac{1}{3!}\left[\frac{\Delta x}{2\beta}\frac{\partial^2}{\partial\varphi^2} - \frac{1}{2}\Delta x\beta U, \left[\frac{\partial^2}{\partial\varphi^2}, \frac{1}{2}\Delta x\beta U \right] \right] \right) \Psi_n(\varphi) = \exp(-\beta\Delta x U\epsilon_n)\Psi_n(\varphi). \tag{3.64}$$

Equivalently, the Schrödinger-type equation is of the form

$$\left(\frac{1}{2\beta^2}\frac{\partial^2}{\partial\varphi^2} + U - \frac{1}{48}\Delta x^2 \left[\frac{1}{\beta^2}\frac{\partial^2}{\partial\varphi^2} - U, \left[\frac{\partial^2}{\partial\varphi^2}, U \right] \right] \right) \Psi_n(\varphi) = \epsilon_n \Psi_n(\varphi). \tag{3.65}$$

The expansion of the commutator term on the left hand side is straightforward but tedious. Because its final form is of extreme importance to this study, full details have been included in appendix A. With expansion, the commutator term reads,

$$\left[\frac{1}{\beta^2}\frac{\partial^2}{\partial\varphi^2} - U, \left[\frac{\partial^2}{\partial\varphi^2}, U \right] \right] = \frac{1}{\beta^2}\left(\frac{\partial^4 U}{\partial\varphi^4}\Psi_n + 4\frac{\partial^3 U}{\partial\varphi^3}\frac{\partial\Psi_n}{\partial\varphi} + 4\frac{\partial^2 U}{\partial\varphi^2}\frac{\partial^2\Psi_n}{\partial\varphi^2} \right) + 2\left(\frac{\partial U}{\partial\varphi} \right)^2 \Psi_n \tag{3.66}$$

The Schrödinger-type equation of eq.(3.65) is now of the form,

$$\left[-\frac{1}{2\beta^2}\frac{\partial^2}{\partial\varphi^2} + U + \frac{\Delta x^2}{48}\left(\frac{1}{\beta^2}\left(\frac{\partial^4 U}{\partial\varphi^4} + 4\frac{\partial^3 V}{\partial\varphi^3}\frac{\partial}{\partial\varphi} + 4\frac{\partial^2 V}{\partial\varphi^2}\frac{\partial^2}{\partial\varphi^2}\right) + 2\left(\frac{\partial V}{\partial\varphi}\right)^2\right)\right]\Psi_n = \epsilon_n\Psi_n. \tag{3.67}$$

This is of the form $\mathscr{L}\Psi_n = \epsilon\Psi_n$. The operator $\mathscr{L}$, which consists of the contents within the [ ] brackets of eq.(3.67), can be shown to be self-adjoint by writing it in the Sturm-Lioville form

$$\mathscr{L}\Psi_n = \frac{\partial}{\partial\varphi}\left[p(\varphi)\frac{\partial}{\partial\varphi}\right]\Psi_n + q(\varphi)\Psi_n \tag{3.68}$$

where,

$$p(\varphi) = \left\{ -\frac{1}{2\beta^2}\left(1 - \frac{\Delta x^2}{6}\frac{\partial^2 U}{\partial\varphi^2}\right)\right\}, \tag{3.69}$$

and

$$q(\varphi) = U + \frac{\Delta x^2}{48}\left\{\frac{1}{\beta^2}\frac{\partial^4 U}{\partial\varphi^4} + 2\left(\frac{\partial U}{\partial\varphi}\right)^2\right\}. \tag{3.70}$$

With eq.(3.68) satisfied, $\mathscr{L}$ is by definition self-adjoint. Self-adjoint operators have three properties [19] of extreme importance to this study.

1. The eigenvalues of a self-adjoint operator are real.

2. The eigenfunctions of a self-adjoint operator are orthogonal.

3. The eigenfunctions form a complete set.

Properties **2** and **3** were asserted in the bilinear expansion of the delta function, eq.(3.27). The first property assures that the evaluation of the partition function, eq.(3.40), gives sensible results.

With the self-adjoint form of eq.(3.65),

$$\frac{\partial}{\partial\varphi}\left[-\frac{1}{2\beta^2}\left(1 - \frac{\Delta x^2}{6}\frac{\partial^2 U}{\partial\varphi^2}\right)\frac{\partial}{\partial\varphi}\right]\Psi_n + \left[U + \frac{\Delta x^2}{48}\left\{\frac{1}{\beta^2}\frac{\partial^4 U}{\partial\varphi^4} + 2\left(\frac{\partial U}{\partial\varphi}\right)^2\right\}\right]\Psi_n = \epsilon_n\Psi_n, \tag{3.71}$$

a series of transformations were carried out to put eq.(3.71) in its most convenient form. The procedure with notation was to perform each functional transform

or change of variable then revert back to the original notation. The first order derivative of the eigenfunction $\Psi_n(\varphi)$ was eliminated by performing the functional transform,

$$\Psi_n = \exp\left(\frac{\Delta x^2}{12}\frac{\partial^2 U}{\partial\varphi^2}\right)\Phi_n. \tag{3.72}$$

With this,

$$\begin{aligned}
\frac{\partial^2\Psi_n}{\partial\varphi^2} &= \frac{\partial}{\partial\varphi}\frac{\partial}{\partial\varphi}\left[\exp\left(\frac{\Delta x^2}{12}\frac{\partial^2 U}{\partial\varphi^2}\right)\Phi_n\right] \\
&= \frac{\partial}{\partial\varphi}\left[\exp\left(\frac{\Delta x^2}{12}\frac{\partial^2 U}{\partial\varphi^2}\right)\frac{\partial\Phi_n}{\partial\varphi} + \frac{\Delta x^2}{12}\frac{\partial^3 U}{\partial\varphi^3}\exp\left(\frac{\Delta x^2}{12}\frac{\partial^2 U}{\partial\varphi^2}\right)\Phi_n\right] \\
&= \frac{\Delta x^2}{12}\frac{\partial^4 U}{\partial\varphi^4}\exp\left(\frac{\Delta x^2}{12}\frac{\partial^2 U}{\partial\varphi^2}\right)\Phi_n + \frac{\Delta x^4}{144}\left(\frac{\partial^3 U}{\partial\varphi^3}\right)^2\exp\left(\frac{\Delta x^2}{12}\frac{\partial^2 U}{\partial\varphi^2}\right)\Phi_n \\
&\quad + \frac{\Delta x^2}{6}\frac{\partial^3 U}{\partial\varphi^3}\exp\left(\frac{\Delta x^2}{12}\frac{\partial^2 U}{\partial\varphi^2}\right)\frac{\partial\Phi_n}{\partial\varphi} + \exp\left(\frac{\Delta x^2}{12}\frac{\partial^2 U}{\partial\varphi^2}\right)\frac{\partial^2\Phi_n}{\partial\varphi^2},
\end{aligned} \tag{3.73}$$

which, to order $\mathcal{O}(\Delta x^2)$, reduces to

$$\begin{aligned}
\frac{\partial^2\Psi_n}{\partial\varphi^2} \simeq \frac{\Delta x^2}{12}\frac{\partial^4 U}{\partial\varphi^4}\exp\left(\frac{\Delta x^2}{12}\frac{\partial^2 U}{\partial\varphi^2}\right)\Phi_n + \frac{\Delta x^2}{6}\frac{\partial^3 U}{\partial\varphi^3}\exp\left(\frac{\Delta x^2}{12}\frac{\partial^2 U}{\partial\varphi^2}\right)\frac{\partial\Phi_n}{\partial\varphi} \\
+ \exp\left(\frac{\Delta x^2}{12}\frac{\partial^2 U}{\partial\varphi^2}\right)\frac{\partial^2\Phi_n}{\partial\varphi^2}.
\end{aligned} \tag{3.74}$$

Likewise, to order $\mathcal{O}(\Delta x^2)$,

$$\begin{aligned}
\frac{\Delta x^2}{12}\frac{\partial^3 U}{\partial\varphi^3}\frac{\partial\Psi_n}{\partial\varphi} &= \frac{\Delta x^2}{12}\frac{\partial^3 U}{\partial\varphi^3}\left[\exp\left(\frac{\Delta x^2}{12}\frac{\partial^2 U}{\partial\varphi^2}\right)\frac{\partial\Phi_n}{\partial\varphi} + \frac{\Delta x^2}{12}\frac{\partial^3 U}{\partial\varphi^3}\exp\left(\frac{\Delta x^2}{12}\frac{\partial^2 U}{\partial\varphi^2}\right)\Phi_n\right] \\
&\simeq \frac{\Delta x^2}{12}\frac{\partial^3 U}{\partial\varphi^3}\exp\left(\frac{\Delta x^2}{12}\frac{\partial^2 U}{\partial\varphi^2}\right)\frac{\partial\Phi_n}{\partial\varphi}.
\end{aligned} \tag{3.75}$$

Eq.(3.71) now reads

$$\begin{aligned}
-\frac{1}{2\beta^2}\left(1 - \frac{\Delta x^2}{6}\frac{\partial^2 U}{\partial\varphi^2}\right)\frac{\partial^2\Psi_n}{\partial\varphi^2} + \left[U + \frac{\Delta x^2}{48}\left(2\left(\frac{\partial U}{\partial\varphi}\right)^2 - \frac{1}{\beta^2}\frac{\partial^4 U}{\partial\varphi^4}\right)\right]\Psi_n \\
= \epsilon_n\Psi_n,
\end{aligned} \tag{3.76}$$

where Φ_n's have been rewritten as Ψ_n's to keep the original notation.

The first term of eq.(3.76) further simplified by performing the change of variable

$$u = \varphi + \frac{\Delta x^2}{12}\frac{\partial U}{\partial\varphi}. \tag{3.77}$$

The potential term becomes,

$$\begin{aligned} U(\varphi) &= U(u - \frac{\Delta x^2}{12}\frac{\partial U}{\partial \varphi}) \\ &= U(u) + \frac{\partial U}{\partial u}\delta u + \dots \\ &= U(u) + \frac{\partial U}{\partial u}\left(-\frac{\Delta x^2}{12}\frac{\partial U}{\partial \varphi}\right) + \dots \\ &= U(u) - \frac{\Delta x^2}{12}\frac{\partial U}{\partial u}\left(\frac{\partial U}{\partial u}\frac{\partial u}{\partial \varphi}\right) + \dots \\ &= U(u) - \frac{\Delta x^2}{12}\frac{\partial U}{\partial u}\frac{\partial U}{\partial u}\left(1 + \frac{\Delta x^2}{12}\frac{\partial^2 U}{\partial \varphi^2}\right) + \dots . \end{aligned} \tag{3.78}$$

Considering terms to the order $\mathcal{O}(\Delta x^2)$ gives

$$U(\varphi) \simeq U(u) - \frac{\Delta x^2}{12}\left(\frac{\partial U}{\partial u}\right)^2. \tag{3.79}$$

Likewise,

$$\begin{aligned} \frac{\partial^2 \Psi_n}{\partial \varphi^2} &= \frac{\partial}{\partial \varphi}\left(\frac{\partial \Psi_n}{\partial u}\frac{\partial u}{\partial \varphi}\right) \\ &= \frac{\partial}{\partial \varphi}\left(\frac{\partial \Psi_n}{\partial u}\left(1 + \frac{\Delta x^2}{12}\frac{\partial^2 U}{\partial \varphi^2}\right)\right) \\ &= \frac{\partial}{\partial u}\left(\frac{\partial \Psi_n}{\partial u}\left(1 + \frac{\Delta x^2}{12}\frac{\partial^2 U}{\partial \varphi^2}\right)\right)\left(1 + \frac{\Delta x^2}{12}\frac{\partial^2 U}{\partial \varphi^2}\right) \\ &= \left(\frac{\partial^2 \Psi_n}{\partial u^2} + \frac{\Delta x^2}{12}\frac{\partial \Psi_n}{\partial u}\frac{\partial}{\partial u}\frac{\partial^2 U}{\partial \varphi^2} + \frac{\Delta x^2}{12}\frac{\partial^2 U}{\partial \varphi^2}\frac{\partial^2 \Psi_n}{\partial u^2}\right)\left(1 + \frac{\Delta x^2}{12}\frac{\partial^2 U}{\partial \varphi^2}\right) \\ &= \frac{\partial^2 \Psi_n}{\partial u^2} + \frac{\Delta x^2}{12}\frac{\partial \Psi_n}{\partial u}\frac{\partial}{\partial u}\frac{\partial^2 U}{\partial \varphi^2} + \frac{\Delta x^2}{12}\frac{\partial^2 U}{\partial \varphi^2}\frac{\partial^2 \Psi_n}{\partial u^2} + \frac{\Delta x^2}{12}\frac{\partial^2 U}{\partial \varphi^2}\frac{\partial^2 \Psi_n}{\partial u^2} + \mathcal{O}(\Delta x^4) \\ &\simeq \left(1 + \frac{\Delta x^2}{6}\frac{\partial^2 U}{\partial \varphi^2}\right)\frac{\partial^2 \Psi_n}{\partial u^2} + \frac{\Delta x^2}{12}\frac{\partial \Psi_n}{\partial u}\frac{\partial}{\partial u}\frac{\partial^2 U}{\partial \varphi^2}. \end{aligned} \tag{3.80}$$

With $\Delta x^2 \frac{\partial u}{\partial \varphi} \sim 1$ and to order $\mathcal{O}(\Delta x^2)$

$$\frac{\partial^2 \Psi_n}{\partial \varphi^2} \simeq \left(1 + \frac{\Delta x^2}{6}\frac{\partial^2 U}{\partial u^2}\right)\frac{\partial^2 \Psi_n}{\partial u^2} + \frac{\Delta x^2}{12}\frac{\partial^3 U}{\partial u^3}\frac{\partial \Psi_n}{\partial u}. \tag{3.81}$$

Reverting back to the original notation of φ's, eq.(3.71) has the form

$$\begin{aligned} -\frac{1}{2\beta^2}\frac{\partial^2 \Psi_n}{\partial \varphi^2} + \frac{1}{2\beta^2}\frac{\Delta x^2}{12}\frac{\partial^3 U}{\partial \varphi^3}\frac{\partial \Psi_n}{\partial \varphi} \\ + \left[U - \frac{\Delta x^2}{48}\left(2\left(\frac{\partial U}{\partial \varphi}\right)^2 - \frac{1}{\beta^2}\frac{\partial^4 U}{\partial \varphi^4}\right)\right]\Psi_n = \epsilon_n \Psi_n. \end{aligned} \tag{3.82}$$

Lastly, the functional transform,

$$\Psi_n = \exp\left(\frac{\Delta x^2}{24}\frac{\partial^2 U}{\partial\varphi^2}\right)\Phi_n. \tag{3.83}$$

was performed, such that

$$\frac{\partial\Psi_n}{\partial\varphi} = -\frac{\Delta x^2}{24}\frac{\partial^3 U}{\partial\varphi^3}\exp\left(\frac{\Delta x^2}{24}\frac{\partial^2 U}{\partial\varphi^2}\right)\Phi_n + \exp\left(\frac{\Delta x^2}{24}\frac{\partial^2 U}{\partial\varphi^2}\right)\frac{\partial\Phi_n}{\partial\varphi}, \tag{3.84}$$

and,

$$\begin{aligned}\frac{\partial^2\Psi_n}{\partial\varphi^2} = &-\frac{\Delta x^2}{24}\frac{\partial^4 U}{\partial\varphi^4}\exp\left(\frac{\Delta x^2}{24}\frac{\partial^2 U}{\partial\varphi^2}\right)\Phi_n + \frac{\Delta x^4}{576}\left(\frac{\partial^3 U}{\partial\varphi^3}\right)^2\exp\left(\frac{\Delta x^2}{24}\frac{\partial^2 U}{\partial\varphi^2}\right)\Phi_n \\ &-\frac{\Delta x^2}{24}\frac{\partial^3 U}{\partial\varphi^3}\exp\left(\frac{\Delta x^2}{24}\frac{\partial^2 U}{\partial\varphi^2}\right)\frac{\partial\Phi_n}{\partial\varphi} + \exp\left(\frac{\Delta x^2}{24}\frac{\partial^2 U}{\partial\varphi^2}\right)\frac{\partial^2\Phi_n}{\partial\varphi^2}.\end{aligned} \tag{3.85}$$

To order $\mathcal{O}(\Delta x^2)$ this gives

$$\frac{1}{2\beta^2}\frac{\Delta x^2}{12}\frac{\partial^3 U}{\partial\varphi^3}\frac{\partial\Psi_n}{\partial\varphi} \simeq \frac{1}{2\beta^2}\frac{\Delta x^2}{12}\frac{\partial^3 U}{\partial\varphi^3}\frac{\partial\Phi_n}{\partial\varphi}\exp\left(\frac{\Delta x^2}{24}\frac{\partial^2 U}{\partial\varphi^2}\right), \tag{3.86}$$

and,

$$\frac{\partial^2\Psi_n}{\partial\varphi^2} \simeq \left(-\frac{\Delta x^2}{24}\frac{\partial^4 U}{\partial\varphi^4}\Phi_n - \frac{\Delta x^2}{24}\frac{\partial^3 U}{\partial\varphi^3}\frac{\partial\Phi_n}{\partial\varphi} + \frac{\partial^2\Phi_n}{\partial\varphi^2}\right)\exp\left(\frac{\Delta x^2}{24}\frac{\partial^2 U}{\partial\varphi^2}\right). \tag{3.87}$$

With these substitutions and in original notation, the Schrödinger-type equation reduces to

$$\left[-\frac{1}{2\beta^2}\frac{\partial^2}{\partial\varphi^2} + U - \frac{\Delta x^2}{24}\left(\frac{\partial U}{\partial\varphi}\right)^2\right]\Psi_n = \epsilon_n\Psi_n. \tag{3.88}$$

From eq.(3.88), an effective potential was extracted. Firstly, eq.(3.88) suggests the modification of $U(\varphi)$ to

$$\begin{aligned}&U - \frac{\Delta x^2}{24}\left(\frac{\partial U}{\partial\varphi}\right)^2 \\ &\quad = \Delta y\sum_j^N\left[V(\phi) - \frac{2\langle\phi\rangle}{\Delta y^2}\phi\right] - \frac{\Delta x^2}{24}\left(\Delta y\sum_j^N\frac{\partial}{\partial\phi}\left[V(\phi) - \frac{2\langle\phi\rangle}{\Delta y^2}\phi\right]\right) \\ &\quad ,\end{aligned} \tag{3.89}$$

where lattice indices have been omitted. From this form of $U(\varphi)$, the following local potential was constructed

$$V_{\text{latt}}(\phi) = V_{MF}(\phi) + \frac{\Delta x^2}{24}\left(\frac{\partial}{\partial\phi}V_{MF}(\phi)\right)^2 \tag{3.90}$$

The term within the square brackets of eq.(3.89) have been labelled $V_{MF}(\phi)$ for brevity. We propose that the replacement of the bare potential, eq.(2.8), in Langevin simulations with eq.(3.90) would lead to the cancellation of lattice dependence to order $\mathcal{O}(\Delta x^2)$ as it appears in eq.(3.89). The leading error would then be of the order $\mathcal{O}(\Delta x^4)$ which becomes negligible for a small choice of Δx.

When $V(\phi)$ is of the ϕ^4 form in eq.(2.8), the lattice potential of eq.(3.90) has terms of the order ϕ^6. V_{latt} is of the form,

$$\begin{aligned} V(\phi)_{latt} = &- \frac{m^2}{2}\phi^2 + \frac{\lambda}{4}\phi^4 - \frac{2\langle\phi\rangle}{\Delta y^2}\phi \\ &+ \frac{\Delta x^2}{24}\left(\frac{\partial}{\partial\phi}\left[-\frac{m^2}{2}\phi^2 + \frac{\lambda}{4}\phi^4 - \frac{2\langle\phi\rangle}{\Delta y^2}\phi\right]\right)^2 \end{aligned} \tag{3.91}$$

or, in a rescaled form consistent with the prescription in chapter 2,

$$\begin{aligned} V(\phi)_{latt} = &- \frac{2\langle\phi\rangle}{\Delta y^2}\left(1 - \frac{\Delta x^2}{24}\right)\phi - \frac{1}{2}\left(1 - \frac{\Delta x^2}{12}\right)\phi^2 - \frac{\langle\phi\rangle}{6}\frac{\Delta x^2}{\Delta y^2}\phi^3 \\ &+ \frac{1}{4}\left(1 - \frac{\Delta^2}{3}\right)\phi^4 + \frac{\Delta x^2}{24}\phi^6 \end{aligned} \tag{3.92}$$

The ϕ^4 (technically, a ϕ^6 polynomial) lattice potential contains terms that give it an asymmetric form depending on the value of $\langle\phi\rangle$. Low temperatures and small lattice spacings were used in this study. So thermal fluctuations, and the factors $\langle\phi\rangle$ and Δx^2 were small enough such that the dynamics of the ϕ^6 potential were similar to those of eq.(2.8).

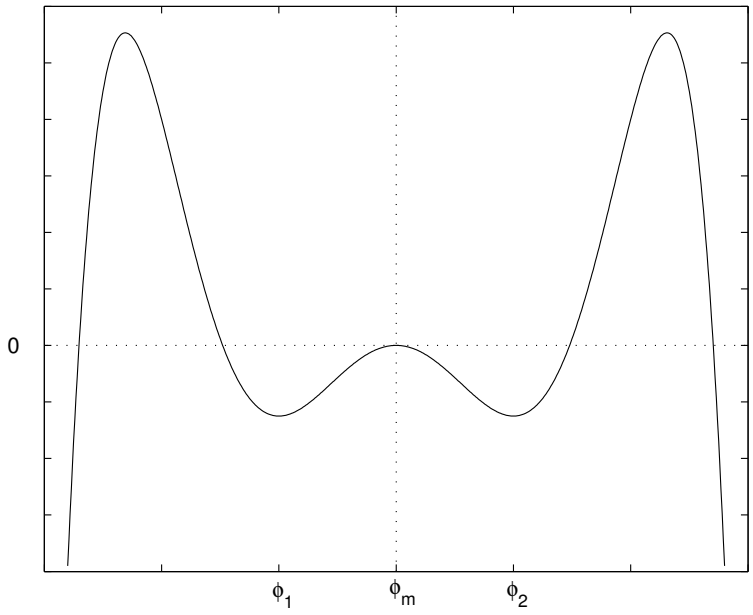

Figure 3.3: The lattice potential of eq.(3.89). For illustrative purposes, the following parameter choices were made; $\Delta x = 0.2$, $\Delta y = 1.0$ and $\langle \phi \rangle = 0$.

Chapter 4

The One-loop Renormalization Counterterm

An alternative method for suppressing lattice spacing dependence uses techniques from renormalization theory. Parisi [24] suggested the introduction of renormalization counterterms to eliminate dependence on the ultraviolet cutoff imposed by the lattice spacing. The conjecture was that the field theory studied on a lattice is equivalent to a continuum theory with an ultraviolet momentum cutoff, $\Lambda = \pi/\Delta x$, where Δx is the lattice spacing. This ultraviolet cutoff then sets the scale for the smallest possible spatial fluctuations that may be induced by the heat bath. In the language of field theory, this has an influence on the form of the thermal corrections to the classical field theory. Such thermal corrections change the behaviour of the classical potential and act as a mechanism for non-perturbative phenomena such as symmetry breaking.

For this reason, an effective potential, V_{eff}, which incorporates thermal corrections set by the lattice spacing must be considered. The effective potential, V_{eff}, unlike the classical (tree-level) potential, does not have a closed form. Its structure has to be studied using perturbation theory. Usually, a perturbative expansion of V is in terms of the number of loops of a Feynman diagram coinciding with an expansion in powers of T is performed. This study is restricted to one-

loop order, consistent with previous studies [13][14], such that

$$V = V_o + TV_1 + \dots \tag{4.1}$$

where "..." represents corrections $\mathcal{O}(T^2)$ and higher.

Section 4.1 begins with a very brief discussion on an apparent equivalence between Euclidean quantum field theory (QFT) and classical thermal field theory (CFT). Then, the well-known derivation of the one-loop effective potential for a zero-temperature (1+1)-dimensional Minkowskian QFT is outlined. Care is taken to make every assumption clear. In section 4.2, anisotropy conditions are imposed and the one-loop effective potential is explicitly evaluated. In section 4.3, a renormalization procedure is then used to formulate a lattice potential specific to the case of the degenerate ϕ^4 model introduced in chapter 2.

4.1 The One-Loop Effective Potential

One-loop quantum corrections were calculated for the effective potential of a (1+1)-dimensional Minkowskian QFT following the procedure in [25]. A Wick rotation [26] into a 2-dimensional Euclidean QFT related the result back to the CFT by a well-known mapping ($\hbar \to k_B T$) between the two theories. Such corrections in the CFT are considered to be entropic in nature.

The path integral formulation of a Minkowskian quantum field theory in $d-1$ spatial and one time dimension is concerned with the computation of path integral averages that look like,

$$\langle \mathcal{O}_j \rangle = \frac{\int \mathcal{D}\phi \mathcal{O}_j e^{\mathrm{i}S_M/\hbar}}{Z_M}, \qquad Z_M = \int \mathcal{D}[\phi] e^{\mathrm{i}S_M/\hbar}, \tag{4.2}$$

where

$$S_M = \int \mathrm{d}t \int \mathrm{d}\mathbf{x}^{d-1} \mathscr{L} \tag{4.3}$$

is the Minkowskian action in terms of the Lagrangian density, $\mathscr{L}$, with the Minkowskian metric, $ds^2 = -(dt^2) + d\mathbf{x}^2$.

The Minkowskian metric becomes Euclidean when t is restricted to the imaginary axis. Under the substitution, $t \to \tau \equiv \mathrm{i}t$, $\tau \in \mathbb{R}$ the set of coordinates $x_\mu \equiv (x_o, \mathbf{x})$ in Minkowski space become real Euclidean coordinates $x_\mu \equiv (\mathbf{x}_E, x_2)$. This procedure, known as a Wick rotation, is useful when it is easier to solve an equivalent Euclidean problem related to a given Minkowskian problem. The term rotation is used because multiplying real t values on a complex plane by i is equivalent to rotating the vector representing t by an angle of $\pi/2$. Performing a Wick rotation gives the Euclidean metric,

$$ds^2 = d\tau^2 + d\mathbf{x}^2. \tag{4.4}$$

The path integral formulation of Euclidean quantum field theory is

$$\langle \mathcal{O}_j \rangle = \frac{\int \mathcal{D}\phi \mathcal{O}_j e^{-S_E/h}}{Z_E}, \qquad Z_E = \int \mathcal{D}[\phi] e^{-S_E/h}, \tag{4.5}$$

where the Euclidean action is $S_E = \int \mathrm{d}x^d \mathscr{L}$.

In contrast, classical statistical mechanics is concerned with the computation of thermal expectation values of an arbitrary observable $\mathcal{O}_j$,

$$\langle \mathcal{O}_j \rangle = \frac{\sum_n \mathcal{O}_j e^{-\beta E_n}}{Z}, \qquad Z = \sum_n e^{-\beta E_n} \tag{4.6}$$

where E_n, Z and β are as defined in the previous chapters. Eq.(4.5) and eq.(4.6) are formally the same and thus it may be expected that there is a relation between these subjects [27]. That is to say, the path integral over all field configurations corresponds to the canonical sum over states (the canonical partition function). In fact, under $k_B T \to \hbar$, the equilibrium correlation functions of the classical theory map exactly onto the zero-temperature Green's functions of the quantum theory, and the free energy maps onto the effective action [13].

This provides a formal mathematical connection between two theories that describe very different physics. It serves as a starting point for constructing an analogy between classical $(d+1)$-dimensional scalar field theory and zero-temperature quantum field theory in d-dimensional Euclidean space-time. This

equivalence was utilized in the derivation of the one-loop effective potential that follows.

We begin with the generating functional

$$\begin{aligned} Z[J] &= \exp\left(\frac{\mathrm{i}}{\hbar}W[J]\right) \\ &= \int \mathcal{D}[\phi]\exp\left(\frac{\mathrm{i}}{\hbar}S^J[\phi]\right), \end{aligned} \tag{4.7}$$

where $S^J[\phi]$ is the Minkowskian action of a scalar field theory in the presence of a source term, J. The action $S^J[\phi]$ is

$$\begin{aligned} S^J[\phi] &= \int \mathrm{d}x^2 \left[\frac{1}{2}\partial_\mu\phi\partial^\mu\phi - V + J\phi\right] \\ &= S[\phi] + \int \mathrm{d}x^2 J\phi. \end{aligned} \tag{4.8}$$

where the classical action,

$$S[\phi] = \int \mathrm{d}x^2 \left[\frac{1}{2}\partial_\mu\phi\partial^\mu\phi - V\right] \tag{4.9}$$

has been inserted. V is the tree-level potential (the ϕ^4 model of eq.(2.4) will be used later in this chapter). The field, ϕ, is decomposed in the usual perturbative way,

$$\phi = \phi_o + \sqrt{\hbar}\chi, \tag{4.10}$$

where ϕ_o is the classical solution to the tree-level Euler-Lagrange equation that follows from,

$$\left.\frac{\delta S^J(\phi)}{\delta\phi}\right|_{\phi=\phi_o} = 0, \tag{4.11}$$

and χ is a fluctuation field about the classical solution. Consequently, the action

can be expanded around the classical solution also, giving

$$\begin{aligned} S^J[\phi] &= S^J[\phi_o + \chi] \\ &= S^J[\phi_o] + \sqrt{\hbar}\int \mathrm{d}^2x\chi(x)\frac{\delta S^J(\phi)}{\delta\phi(x)}\bigg|_{\phi=\phi_o} \\ &\quad + \frac{\hbar}{2}\int \mathrm{d}^2x\mathrm{d}^2y\chi(x)\frac{\delta^2 S^J(\phi)}{\delta\phi(x)\delta\phi(y)}\bigg|_{\phi=\phi_o}\chi(y) + \dots \\ &= S^J[\phi_o] - \frac{\hbar}{2}\int \mathrm{d}^2x\mathrm{d}^2y\chi(x)\mathcal{G}^{-1}(x,y)\chi(y) + \dots, \end{aligned} \tag{4.12}$$

where $\mathcal{G}^{-1}(x,y)$ has been defined as

$$\mathcal{G}^{-1}(x,y) = -\frac{\delta^2 S^J(\phi)}{\delta\phi(x)\delta\phi(y)}\bigg|_{\phi=\phi_o}. \tag{4.13}$$

Note that the term linear in χ vanishes because of the relation, eq.(4.11). The terms represented by "..." are $\mathcal{O}(\chi^3)$ and higher. These terms introduce higher powers in $\hbar$ and are therefore neglected. Substitution of the expansion eq.(4.12) into the generating functional gives,

$$\begin{aligned} Z[J] &= \exp\left(\frac{\mathrm{i}}{\hbar}S[\phi_o]\right)\int \mathcal{D}[\chi]\exp\left(-\frac{\mathrm{i}}{2}\chi x\frac{\delta^2 S^J(\phi)}{\delta\phi(x)\delta\phi(y)}\bigg|_{\phi=\phi_o}\chi(y)\right) \\ &= \exp\left(\frac{\mathrm{i}}{\hbar}S[\phi_o]\right)\left[\det(\mathcal{G}^{-1})\right]^{1/2} \end{aligned} \tag{4.14}$$

It follows that the generating functional for connected Greens functions, W[J], can be found by the Gaussian integration of eq.(4.14) (see Appendix B)

$$\begin{aligned} W[J] &= S^J[\phi_o] + \frac{\hbar}{\mathrm{i}}\ln\det(\mathcal{G}^{-1})]^{-1/2} \\ &= S^J[\phi_o] + \frac{\mathrm{i}\hbar}{2}\mathrm{tr}\ln\mathcal{G}^{-1} \end{aligned} \tag{4.15}$$

The effective action, $\Gamma[\phi_c]$, from which the effective potential follows, is the generating functional for one particle irreducible (1PI) graphs (diagrams that do not dissociate into two when a single line is cut). It follows from the Legendre transformation of the generating functional, $W[J]$, given by

$$\Gamma[\phi_c] = W[J] - \int \mathrm{d}^2x\phi_c(x)J(x). \tag{4.16}$$

The classical field, ϕ_c, can be expanded in powers of $\hbar$. However, since it satisfies the Euler-Lagrange equation eq.(4.11) in the limit $\hbar \to 0$, it can be expanded as follows

$$\phi_c(x) = \phi_o(x) + \phi_1(x) + \ldots, \tag{4.17}$$

where $\phi_1(x)$ is understood to be of order $\hbar$ and "..." represent terms $\mathcal{O}(\hbar^2)$ or higher. From eq.(4.17), the action becomes,

$$\begin{aligned} S(\phi_c) &\simeq S(\phi_o + \phi_1) \\ &= S(\phi_o) + \int \mathrm{d}^2x \phi_1 \frac{\delta S}{\delta \phi(x)}\bigg|_{\phi_o} \\ &= S(\phi_o) - \int \mathrm{d}^2x J(x)\phi_1(x). \end{aligned} \tag{4.18}$$

With these substitutions and the result of eq.(4.15), $\Gamma[\phi_c]$ to first order in $\hbar$, reads

$$\begin{aligned} \Gamma[\phi_c] &= S^J[\phi_o] + \frac{\mathrm{i}\hbar}{2}\mathrm{Tr}\ln\mathcal{G}^{-1} - \int \mathrm{d}^2x \phi_c(x)J(x) \\ &= S[\phi_o] + \int \mathrm{d}x^2 \phi_o J(x) + \frac{\mathrm{i}\hbar}{2}\mathrm{Tr}\ln\mathcal{G}^{-1} - \int \mathrm{d}^2x(\phi_o + \phi_1)J(x) \\ &= S[\phi_o] - \int \mathrm{d}x^2 \phi_1 J(x) + \frac{\mathrm{i}\hbar}{2}\mathrm{Tr}\ln\mathcal{G}^{-1} \\ &= S[\phi_c] + \frac{\mathrm{i}\hbar}{2}\mathrm{Tr}\ln\mathcal{G}^{-1}. \end{aligned} \tag{4.19}$$

To understand the relation between the effective action, $\Gamma(\phi_c)$, and the effective potential, $V(\phi_c)$, consider the expansion of the effective action in powers of momentum,

$$\Gamma[\phi_c] = \int \mathrm{d}^2x \left[-V_{eff}(\phi_c) + \frac{1}{2}\partial_\mu\phi_c\partial^\mu\phi_c + \cdots\right]. \tag{4.20}$$

When $J \to 0$, the classical field becomes $\phi_c = \phi$ which is a constant. Therefore, all derivative terms in eq.(4.20) vanish leaving,

$$\begin{aligned} \Gamma[\phi_c] &= -(2\pi)^2\delta(0)V_{eff}(\phi_c) \\ &= -\Omega V_{eff}(\phi_c) \end{aligned} \tag{4.21}$$

where Ω is the space-time volume. From eq.(4.19) and the form of the classical action,

$$\Gamma[\phi_c] = -\Omega V(\phi_o) + \frac{\mathrm{i}\hbar}{2}\mathrm{Tr}\ln\mathcal{G}^{-1} \tag{4.22}$$

or,

$$V(\phi_c) = V(\phi_o) - \frac{\mathrm{i}\hbar}{2}\Omega^{-1}\mathrm{Tr}\ln\mathcal{G}^{-1} \tag{4.23}$$

From the definition of $\mathcal{G}^{-1}(x,y)$ in eq.(4.13) and the classical action given in eq.(4.9),

$$\langle x|\mathcal{G}^{-1}|y\rangle = \mathcal{G}^{-1}(x,y) = (\Box + V^{''})\delta^2(x-y) \tag{4.24}$$

This shows that in the calculation of the effective potential, $\mathcal{G}$ behaves like a propagator with an effective mass $V^{''}$ such that

$$\mathrm{Tr}\ \ln\ \mathcal{G}^{-1} = \int \mathrm{d}^2x\langle x|\ln\mathcal{G}^{-1}|x\rangle. \tag{4.25}$$

Even though $\mathcal{G}^{-1}$ is not diagonal in the coordinate basis, it is in the momentum basis and has the form

$$\langle k|\mathcal{G}^{-1}|k'\rangle = \mathcal{G}^{-1}(k,k') = (-k^2 + V^{''})\delta^2(k-k') \tag{4.26}$$

Consequently, using the fact that for a diagonal matrix,

$$\langle i|\ln A_D|j\rangle = \ln\langle i|A_D|j\rangle \tag{4.27}$$

the one-loop correction may be written in the more convenient form,

$$\begin{aligned}
\mathrm{Tr}\ln\mathcal{G}^{-1} &= \int \mathrm{d}^2x\langle x|\ln\mathcal{G}^{-1}|x\rangle \\
&= \int \mathrm{d}^2x\mathrm{d}^2k\mathrm{d}^2k'\langle x|k\rangle\langle k|\ln\mathcal{G}^{-1}|k'\rangle\langle k'|x\rangle \\
&= \int \mathrm{d}^2x\mathrm{d}^2k\mathrm{d}^2k'\frac{e^{-i(k-k').x}}{(2\pi)^2}\ln(-k^2+V^{''})\delta^2(k-k') \\
&= \int \mathrm{d}^2x\frac{\mathrm{d}^2k}{(2\pi)^2}\ln(-k^2+V^{''}) \\
&= \Omega\int \frac{\mathrm{d}^2k}{(2\pi)^2}\ln(-k^2+V^{''}).
\end{aligned} \tag{4.28}$$

Thus, for scalar field theories, the one-loop correction to the effective potential is given by

$$V_{1L} = \frac{1}{2}\int_0^\infty \frac{\mathrm{d}^2 k}{(2\pi)^2}\ln(-k^2 + V'') \tag{4.29}$$

A Wick rotation on the complex k_o plane is performed. The procedure is based on the assumption of analytic continuation, so particular caution needs to be taken with such rotations in momentum space. Consider the self-energy graph, $\int \mathrm{d}^2 k\mathcal{G}$. From eq.(4.26), it is clear that, what are termed, "mass-shell" singularities [26] (or poles) exist at $k^2 = V''$. Written more explicitly, the integral reads

$$\int \mathrm{d}\mathbf{k}\int_{-\infty}^{\infty}\mathrm{d}k_o \frac{1}{k_o^2 - (\mathbf{k}^2 + V'') - \mathrm{i}\eta} \tag{4.30}$$

with poles now situated at $k_o = \pm\sqrt{\mathbf{k}^2 + V_o'' - \mathrm{i}\eta}$. The $-\mathrm{i}\eta$ displaces the mass-shell poles away from the path of integration along the real k_o axis. This is to ensure that no singularities are encountered in the process of contour integration.

With the mass-shell poles situated above the negative k_o axis and below the positive k_o axis (see fig.(4.1) below), a Wick rotation may now be performed by the transformation,

$$k_o \to \mathrm{i}k_2 \qquad\qquad k_2 \in \mathbb{R}. \tag{4.31}$$

The transformation is the rotation on the complex k_2 plane illustrated graphically in fig.(4.1).

The self-energy graph now reads,

$$-\mathrm{i}\int \mathrm{d}\mathbf{k}_E \int_{-\infty}^{\infty}\mathrm{d}k_2 \frac{1}{\mathbf{k}_E^2 + k_2^2 + V''} \tag{4.32}$$

where the limit $\eta \to 0$ has been taken. Note that the integral eq.(4.32) is over variables of a 2-component Euclidean momentum vector, $k_E \equiv (\mathbf{k}_E, k_2) = (k_1, k_2)$. With the transformation eq.(4.31), eq.(4.29) becomes

$$V_{1L} = -\frac{\mathrm{i}\hbar}{2}\int_0^\infty \frac{\mathrm{i}\mathrm{d}^2 k_E}{(2\pi)^2}\ln(k_E^2 + V''), \tag{4.33}$$

Finally, dropping the quantum k notation in favor of the classical p notation for momentum and performing the transform $\hbar \to k_B T$, the one-loop counterterm

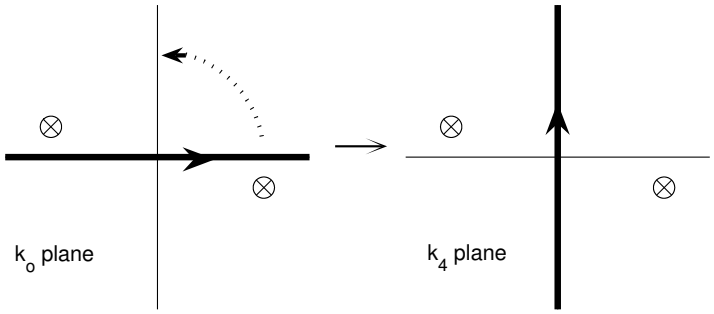

Figure 4.1: Wick rotation in momentum space. The ⊗'s indicate poles that are present.

becomes

$$V_{1L} = \frac{T}{2}\int_0^\infty \frac{\mathrm{d}^2 p}{(2\pi)^2}\ln(p^2 + V'').\tag{4.34}$$

4.2 Lattice Regularization

As is well known, integrals of the type eq.(4.34) are severly ultraviolet divergent. Numerous methods exist for regularizing such integrals, a few popular ones being dimensional regularization, Pauli-Villars regularization, zeta function regularization and lattice regularization. Ultraviolet cutoffs are inherent to a field theory formulated on a lattice, so lattice regularization is the obvious choice.

From the result eq.(4.34), the one-loop effective potential for the isotropic version of our (2+1)-dimensional scalar field is straightfoward to calculate. With the ultraviolet lattice cutoff, Λ,

$$V_{eff}(\phi) = V + \frac{T}{2}\int_0^\Lambda \frac{\mathrm{d}^2 p}{(2\pi)^2}\ln(p^2 + V'')\tag{4.35}$$

The evaluation of the momentum integral can be simplified by the transformation to polar coordinates $\{p_x = p\cos(\theta), p_y = p\sin(\theta)\}$. This gives,

$$\begin{aligned}\int_0^\Lambda \frac{\mathrm{d}^2p}{(2\pi)^2}\ln(p^2+V'') &= \frac{1}{(2\pi)^2}\int_0^{2\pi}\mathrm{d}\theta\int_0^\Lambda \mathrm{d}p p\ln(p^2+V'') \\ &= \frac{1}{8\pi}\left[(\Lambda^2+V'')\ln(\Lambda^2+V'')-\Lambda^2-V''\ln(V'')\right]\end{aligned} \tag{4.36}$$

With the integrand having no θ dependence, integration over θ simply introduces a factor of 2π. With $V'' \ll \Lambda^2$, a Taylor series expansion about V'' to first-order is performed. Also, constant terms like Λ^2 have no effect on the dynamics of the model and may be omitted. The one-loop effective potential to order $\mathcal{O}(V'')$ is

$$V_{eff} = V + \frac{T}{8\pi}V''\left[1-\ln\left(\frac{V''}{\Lambda^2}\right)\right]. \tag{4.37}$$

The evaluation of the anisotropic momentum integral was somewhat less trivial. The one-loop effective potential is of the form,

$$V_{eff} = V + \frac{T}{2}\frac{1}{(2\pi)^2}\int_0^{\Lambda_x}\mathrm{d}p_x\int_0^{\sqrt{\Lambda_y\left(1-\frac{p_x^2}{\Lambda_x}\right)}}\mathrm{d}p_y\ln\left(p_x^2+p_y^2+V''\right). \tag{4.38}$$

Anisotropy in the field theory complicates the θ integration as one now has to consider two cutoffs, Λ_x and Λ_y. Instead of having rotational symmetry and therefore no θ dependence, the integration here is over an elliptic region in momentum space illustrated in fig.(4.2) To evaluate eq.(4.38) it was useful to transform to the set of polar coordinates, $\{p_x = p\cos\theta, p_y = p\sin\theta\}$. As a consequence, the upper bound of the radial quantity $p = \sqrt{p_x^2+p_y^2}$ varies with θ. That is, the upper bound is traced out by the elliptic curve

$$p_{max} = \sqrt{\Lambda_x^2\sin^2\theta + \Lambda_y^2\cos^2\theta}. \tag{4.39}$$

illustrated in fig.(4.2). For later convenience, $\theta = 0$ was set at the positive p_y axis.

One of the trigonometric functions in eq.(4.39) may be eliminated by re-defining one of the cutoffs. Because $\Lambda_x > \Lambda_y$ by the anisotropy condition of

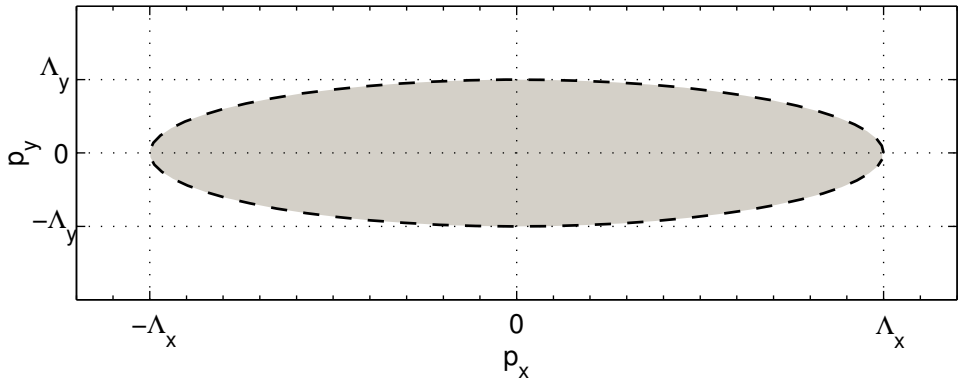

Figure 4.2: Momentum space. The shaded region illustrates the area of momentum space integrated over in the evaluation of the anisotropic one-loop effective potential.

eq.(3.53), a quantity, b^2, was defined as the difference in squares

$$b^2 = \Lambda_x^2 - \Lambda_y^2. \tag{4.40}$$

With this, p_{max} simplifies to

$$\begin{aligned} p_{max} &= \sqrt{\left(b^2 + \Lambda_y^2\right)\sin^2\theta + \Lambda_y^2\cos^2\theta} \\ &= \sqrt{b^2\sin^2\theta + \Lambda_y^2} \end{aligned} \tag{4.41}$$

The momentum integral of eq.(4.38) now reads,

$$\frac{1}{(2\pi)^2}\int_0^{2\pi} \mathrm{d}\theta \int_0^{\sqrt{b^2\sin^2\theta+\Lambda_y^2}} \mathrm{d}p\, p \ln(p^2 + V'') \tag{4.42}$$

In [14], the logarithmic function to be integrated over was seperated, in this case giving

$$\frac{1}{(2\pi)^2}\int_0^{2\pi}\mathrm{d}\theta\left\{\int_0^{\sqrt{b^2\sin^2\theta+\Lambda_y^2}}\mathrm{d}pp\ln(p^2)+\int_0^{\sqrt{b^2\sin^2\theta+\Lambda_y^2}}\mathrm{d}pp\ln\left(1+\frac{V''}{p^2}\right)\right\} \tag{4.43}$$

The first term in the brackets is a constant and are usually subtracted from the calculation. Constants are of no consequence to the functional form of the effective potential as they simply act to shift the potential up and down the $V(\phi)$ axis. However, such constants will not be subtracted till the very end. Integration of the first term with respect to p gives,

$$\begin{aligned}&\frac{1}{(2\pi)^2}\int_0^{2\pi}\mathrm{d}\theta\int_0^{\sqrt{b^2\sin^2\theta+\Lambda_y^2}}\mathrm{d}pp\ln(p^2)\\&\quad=\frac{1}{2(2\pi)^2}\int_0^{2\pi}\mathrm{d}\theta\left\{\left(b^2\sin^2\theta+\Lambda_y^2\right)\ln\left(b^2\sin^2\theta+\Lambda_y^2\right)-\left(b^2\sin^2\theta+\Lambda_y^2\right)\right\}\end{aligned} \tag{4.44}$$

Integration of the second term with respect to p gives,

$$\begin{aligned}&\frac{1}{(2\pi)^2}\int_0^{2\pi}\mathrm{d}\theta\int_{V''}^{\sqrt{b^2\sin^2\theta+\Lambda_y^2}}\mathrm{d}p\ln\left(1+\frac{V''}{p^2}\right)\\&=\frac{1}{2(2\pi)^2}\int_0^{2\pi}\mathrm{d}\theta\Bigg[\left(b^2\sin^2\theta+A\right)\ln\left(b^2\sin^2\theta+A\right)\\&\qquad\qquad-\left(b^2\sin^2\theta+\Lambda_y^2\right)\ln\left(b^2\sin^2\theta+\Lambda_y^2\right)-V''\ln\left(V''\right)\Bigg],\end{aligned} \tag{4.45}$$

where $A=\Lambda_y^2+V''$ has been introduced for brevity. Combining eq.(4.44) and

eq.(4.45), the one-loop counterterm eq.(4.43) becomes

$$\begin{aligned}
&\frac{1}{2(2\pi)^2}\int_0^{2\pi} \mathrm{d}\theta \Bigg[\left(b^2\sin^2\theta + A\right)\ln\left(b^2\sin^2\theta + A\right) - \left(b^2\sin^2\theta + \Lambda_y^2\right) - V''\ln\left(V''\right) \Bigg] \\
&= \frac{1}{2(2\pi)^2}\int_0^{2\pi} \mathrm{d}\theta \Bigg[\left(b^2\sin^2\theta + A\right)\ln\left[A\left(\frac{b^2}{A}\sin^2(\theta)+1\right)\right] \\
&\qquad\qquad - \left(b^2\sin^2\theta + \Lambda_y^2\right) - V''\ln\left(V''\right) \Bigg] \\
&= \frac{1}{2(2\pi)^2}\int_0^{2\pi} \mathrm{d}\theta \Bigg[\left(b^2\sin^2(\theta) + A\right)\ln\left(1+\frac{b^2}{A}\sin^2(\theta)\right) \\
&\qquad\qquad + \left(b^2\sin^2(\theta) + A\right)\ln(A) - \left(b^2\sin^2\theta + \Lambda_y^2\right) - V''\ln\left(V''\right) \Bigg]
\end{aligned} \tag{4.46}$$

Integrating the first term in the square brackets [28] gives

$$\begin{aligned}
&\frac{1}{2(2\pi)^2}\int_0^{2\pi} \mathrm{d}\theta \left(b^2\sin^2\theta + A\right)\ln\left(\frac{b^2}{A}\sin^2(\theta)+1\right) \\
&\qquad = \frac{b^2}{2(2\pi)^2}\int_0^{2\pi} \mathrm{d}\theta\sin^2\theta\ln\left(\frac{b^2}{A}\sin^2\theta+1\right) \\
&\qquad\quad + \frac{A}{2(2\pi)^2}\int_0^{2\pi} \mathrm{d}\theta\ln\left(\frac{b^2}{A}\sin^2\theta+1\right) \\
&\qquad = \frac{b^2}{4\pi}\left[\ln\left(\frac{1+\sqrt{1+\frac{b^2}{A}}}{2}\right) - \frac{1}{2}\frac{1-\sqrt{1+\frac{b^2}{A}}}{1+\sqrt{1+\frac{b^2}{A}}}\right] \\
&\qquad\quad + \frac{A}{2\pi}\ln\left(\frac{1+\sqrt{1+\frac{b^2}{A}}}{2}\right)
\end{aligned} \tag{4.47}$$

The only θ dependence left in eq.(4.47) are terms of the form $\sin^2\theta$. So θ integration can be carried out with relative ease. The one-loop effective potential

reads,

$$
\begin{aligned}
V_{eff}(\phi) = V(\phi) + \frac{T}{8\pi}\Bigg\{ & A\ln(A) - \Lambda_y^2 + \frac{b^2}{2}\ln(A) - \frac{b^2}{2} \\
& +2b^2\left[\ln\left(\frac{1+\sqrt{1+\frac{b^2}{A}}}{2}\right) - \frac{1}{2}\frac{1-\sqrt{1+\frac{b^2}{A}}}{1+\sqrt{1+\frac{b^2}{A}}}\right] \\
& +4A\ln\left(\frac{1+\sqrt{1+\frac{b^2}{A}}}{2}\right) - V''\ln(V'')\Bigg\} \\
= V(\phi) + \frac{T}{8\pi}\Bigg\{ & \left(\frac{1}{2}\left(\Lambda_x^2+\Lambda_y^2\right)+V''\right)\ln\left(\Lambda_y^2+V''\right) - \frac{1}{2}\left(\Lambda_x^2+\Lambda_y^2\right) \\
& +4\left(\frac{1}{2}\left(\Lambda_x^2+\Lambda_y^2\right)+V''\right)\ln\left(\frac{1+\sqrt{1+\frac{\left(\Lambda_x^2-\Lambda_y^2\right)^2}{\left(\Lambda_y^2+V''\right)}}}{2}\right) \\
& -\left(\Lambda_x^2-\Lambda_y^2\right)\frac{1-\sqrt{1+\frac{\left(\Lambda_x^2-\Lambda_y^2\right)^2}{\left(\Lambda_y^2+V''\right)}}}{1+\sqrt{1+\frac{\left(\Lambda_x^2-\Lambda_y^2\right)^2}{\left(\Lambda_y^2+V''\right)}}} - V''\ln(V'')\Bigg\} \qquad (4.48)
\end{aligned}
$$

where the definitions for b and A have been substituted back in.

To keep consistent with the methodology presented in [13][14], a series expansion about V'' was performed to order $\mathcal{O}(V'')$. This simplification is possible since the conditions

$$\Lambda_x^2 \simeq \Lambda_y^2 \gg V'' \qquad (4.49)$$

are satified. Λ^2 terms are generally of order 10^2, whereas V'' is of order unity. Dealing with the result from this series expansion, drastically simplifies the renormalization procedure presented in the next section. With V'' as the small pa-

rameter, a series expansion yields,

$$\begin{aligned}
&\frac{T}{8\pi}\Bigg[\frac{1}{2}\left(\Lambda_x^2+\Lambda_y^2\right)\left(\ln\left(\Lambda_y^2\right)-1\right)\\
&\qquad+\frac{1}{\left(1+\sqrt{\frac{\Lambda_x^2}{\Lambda_y^2}}\right)}\Bigg(2\left(\Lambda_x^2+\Lambda_y^2\right)\left(1+\sqrt{\frac{\Lambda_x^2}{\Lambda_y^2}}\right)\ln\left(\frac{1+\sqrt{\frac{\Lambda_x^2}{\Lambda_y^2}}}{2}\right)\\
&\qquad\qquad-\left(\Lambda_x^2-\Lambda_y^2\right)\left(1-\sqrt{\frac{\Lambda_x^2}{\Lambda_y^2}}\right)\Bigg)\Bigg]\\
&+\frac{T}{8\pi}\Bigg[\frac{1}{2}\left(1+\frac{\Lambda_x^2}{\Lambda_y^2}\right)-\ln\left(\frac{V''}{\Lambda_y^2}\right)\\
&\qquad-\frac{\left(\Lambda_x+\Lambda_y\right)^2}{\left(\Lambda_y^2+\Lambda_x\Lambda_y\right)^2}\left(\Lambda_x^2-4\Lambda_y^2\ln\left(\frac{1+\sqrt{\frac{\Lambda_x^2}{\Lambda_y^2}}}{2}\right)-\Lambda_y^2\right)\Bigg]V''\\
&+\ldots
\end{aligned}\tag{4.50}$$

where the ... represent terms $\mathcal{O}(V''^2)$ and higher. Terms that are zeroth order in V'' were subtracted from the calculation. Therefore the one-loop effective potential reads

$$\begin{aligned}
V_{eff}(\phi)=V(\phi)+\frac{T}{8\pi}\Bigg[&\frac{1}{2}\left(1+\frac{\Lambda_x^2}{\Lambda_y^2}\right)-\ln\left(\frac{V''}{\Lambda_y^2}\right)\\
&-\frac{\left(\Lambda_x+\Lambda_y\right)^2}{\left(\Lambda_y^2+\Lambda_x\Lambda_y\right)^2}\left(\Lambda_x^2-4\Lambda_y^2\ln\left(\frac{1+\sqrt{\frac{\Lambda_x^2}{\Lambda_y^2}}}{2}\right)-\Lambda_y^2\right)\Bigg]V''(\phi)
\end{aligned}\tag{4.51}$$

At this point it was crucial that the isotropic effective potential, eq.(4.37), may be recovered. In the isotropic limit, $\Lambda_x=\Lambda_y\equiv\Lambda$. Implementing this equality in eq.(4.51), the argument of the second natural log term is unity. Therefore, in the isotropic limit

$$\begin{aligned}
V_{eff}(\phi)=V(\phi)+\frac{T}{8\pi}\Bigg[&\frac{1}{2}\left(1+1\right)-\ln\left(\frac{V''}{\Lambda^2}\right)\\
&-\frac{1}{\Lambda^2}\left(0\right)\Bigg]V''.
\end{aligned}\tag{4.52}$$

Comparison with eq.(4.37) shows that the isotropic one-loop effective potential has been reproduced exactly. This indicates that the anisotropic calculation was carried out in a correct and self-consistent way.

Fig.(4.3) shows the form of the one-loop counterterm in eq.(4.51). Each curve in the figure was produced by varying Δy from $\Delta x \leq \Delta y \leq 10\Delta x$ with Δx fixed. The $\times$'s indicate when $\Delta y = \Delta x$. The figure shows plots of the counterterm for the set of values, $\Delta x = 0.1, 0.2, 0.5, 1.0, 2.5, 5.0$. For each plot $V'' = 1$ and $T = 8\pi$. The bold line is the isotropic counterterm plotted for $0.1 \leq \Delta x \leq 5$. In the isotropic limit, the $\times$'s obtained from eq.(4.51) lie on this curve. This indicates the counterterm of eq.(4.51) is behaving self-consistently.

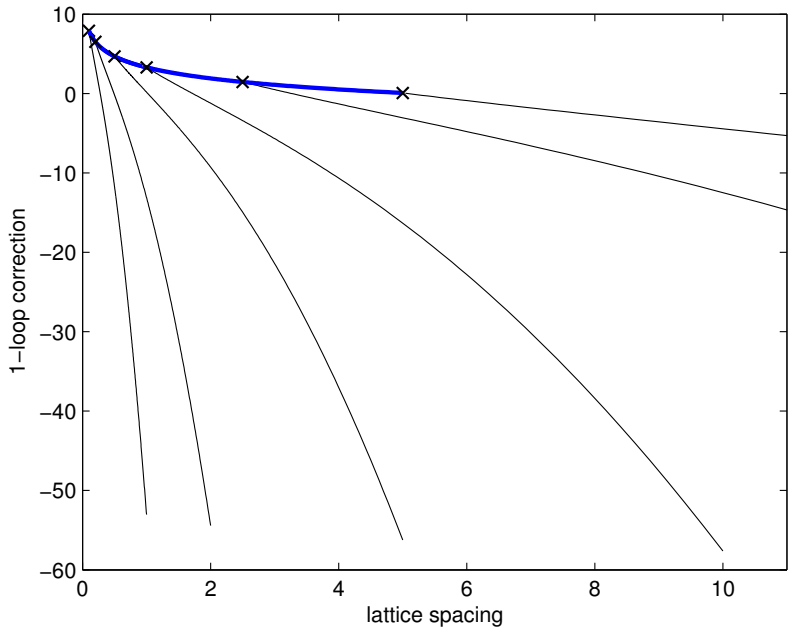

Figure 4.3: The one-loop counterterm of eq.(4.51). The bold line is the isotropic counterterm plotted for $0.1 \leq \Delta x \leq 5$. Each line branching of the isotropic curve represents values of the anisotropic counterterm.

4.3 Renormalization Counterterms

At this point, the form of $V(\phi)$ is specified to be the ϕ^4 model of eq.(2.4). Following the renormalization procedure of [14], a renormalization condition is imposed at some energy scale M

$$V_{eff}^{''}(\phi = \sqrt{M}) = V^{''}(\phi = \sqrt{M}) \tag{4.53}$$

The second derivative of eq.(4.51) with respect to ϕ gives

$$\begin{aligned} V_{eff}^{''}(\phi) = V^{''}(\phi) - \frac{T}{8\pi}\Bigg[V^{''''}\Bigg(\ln\left(\frac{V^{''}}{\Lambda_y^2}\right) + \frac{1}{2}\left(1 - \frac{\Lambda_x^2}{\Lambda_y^2}\right) \\ + \frac{(\Lambda_x + \Lambda_y)^2}{\left(\Lambda_y^2 + \Lambda_x\Lambda_y\right)^2}\left(\Lambda_x^2 - 4\Lambda_y^2 \ln\left(\frac{1+\sqrt{\frac{\Lambda_x^2}{\Lambda_y^2}}}{2}\right) - \Lambda_y^2\right)\Bigg) \\ + \frac{\left(V^{'''}\right)^2}{V^{''}}\Bigg]. \end{aligned} \tag{4.54}$$

To satisfy the renormalization condition, eq.(4.53), the following renormalized one-loop effective potential was constructed,

$$\begin{aligned} V_{eff}(\phi) = V(\phi) + \frac{T}{8\pi}\left[\frac{1}{2}\left(1 + \frac{\Lambda_x^2}{\Lambda_y^2}\right) - \ln\left(\frac{V^{''}}{\Lambda_y^2}\right) - C\right]V^{''} \\ + \frac{T}{16\pi}\left[V^{''''}\left(\ln\left(\frac{V^{''}}{\Lambda_y^2}\right) + \frac{1}{2}\left(1 - \frac{\Lambda_x^2}{\Lambda_y^2}\right) + C\right) + \frac{\left(V^{'''}\right)^2}{V^{''}}\right]\Bigg|_{\phi=\sqrt{M}}\phi^2, \end{aligned} \tag{4.55}$$

where

$$C = \frac{(\Lambda_x + \Lambda_y)^2}{\left(\Lambda_y^2 + \Lambda_x\Lambda_y\right)^2}\left(\Lambda_x^2 - 4\Lambda_y^2 \ln\left(\frac{1+\sqrt{\frac{\Lambda_x^2}{\Lambda_y^2}}}{2}\right) - \Lambda_y^2\right). \tag{4.56}$$

The term of order ϕ^2 has been added so that it's second derivative cancels with the excess terms in eq,(4.54) and hence the condition eq.(4.53) will be satisfied. The above effective potential of eq.(4.55) includes thermal fluctuations of order $\mathcal{O}(T)$ to the bare potential at some energy scale M. Note the Δx and Δy dependence of these fluctuations

For a scalar ϕ^4 field theory the lattice corrections to the mass shift will be of the form

$$V_{latt} = V_o + a\phi^2 \tag{4.57}$$

A renormalization point was conveniently chosen to be

$$\phi_{RN} = \sqrt{\frac{M^2 + m^2}{3\lambda}}. \tag{4.58}$$

such that

$$\begin{aligned} V_o^{''}(\phi_{RN}) &= M^2, \\ V_o^{'''}(\phi_{RN}) &= 2\sqrt{3\lambda\,(M^2 + m^2)}, \\ V_o^{''''}(\phi_{RN}) &= 6\lambda, \end{aligned}$$

The lattice potential of eq.(4.57) has the form.

$$V_{latt} = -\frac{m^2}{2}\phi^2 + \frac{\lambda}{4}\phi^4 + \frac{3T\lambda}{4\pi}\left[\ln\left(\frac{M}{\Lambda_y}\right) + \frac{1}{2}\left(1 - \frac{\Lambda_x^2}{\Lambda_y^2}\right) + C + \frac{M^2 + m^2}{M^2}\right]\phi^2, \tag{4.59}$$

or, with the rescaling prescription given in chapter 2,

$$V_{latt} = -\frac{1}{2}\phi^2 + \frac{1}{4}\phi^4 + \frac{3}{4\pi\beta}\left[\ln\left(\frac{M}{\Lambda_y}\right) + \frac{1}{2}\left(1 - \frac{\Lambda_x^2}{\Lambda_y^2}\right) + C + \frac{M^2 + 1}{M^2}\right]\phi^2, \tag{4.60}$$

This lattice potential, it is proposed, will cancel lattice spacing dependence in numerical simulations of the discrete system in chapter 2. In this study, we used $M = \sqrt{2}$ consistent with [14]. Testing of eq.(4.60) in chapter 6 showed results to be relatively independent of this choice.

Chapter 5

Lattice Simulations

In the previous two chapters, two methods were formulated for suppressing lattice spacing dependence in numerical simulations of the system presented in chapter 2). The result was two lattice potentials, eq.(3.92) and eq.(4.60), each claiming to correct for lattice spacing dependence. Given their apparent functional differences, one is lead to ask which is more valid. To answer this, a numerical study was carried out using Langevin simulations. The advantage of such simulations is that field configurations were readily available after each iteration making computation of statistical mechanical quantities possible. Such an analysis is not possible with Monte Carlo techniques.

It was crucial that accurate algorithms were used for the numerical testing. Before the results of the numerical study are presented, we discuss of some apsects of Langevin simulations that must be carefully considered. This chapter begins with an introduction to the phenomenological Langevin equation, a stochastic partial differential equation propagated using time-stepping procedures. In section 5.2 we present a discussion of time-step error and ways to render it subdominent in Langevin simulations. In section 5.3, the time-stepping method is presented. A higher-order scheme is opted for due to initially poor test results obtained by an Euler method. In section 5.4, the effects of truncation error are illustrated by comparing nucleation times obtained using the Euler method and a higher-order method. The procedure for extracting correlation lengths from

field configurations is introduced in section 5.5. In section 5.6, the results of the $(1+1)$-dimensional study presented in [12] are successfully reproduced.

5.1 The Phenomenological Langevin Equation

The Langevin equation is a continuum stochastic partial differential equation (SPDE). The use of a Langevin equation for the stochastic evolution of the field-system in chapter 2 is based purely on phenomenological grounds. The idea is to supplement the Euler-Lagrange equation of motion with noise and viscosity terms so that the system is driven to an equilibrium state. Noise and viscosity terms are usually related via a fluctuation-dissipation theorem.

Langevin equations borrow much of their inspiration from Langevin's treatment of the Brownian particle [29]. The Brownian particle is a device originally used by Einstein to describe apparent random motion in fluids. His suggestion was that while a particle suspended in a fluid experiences random kicks which will change its velocity, viscosity in the fluid decelerates the particle. This occurs repeatedly, so that the particle travels through the medium with short, random displacements.

Langevin later derived a mathematical description of the dynamics of this process. His approach was based on Newtonian mechanics, formulating the equation of motion for a Brownian particle subject to the potential, $V(x)$,

$$\begin{aligned} ma &= \sum_i F_i \\ m\frac{\mathrm{d}^2x(t)}{\mathrm{d}t^2} &= -\frac{\mathrm{d}V(x)}{\mathrm{d}x} - \eta\frac{\mathrm{d}x(t)}{\mathrm{d}t} + \xi(t) \end{aligned} \tag{5.1}$$

The viscous force term, $\eta\dot{x}$, acts to retard the particles motion and the random force term, $\xi(t)$, represents random kicks acting on the Brownian particle. The random kicks are independent on the position of the particle. Variations in its value are more rapid than the changes in $x(t)$. This nature of $\xi(t)$ is represented

by the relation,

$$\langle \xi(t)\xi(t') \rangle = 2\zeta kT\delta(t-t'), \tag{5.2}$$

where $\langle \dots \rangle$ is the statistical average and ζ is the spectral index of the fluctuation.

In the case of a scalar field theory, we begin with the Euler-Lagrange equation of motion,

$$\Box\phi = \frac{\partial^2\phi(\mathbf{x},t)}{\partial t^2} - \frac{\partial^2\phi(\mathbf{x},t)}{\partial \mathbf{x}^2} = -\frac{\delta V}{\delta\phi}. \tag{5.3}$$

with a Minkowskian metric. Introducing the supplementary terms made for the Brownian particle, gives the phenomenological Langevin equation

$$\frac{\partial^2\phi(\mathbf{x},t)}{\partial t^2} - \frac{\partial^2\phi(\mathbf{x},t)}{\partial \mathbf{x}^2} + \eta\frac{\partial\phi(\mathbf{x},t)}{\partial t} = -\frac{\delta}{\delta\phi}V[\phi] + \xi(\mathbf{x},t). \tag{5.4}$$

The random force term, $\xi(\mathbf{x},t)$, or noise term as it shall be called, represents the coupling of the field to a thermal bath. Notice that the noise term in eq.(5.4) is linear. This is referred to as additive noise. This is the simplest way to model thermal noise. However, there is no reason why noise shouldn't manifest itself nonlinearly in the phenomenological Langevin equation. Recent studies [30][31] into nonlinear noise terms in Langevin studies have been performed. Attempts to derive the nature of the noise term analytically have also been made [32].

The noise term, $\xi(\mathbf{x},t)$, and the viscosity coefficient, η, are related through the fluctuation-dissipation relation,

$$\langle \xi(\mathbf{x},t)\xi(\mathbf{x}',t') \rangle = 2\eta\beta^{-1}\delta(\mathbf{x}-\mathbf{x}')\delta(t-t'). \tag{5.5}$$

where β is as before. A thorough discussion of its origins can be found in [30]. The probability distribution of the noise is assumed to be Gaussian of the form,

$$\mathrm{d}\,P[\xi] = \frac{1}{\sqrt{4\pi\eta T}}D\xi\exp\left(-\frac{1}{2}\int \xi^2\frac{(\mathbf{x},t)}{2\eta T}\mathrm{d}\mathbf{x}\mathrm{d}t\right). \tag{5.6}$$

In principle, knowledge of the physical nature of the heat bath would enable one to calculate the value of η [32] [11]. However, as it was the final equilibrium field configuration that was of interest in this work, the viscosity coefficient, η, was arbitrarily set to unity.

Applying the dimensionless rescaling of chapter 2 to eq.(5.4) gives

$$(m^2a)\frac{\partial^2\tilde{\phi}(\tilde{\mathbf{x}},\tilde{t})}{\partial\tilde{t}^2} - (m^2a)\frac{\partial^2\tilde{\phi}(\tilde{\mathbf{x}},\tilde{t})}{\partial\tilde{\mathbf{x}}^2} + (m^2a)\tilde{\eta}\frac{\partial\tilde{\phi}(\tilde{\mathbf{x}},\tilde{t})}{\partial\tilde{t}} = -(m^2a)\frac{\delta}{\delta\tilde{\phi}}V[\tilde{\phi}] + (m^2a)\tilde{\xi}(\tilde{\mathbf{x}},\tilde{t}). \tag{5.7}$$

The definitions,

$$\tilde{\eta} = \frac{\eta}{m} \tag{5.8}$$

$$\tilde{\xi} = \frac{\sqrt{\lambda}}{m^3}\xi \tag{5.9}$$

have been made to keep the dimensions of each term consistent. Cancelling the (m^2a) factors and dropping the tildes gives the final form of the phenomenological Langevin equation used in this study.

$$\frac{\partial^2\phi(\mathbf{x},t)}{\partial t^2} - \frac{\partial^2\phi(\mathbf{x},t)}{\partial\mathbf{x}^2} + \eta\frac{\partial\phi(\mathbf{x},t)}{\partial t} = -\frac{\delta}{\delta\phi}V[\phi] + \xi(\mathbf{x},t). \tag{5.10}$$

The rescaled form of the fluctuation-dissipation relation is,

$$\langle\xi_{\mathbf{x},t}\xi_{\mathbf{x}',t'}\rangle = \frac{2\eta\beta^{-1}}{\Delta x\Delta y\Delta t}\delta_{\mathbf{x},\mathbf{x}'}\delta_{t,t'}, \tag{5.11}$$

where the lattice spacings and time-step have been inserted to compensate for the lack of dimensionality of the Kronecker deltas.

The lattice formulation of eq.(5.10) is

$$\frac{\partial^2\phi_{i,j}(t)}{\partial t^2} - (\nabla_{lat}\phi_{i,j}(t))^2 + \eta\frac{\partial\phi(\mathbf{x},t)}{\partial t} = -V'_{lat}(\phi_{i,j}(t)) + \xi_{i,j}(t). \tag{5.12}$$

where $(\nabla_{lat}\phi_{i,j}(t))^2$ is as defined in eq.(2.10) and $V'_{lat}(\phi_{i,j}(t))$ it first derivative of either eq.(2.1), eq.(3.92) or eq.(4.60) with respect to ϕ. The discrete form of the fluctuation-dissipation relation is,

$$\xi_{i,j}(t) = \sqrt{\frac{2\eta\beta^{-1}}{\Delta x\Delta y\Delta t}}G_{i,j}(t) \tag{5.13}$$

where $G_{i,j}(t)$ is Gaussian noise with unit divergence. A finite-difference approximation to the second-order time derivative is made in section 5.3. Note that a complication with $(\nabla_{lat}\phi_{i,j}(t))^2$ will arise for lattice sites situated on the boundary. To rectify this, the lattice is wrapped up in such a way that it forms a torus, as shown in fig.(5.1). With these toroidal boundary conditions, each lattice site has four neighbouring lattice sites required for $(\nabla_{lat}\phi_{i,j}(t))^2$.

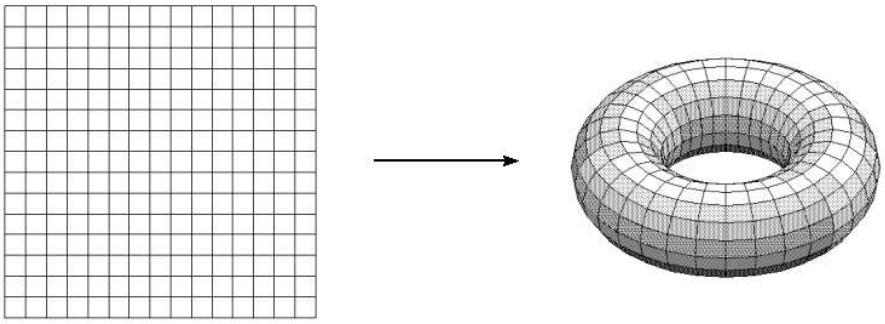

Figure 5.1: The toriodal boundary conditions used in this study.

Generally, accurate Langevin studies require large lattices with long running time. Large system sizes are necessary to get acceptable statistics at low temperatures and to avoid finite size effects. In the Langevin simulations performed in this study, the lattice size was set as large as possible, limited only by the hardware available.

5.2 Time Discretization Error

In the Langevin equation eq.(5.12), t corresponds to computer run-time. But the computer can only evolve the field in discrete time-steps, Δt. The lattice formulation presented in chapter 2 is then discretized in time as well as in space. So we can expect the discretized partition function as calculated in eq.(3.5) to contain both space and time discretization errors. To be confident with the Langevin simulation, it is important to understand the effects of time discretization. Leading order time-step dependence was calculated for the simplest stochastic propagation

scheme, the Euler method, in [12]. The Euler method propagates eq.(5.12) by updating $2MN$ quantities $\{\phi_{ij}(t), \pi_{ij}(t)\}$ where $i = 1, \ldots, M$ and $j = 1, \ldots, N$. The time-stepping algorithm is

$$\pi_{i,j}(t + \Delta t) = \pi_{i,j}(t) + \Delta t \left[\eta \pi_{i,j}(t) - \frac{\partial H_{lat}}{\partial \phi_{i,j}(t)}\right] + \xi_{i,j}(t) \tag{5.14}$$

$$\phi_{i,j}(t + \Delta t) = \phi_{i,j}(t) + \Delta t \pi_{i,j}(t + \Delta t), \tag{5.15}$$

where H_{lat} is the lattice Hamiltonian, eq.(2.9).

The probability density function associated with eq.(5.14) and eq.(5.15) is described by a discrete time differential equation known as the Fokker-Planck equation,

$$\begin{aligned} P[\pi, \phi, t + \Delta t] = \exp\left(-\Delta t \frac{\partial}{\partial \phi_{ij}} \frac{\partial H_{lat}}{\partial \pi_{ij}}\right) \times \\ \exp\left[\Delta t \frac{\partial}{\partial \pi_{ij}} \left(\eta \frac{\partial H_{lat}}{\partial \pi_{ij}} + \frac{\partial H_{lat}}{\partial \phi_{ij}}\right) + \Delta t \frac{\eta}{\beta} \frac{\partial^2}{\partial \pi_{ij}^2}\right] P[\pi, \phi, t] \end{aligned} \tag{5.16}$$

For brevity, indices will be dropped in what follows. The operators in the exponents of eq.(5.16) are non-commuting. A Campbell-Baker-Hausdorff expansion was used to combine the exponents. This gives the Fokker-Planck equation the convenient form,

$$P[\pi, \phi, t + \Delta t] = e^{-\Delta t H_{FP}} P[\pi, \phi, t], \tag{5.17}$$

where to first order in Δt,

$$\begin{aligned} H_{FP} = \frac{\eta}{\beta} \frac{\partial^2}{\partial \pi^2} - \frac{\partial}{\partial \phi} \frac{\partial H_{lat}}{\partial \pi} + \frac{\partial}{\partial \pi} \left(\eta \frac{\partial H_{lat}}{\partial \pi} + \frac{\partial H_{lat}}{\partial \phi}\right) \\ + \frac{1}{2} \Delta t \left[\eta \frac{\partial H_{lat}}{\partial \pi} + \frac{\eta}{\beta} \frac{\partial}{\partial \pi} + \frac{\partial H_{lat}}{\partial \phi}\right] \frac{\partial}{\partial \phi} \\ - \frac{1}{2} \Delta t \frac{\partial H_{lat}}{\partial \pi} \frac{\partial^2 H_{lat}}{\partial \phi^2} \frac{\partial}{\partial \pi} + \mathcal{O}(\Delta t^2). \end{aligned} \tag{5.18}$$

The solution of $H_{FP} P[\pi, \phi] = 0$ is the equilibrium canonical distribution approached by the discretized system. To zeroth order in momenta and first order in Δt,

$$P[\pi, \phi] = \exp\left(-\Delta x \Delta y \sum_i \sum_j \left[\beta(1 + \Delta t \frac{\eta}{2}) \frac{\pi_{ij}^2}{2} + \beta S(\phi_{ij}) - \Delta t \frac{\beta}{2} \pi_{ij} \frac{\partial S}{\partial \phi_{ij}}\right]\right). \tag{5.19}$$

The equilibrium density of configurations of our discretized Hamiltonian, eq.(2.9) is obtained by the Gaussian integration (see appendix B) over the momenta in eq.(5.19) giving,

$$P[\phi] = C\exp\left[-\beta\Delta x\sum_i \Delta y\sum_j\left\{S(\phi_{ij}) - \frac{\Delta t^2}{8}\left(\frac{\partial S}{\partial\phi_{ij}}\right)^2\right\}\right]. \tag{5.20}$$

The effect of the time discretization is explicitly shown. We see that the leading-order time-step dependence is $\mathcal{O}(\Delta t^2)$. By setting $\Delta t \ll \Delta x$, where Δx is the effective lattice spacing, time-step dependence can be rendered subdominant. In the simulations that follow, we used

$$\Delta t = 0.1\Delta x^2. \tag{5.21}$$

5.3 Time-stepping Methods

Using a higher-order time stepping method, rather than the lowest-order Euler method stated in the previous section, will have one main advantage. Truncation error that is introduced after each iteration of the time-step method will be considerably reduced. Truncation error acts as a form of unwanted noise in the simulation. This impairs the evolution of the field-system to thermal equilibrium, and is equivalent to raising the temperature of the system.

A Langevin simulation can be thought of as integrating a discrete approximation to a stochastic partial differential equation (the Langevin equation). To implicate a time-stepping method, finite-difference approximations to the time differential terms in eq.(5.12) are required. Consider the Taylor series expansion of the first derivative

$$\frac{\mathrm{d}\phi_{l+1}}{\mathrm{d}t} = \frac{\mathrm{d}\phi_l}{\mathrm{d}l} + \frac{\mathrm{d}^2\phi_l}{\mathrm{d}t^2}\Delta t + \cdots \tag{5.22}$$

where the subscripts l and $l+1$ denote the discrete time levels, and "..." represent terms higher order in Δt. Truncating the series to order $\mathcal{O}(\Delta t)$ and rearrranging for the second derivative gives

$$\frac{\partial^2\phi_l(\mathbf{x})}{\partial t^2} \simeq \frac{\frac{\partial\phi_{l+1}(\mathbf{x})}{\partial t} - \frac{\partial\phi_l(\mathbf{x})}{\partial t}}{\Delta t}. \tag{5.23}$$

such that the second order derivative is a finite difference approximation of the first derivative. This approximation is accurate with the small choice of Δt in eq.(5.21). Substitution of eq.(5.23) into the Langevin equation eq.(5.12) allows one to identify the update function,

$$\begin{aligned}\frac{\mathrm{d}\phi_{l+1}}{\mathrm{d}t} &= \frac{\mathrm{d}\phi_l}{\mathrm{d}t} + \Delta t\left[\eta\frac{\mathrm{d}\phi_l}{\mathrm{d}t} + (\nabla_{lat}\phi_l)^2 - V'_{latt}\right] + \xi_{i,j}(t) \\ &\equiv f(\phi_l, t)\end{aligned} \tag{5.24}$$

The general stepping procedure is the Taylor series expansion of ϕ_{l+1} about ϕ_l,

$$\phi_{t+1} = \phi_t + \frac{\mathrm{d}\phi_t}{\mathrm{d}t}\Delta t + \frac{\mathrm{d}^2\phi_t}{\mathrm{d}t^2}\frac{\Delta t^2}{2!} + \ldots \tag{5.25}$$

The Euler method truncates the Taylor series expansion to order $\mathcal{O}(\Delta t)$. With $\pi(t) \equiv \mathrm{d}\phi_l/\mathrm{d}t$ and eq.(5.24) the algorithm of eq.(5.14) and eq.(5.15) is produced. The Euler method is the only first-order method.

Higher-order time-steppng methods that include terms of order $\mathcal{O}(\Delta t^2)$ in eq.(5.25) are known as second-order Runge-Kutta methods. The general second-order Runge-Kutta stepping formula [33] is

$$\phi_{l+1} = \phi_l + c_1 k_1 + c_2 k_2 \tag{5.26}$$

where k_1 and k_2 are the Runge-Kutta "constants" of the form

$$k_1 = f(\phi_l, t_l)\Delta t \tag{5.27}$$

$$\begin{aligned}k_2 &= f(\phi_l + a_2 k_1(\phi_l, t_l), t_l + a_2\Delta t)\Delta t \\ &= f(\phi_l + a_2 f(\phi_l, t_l)\Delta t, t_l + a_2\Delta t)\Delta t,\end{aligned} \tag{5.28}$$

The constants c_1, c_2 and a_2 are to be determined. If k_2 is expanded as a Taylor series in two variables, giving

$$\begin{aligned}k_2 &= f(\phi_l + a_2 f(y_l, t_l)\Delta t, t_l + a_2\Delta t)\Delta t \\ &= \left[f(\phi_l, t_l) + f_\phi(\phi_l, t_l)a_2 f(\phi_l, t_l)\Delta t + f_t(\phi_l, t_l)a_2\Delta t\right]\Delta t + \mathcal{O}(\Delta t^3)\end{aligned} \tag{5.29}$$

Substituting eq.(5.27) and eq.(5.29) into eq.(5.26) gives

$$\begin{aligned}\phi_{l+1} &= \phi_l + c_1 f(\phi_l, t_l)\Delta t + c_2[f(\phi_l, t_l) + f_\phi(\phi_l, t_l)a_2 f(\phi_l, t_l)\Delta t \\ &\quad + f_t(\phi_l, t_l)a_2\Delta t]\Delta t + \mathcal{O}(\Delta t^3) \\ &= \phi_l + (c_1 + c_2)f(\phi_l, t_l)\Delta t + c_2[f_\phi(\phi_l, t_l)a_2 f(\phi_l, t_l) \\ &\quad + f_t(\phi_l, t_l)a_2]\Delta t^2 + \mathcal{O}(\Delta t^3) \end{aligned} \tag{5.30}$$

The stepping formula for ϕ_{l+1} has the form of a Taylor series, that is, it is a polynomial of increasing order. The Taylor series expansion of ϕ_{l+1} about ϕ_l of eq.(5.25) has the form,

$$\begin{aligned}\phi_{l+1} &= \phi_l + \frac{\mathrm{d}\phi_l}{\mathrm{d}t}\Delta t + \frac{\mathrm{d}^2\phi_l}{\mathrm{d}t^2}\frac{\Delta t^2}{2!} + \mathcal{O}(\Delta t^3) \\ &= \phi_l + f(\phi_l, t_l)\Delta t + \frac{\mathrm{d}f(\phi_l, t_l)}{\mathrm{d}t}\frac{\Delta t^2}{2!} + \mathcal{O}(\Delta t^3) \end{aligned} \tag{5.31}$$

where $d\phi_l/dt = f(\phi_l, t_l)$ has been inserted. By matching terms in eq.(5.30) and eq.(5.31), we can find information on the constants c_1, c_2 and a_2. To do so, we need $[df(\phi_l, t_l)/dt](\Delta t^2/2!)$ in eq.(5.31) in the form $f_\phi(\phi_l, t_l)a_2 f(\phi_l, t_l) + f_l(\phi_l, t_l)a_2$ in eq.(5.30). This is achieved by chain-rule differentiation giving

$$\begin{aligned}\frac{\mathrm{d}f(\phi_l, t_l)}{\mathrm{d}t} &= \frac{\mathrm{d}f(\phi_l, t_l)}{\mathrm{d}y}\frac{\mathrm{d}y_l}{\mathrm{d}t} + \frac{\mathrm{d}f(\phi_l, t_l)}{\mathrm{d}t} \\ &= f_\phi(\phi_l, t_l)f(\phi_l, t_l) + f_t(\phi_l, t_l). \end{aligned} \tag{5.32}$$

Substituting this into eq.(5.31) gives

$$\begin{aligned}\phi_{l+1} &= \phi_l + f(\phi_l, t_l)\Delta t + [f_\phi(\phi_l, t_l)f(\phi_l, t_l) \\ &\quad + f_t(\phi_l, t_l)a_2]\Delta t^2 + \mathcal{O}(\Delta t^3) \end{aligned} \tag{5.33}$$

By equating coefficients, we find

$$c_1 + c_2 = 1 \tag{5.34}$$

$$c_2 a_2 = \frac{1}{2} \tag{5.35}$$

Since this is a system of two equations involving three unknowns, we can chose one constant arbitrarily. Thus, there are actually an infinite number of second-order Runge-Kutta methods determined by this arbitrary choice.

One choice is to set $c_1 = c_2 = 1/2$ and $a_2 = 1$ giving the second-order Runge-Kutta method

$$\begin{aligned} \phi_{l+1} &= \phi_l + \frac{k_1 + k_2}{2} \\ k_1 &= f(\phi_l, t_l)\Delta t \\ k_2 &= f(\phi_l + f(\phi_l, t_l)\Delta t, t_l + \Delta t)\Delta t \end{aligned} \tag{5.36}$$

This is known as the modified Euler method or Heun method [34]. Note that the method uses an average of the derivative, $d\phi/dt$ at time levels l and $l+1$. The advantage of this stepping method over the Euler method is illustrated in fig.(5.2). From fig.(5.2), considering only the derivative at l can lead to a large

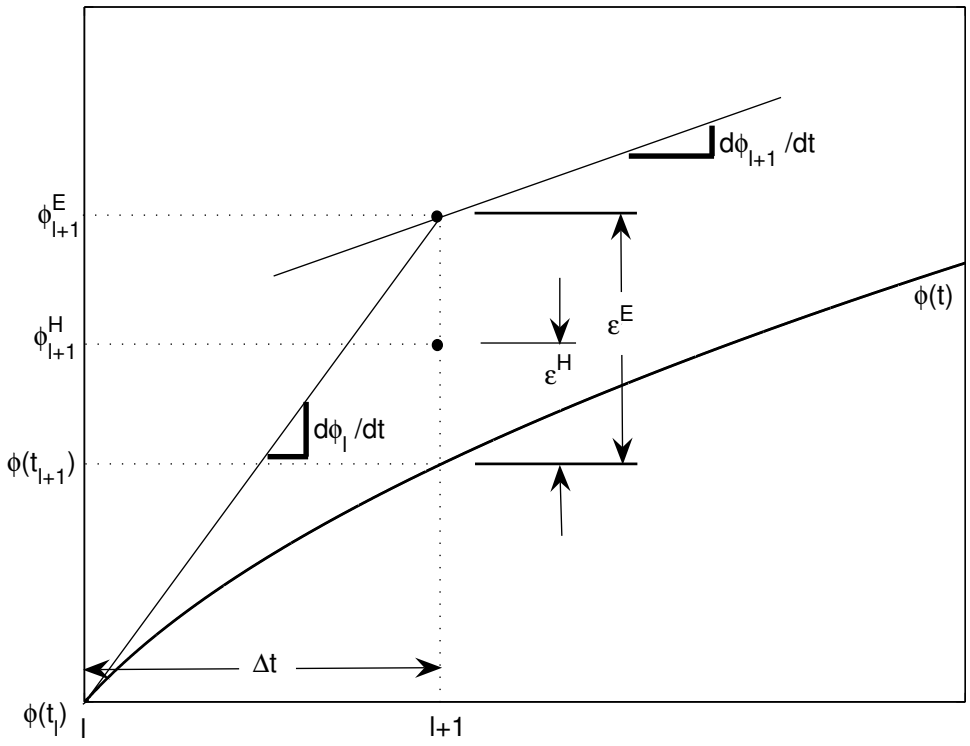

Figure 5.2: The modified Euler method or Heun method.

overshoot of the exact solution and thus, a large truncation error. However, the averaging of the derivatives at l and $l+1$, used in the Heun method, reduces this overshoot and therefore the truncation error.

In a more explicit form, the algorithm for the field-system of interest is

$$\phi_{i,j}(t+\Delta t) = \phi_{i,j}(t) + \frac{\Delta t}{2}\pi_{i,j}(t+\Delta t) + \frac{\Delta t}{2}\psi_{i,j}(t+\Delta t) \tag{5.37}$$

$$\pi_{i,j}(t+\Delta t) = \pi_{i,j}(t) + \Delta t\left[\eta\pi_{i,j}(t) + (\nabla_{lat}\phi_{i,j}(t))^2 - V'_{lat}(\phi_{i,j}(t))\right] + \xi_{i,j}(t) \tag{5.38}$$

$$\psi_{i,j}(t+\Delta t) = \psi_{i,j}(t) + \Delta t\left[\eta\psi_{i,j}(t) + (\nabla_{lat}\varphi_{i,j}(t))^2 - V'_{lat}(\varphi_{i,j}(t))\right] + \xi_{i,j}(t) \tag{5.39}$$

where

$$\varphi_{i,j}(t) = \phi_{i,j}(t) + \Delta t\left[\pi_{i,j}(t) + \Delta t\left[\eta\pi_{i,j}(t) + (\nabla_{lat}\phi_{i,j}(t))^2 - V'_{lat}(\phi_{i,j}(t))\right] + \xi_{i,j}(t)\right] \tag{5.40}$$

is a temporary update for the field. The term, $(\nabla_{lat}\varphi_{i,j}(t))^2$, involves twelve neighbouring field values in its calculations (see fig.(5.3)). Consequently, the algorithm is slower than the Euler method of eq.(5.14) and eq.(5.15). It is also more memory intensive as $3MN$ quantities, $\{\phi_{i,j}(t), \pi_{i,j}(t), \psi_{i,j}(t)\}$, need to be updated for each iteration. Using the second-order Runge-Kutta method, one suffers roughly a factor of two increase in computation run-time and a 33% decrease in lattice size. The advantage is that its accuracy is to order $\mathcal{O}(\Delta t^2)$ meaning the dominant truncation errors are of order $\mathcal{O}(\Delta t^3)$. Therefore, with the small choice for Δt made in eq.(5.21), such errors are of similar magnitude to the round-off error, and hence negligible. To initialize the simulation, the usual procedure is to scatter Gaussian distributed random values for $\phi_{i,j}(t)$, $\pi_{i,j}(t)$ and $\psi_{i,j}(t)$ across the lattice. This procedure was adopted in Langevin simulations performed in this study.

5.4 Decay Times of Metastable States

To illustrate the importance of truncation error, both the Euler method and the second-order modified Euler method were used to generate decay times of

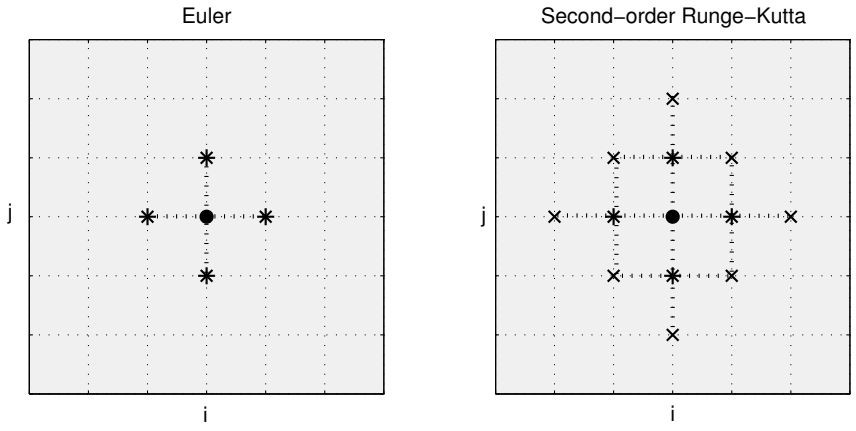

Figure 5.3: Field values involved in the update to the field value at each lattice site. • is the lattice site being updated. The other markers indicate the field values that go into the update at each site i, j.

metastable states. Decay times were extracted from lattice simulations of a (1+1)-dimensional scalar ϕ^4-theory with an asymmetry term in the potential,

$$V(\phi) = \frac{m^2}{2}\phi^2 - \frac{\alpha}{3}\phi^3 + \frac{\lambda}{4}\phi^4 \tag{5.41}$$

The asymmetry term in eq.(5.41) has the effect of making one of the minima in the double-well potential metastable, as shown in fig.(5.4).

To commence the simulation, Gaussian distributed random field values were scattered in a quartic potential until an initial correlation in field value was achieved. This procedure, known as quenching, seems a more natural way to study metastable decay [30]. The duration of the quenching period was set as the longest nucleation time that occurs in a sample of 5000 nucleation times obtained from initially uncorrelated simulations. The quenched potential is simply eq.(5.41) with $\alpha = 0$, giving it the form of a single-well potential (the dashed-dotted curve in fig.(5.4)).

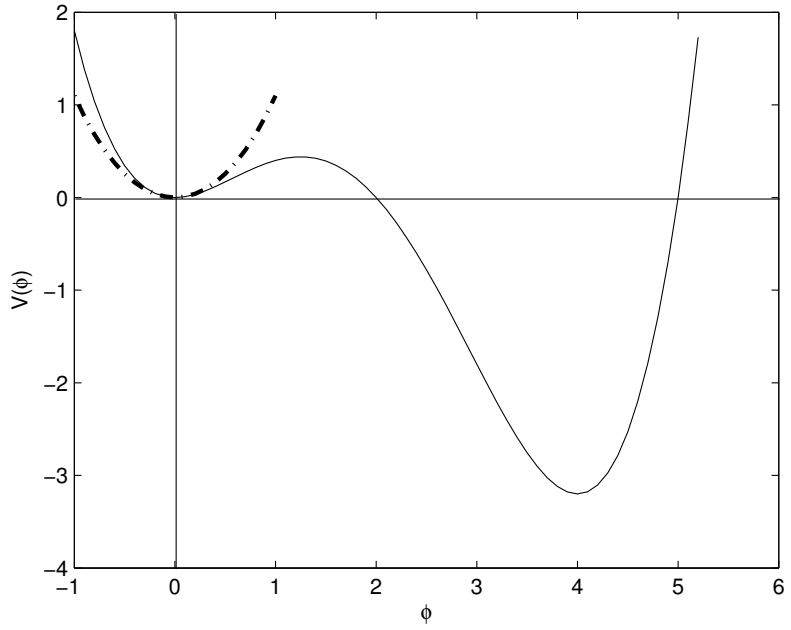

Figure 5.4: The asymmetric potential (full curve) and the quenched potential (dashed-dotted curve).

After scaling out the mass term, m, we arbitrarily set $\eta = 1.0$, $\alpha = 0.7$, $\lambda = 0.1$, $\Delta x = 0.5$. The time-step Δt was determined from eq.(5.21). Using small lattice sizes of $M = 500$, simulations ran until the nucleation of critical-sized "bubbles" formed in the lower-energy minimum. To determine this critical size for bubbles, a catagorizing exercise was carried out. All bubbles that nucleated in the simulation were recorded and their subsequent expansion or annihilation observed. After categorizing 500 critical bubbles, the average size at which bubbles became critical was ~ 12 contiguous lattice sites. Once a bubble reached this critical size the time was recorded.

Samples of 5000 nucleation times were obtained for each value of temperature. A histogram plot of these nucleation times gave a waiting-time distribution, as shown in fig.(5.5). By fitting the distribution with the waiting-time form,

$$\frac{\mathrm{d}N(t)}{\mathrm{d}t}\delta t = K\left(\frac{t}{\tau}\right)^a \exp\left(-\frac{t}{\tau}\right), \tag{5.42}$$

where δt is the bin size of the histogram, The parameter, τ, is identified as the

decay time, a is a fit parameter, and K is a normalization factor.

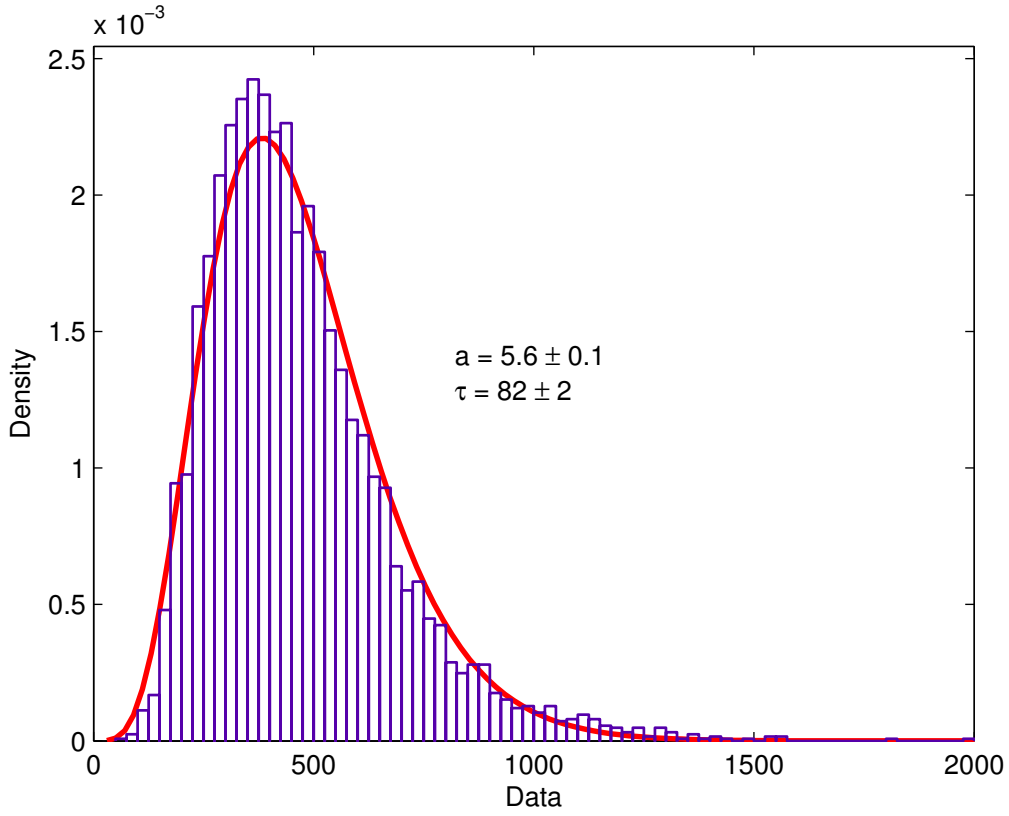

Figure 5.5: The waiting time fit to a distribution of 5000 nucleation times.

The decay rate per unit length [35], in the semi-classical approximation, is given by

$$\Gamma = A \exp\left(-\frac{S_E}{T}\right) \tag{5.43}$$

where S_E is the Euclidean action corresponding to the "bounce solution" to the equation of motion. The prefactor A contains quantum corrections which are discussed in [36]. A simple manipulation puts eq.(5.43) in a straight line form

$$\begin{aligned} \ln\tau &= \ln(\Gamma L)^{-1} \\ &= -\ln(AL) + \frac{S_E}{T} \end{aligned} \tag{5.44}$$

Plots of $\ln \tau$ vs. β are shown in fig.(5.6). Decay times were extracted for a range of temperatures, then the straight line form of eq.(5.44) was fitted. Fig.(5.6) shows the decay times extracted using the Euler ($\Box$'s) and modified Euler ($\diamondsuit$'s) time-stepping methods. The same parameters were used for both methods. The result that Euler decay times are earlier can be attributed to larger truncation error which is effectively the same as having a higher temperature. At higher temperatures, decay of the metastable state is more rapid (as can be inferred from fig.(5.6)).

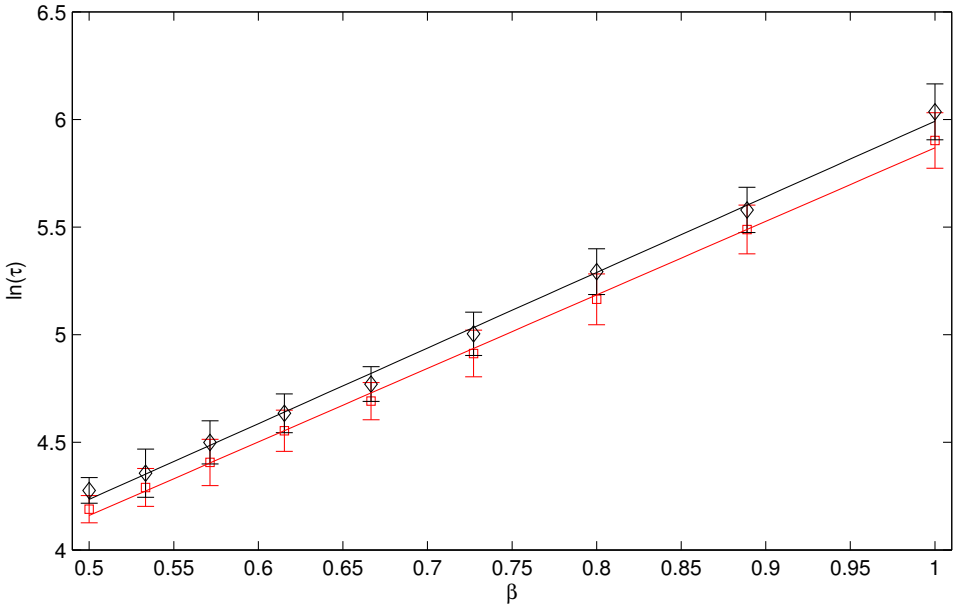

Figure 5.6: Plot of $\ln(\tau)$ vs. β. $\Box$'s and $\diamondsuit$'s represent decay times extracted from simulations using Euler and Modified Euler time stepping methods, respectively.

5.5 Extracting Correlation Lengths

A quantity that will be studied numerically in the following section and in the following chapter is the correlation length. The correlation length is a measure of the range over which fluctuations in one region of space influence (or, are

correlated with) those in another region. Two points which are separated by a distance larger than the correlation length will each have fluctuations which are relatively independent, that is, uncorrelated. Clearly, the correlation length is dependent on both the temperature of the system and the coupling strengths between neighbouring lattice sites.

To extract a correlation length, λ_∞, from numerically determined field configurations, one must determine the two-point correlation function,

$$c(i\Delta x) = \langle \phi(i)\phi(i+\Delta i)\rangle. \tag{5.45}$$

This is a simple average of the product of two field values seperated by a distance, x. The correlation length is $\lambda_\infty = \lim_{x\to\infty} \lambda(x)$, where

$$\lambda(x) = \Delta x \left(\log \left(\frac{c(x)}{c(x+\Delta x)} \right) \right)^{-1} \tag{5.46}$$

In computational practice, a finite lattice is used and therefore λ_∞ cannot be determined exactly. The extraction is further complicated by the fact that at large x the data set size decreases, compromising the calculation of $\lambda(x)$. The procedure used in [12] was to plot $\lambda(x)$ versus x and look for a "plateau" at intermediate values of x. The same procedure was used in this numerical study.

It is important that simulations are allowed to run until thermal equilibrium is reached. At thermal equilibrium, the field configuration consists of critical sized regions of the field in either of the minima, ϕ_1 or ϕ_2. These structures are termed kink/antikink pairs. Thermal equilibrium is satisfied when the equilibrium kink/antikink density across the field configuration is obtained. While fluctuations from the thermal bath are still present in the system, this fluctuation energy and the elastic energy between lattice sites is balanced in such a way that the mean-field value across the lattice is zero. The kink/antikink density is achieved only if the lattice size (i.e. the statistical data set) is large enough.

To identify thermal equilibrium in Langevin simulations, the algorithm was instructed to check the mean-field value after ever iteration. The mean-field

value is simply the ensemble average of the field over the lattice. With the initial conditions stated previously, the mean-field begins with a value of -1 and reaches a value of zero after long evolution times. These times are of the order $10^5 - 10^6$ iterations, depending on the temperature value used. The progression to equilibrium is illustrated in the first frame of fig.(5.7). It shows probability distributions for succesively later times (indicated by lighter shades of gray). The second frame is simply the first frame "flipped" over to illustrate the behaviour of the distribution in the ϕ_2 minimum. This behaviour is obscurred in the first frame by the plot of final probability distribution. The symmetric form of this final distribution indicates that thermal equilibrium has been reached.

To eliminate the effect of thermal noise and phonons (which are still present at equilibrium) on the results, a time-averaging scheme was employed. Values for $\lambda(x)$ were calculated for 500 different equilibrium field configurations then averaged. Generating 500 equilibrium field configurations was a simple matter of evolving 1 such configuration for 500 iterations.

5.6 Controlled One-dimensional Lattice Simulations

As mentioned earlier, methods to control lattice dependence in lattice simulations of (1+1)-dimensional scalar field theories have been thoroughly tested [12]. In this section, the results of [12] are reproduced. The purpose of this exercise was to verify their results, and also, to serve as calibration of the numerical method presented previously in this chapter.

Trullinger and Sasaki [17], and independently Croiteru et.al.[37] applied a TIO method to order $\mathcal{O}(\Delta x^2)$ to obtain the Schrödinger-type equation

$$\left[-\frac{1}{2\beta^2}\frac{\partial^2}{\partial\phi^2} + V(\phi) - \frac{\Delta x^2}{24}\left(\frac{\partial V}{\partial\phi}\right)^2\right]\Psi_n = \epsilon_n\Psi_n. \tag{5.47}$$

From this work, the lattice potential,

$$V_{\text{latt}} = V + \frac{\Delta x^2}{24}\left(\frac{\partial V}{\partial\phi}\right)^2 \tag{5.48}$$

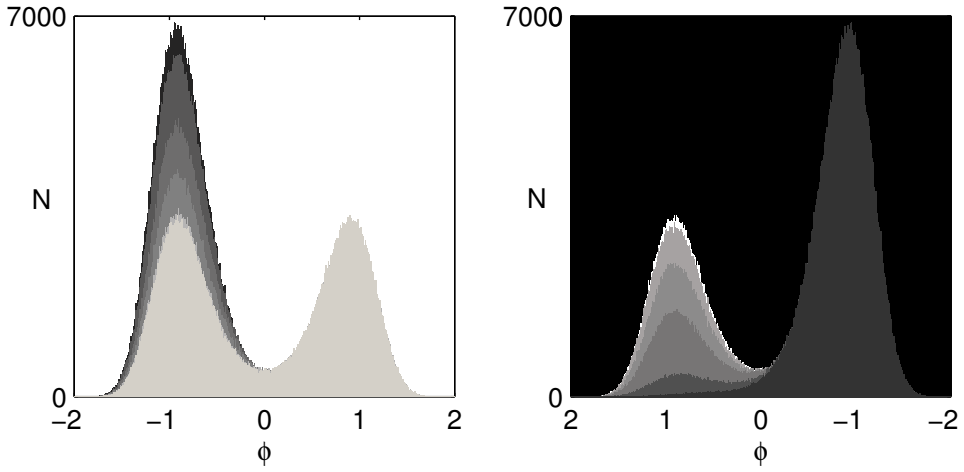

Figure 5.7: Identification of thermal equilibrium. The two figures show the progression of the probability distribution function with time. The figure on the right is the reverse of the figure on the left. The darker distributions were obtained at earlier times than the lighter distributions.

was proposed in [12] such that any lattice dependence is predominantly of order $\mathcal{O}(\Delta x^4)$.

Gleiser and Müller [38] studied the effectiveness of one-loop renormalization counterterms in the one-dimensional case. One-loop momentum integrals in (1+1)-dimensional scalar field theories are relatively straightforward to evaluate. The integral in the continuous case is not ultraviolet divergent i.e. no ultra-violet cutoffs are required to regularize the integral as shown in appendix C. That is not the case for the corresponding discretized theory as an ultraviolet cutoff is inherant with the lattice. The integral with the ultraviolet cutoff is also calculated

in appendix C. With the cutoff, $\Lambda = \pi/\Delta x$, one finds

$$V_{eff} = V + \frac{T}{4}\sqrt{V''} - \frac{T}{4\pi}\frac{V''}{\Lambda} + \mathcal{O}\left(\frac{V''^2}{\Lambda^4}\right) \tag{5.49}$$

The renormalization condition is then imposed at some energy scale M, such that

$$V''_{eff}(\phi = \sqrt{M}) = V''(\phi = \sqrt{M}) \tag{5.50}$$

To impose the condition at this energy level, it is necessary to add counterterms to V_{eff} of the form

$$V_{ct} = \frac{T}{4\pi}\frac{V''}{\Lambda}. \tag{5.51}$$

The lattice potential formulated in [38] is,

$$V_{latt} = V(\phi) + \frac{T\Delta x}{4\pi^2}V''(\phi). \tag{5.52}$$

which is intended to eliminate Δx dependence to one-loop order in T.

To determine which counterterm is more effective, correlation lengths were extracted from their respective simulations and compared. A low-temperature exact value for the correlation length was obtained using a kink-gas phenomenology briefly outlined in appendix D. At low temperatures λ is defined as

$$\lambda = \frac{1}{\beta(\epsilon_{0,a} - \epsilon_{0,s})} = \frac{1}{2\beta t_o}. \tag{5.53}$$

The evaluation of this, using semiclassical methods, is included in appendix D. For $\beta = 5$, the kink-gas phenomenology gave the value $\lambda = 17.81$.

Correlation lengths were extracted from field configurations on a lattice of size $M = 8 \times 10^5$. A segment of the field configuration at thermal equilibrium is shown in fig.(5.8). One-dimensional kink/antikink pairs are clearly present. Fig.(5.9) shows plots $\lambda(x)$ versus x obtained using the modified Euler method outlined previously. The •'s are results obtained from a simulation using the bare potential. The ∘'s are from a simulation using the potential eq.(5.48), and the ■'s from a simulation using eq.(5.52). Our results agree with those presented in [12]. The TIO method agrees well with the exact kink-gas value (the dashed line). The

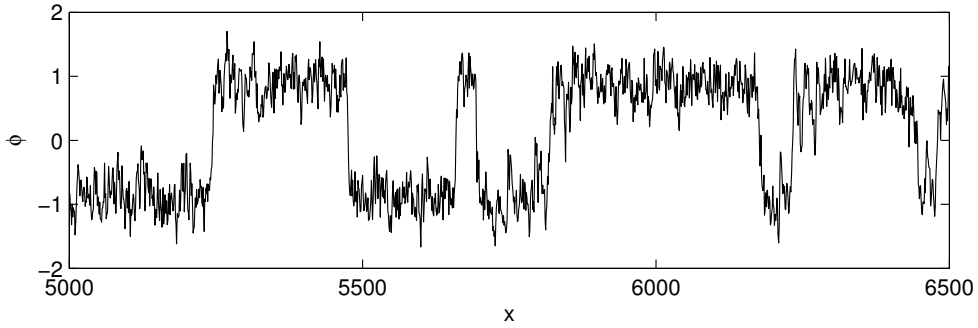

Figure 5.8: A snapshot of the 1D scalar field over a small segment of the lattice.

one-loop renormalization method calculates a correlation length further from the kink-gas value than one gets if no attempt to control lattice dependence is made.

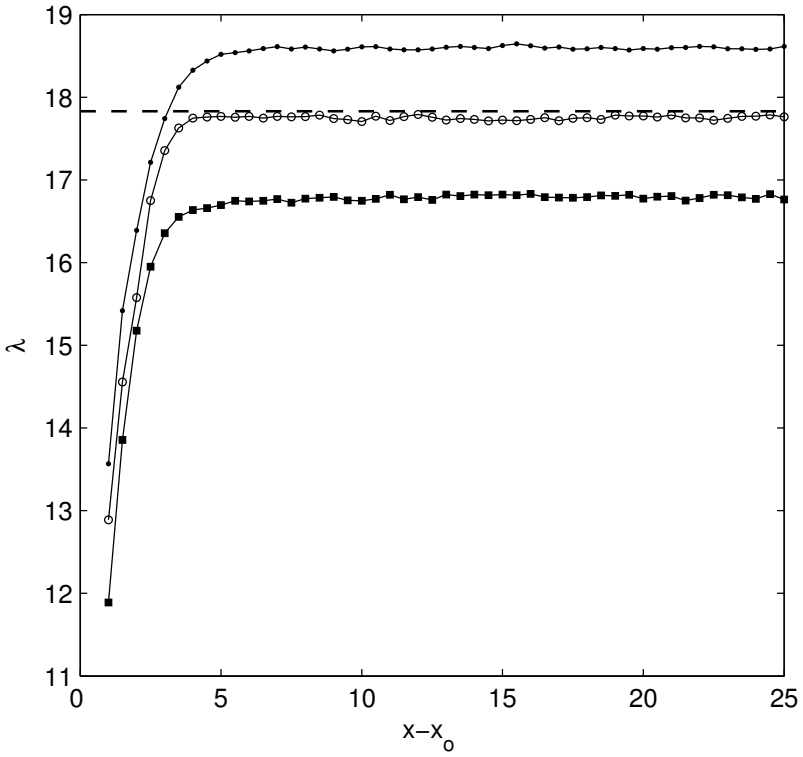

Figure 5.9: Calculations of the correlation length for varying values of the two-point seperation distance.

Chapter 6

Results and Discussion

In the previous chapter, an accurate numerical method was developed. Subsequent testing was successful, and therefore permitted a level of confidence in its precision. This was a crucial step if conclusions are to be drawn from the results presented in this chapter. Here, the results of applying the effective potentials, eq.(3.92) and eq.(4.60), to ϕ^4 model are presented and discussed. Note that all field dynamics discussed in this chapter are in the context of the ϕ^4 model.

First, a discussion is given on the application of Ising methods to the ϕ^4 system. The intention of this exercise was to obtain an exact correlation length to use as a benchmark for extracted values, in the same way the kink-gas phenomenology (see appendix D) was used in the one-dimensional study. These Ising methods are applicable only at the low temperatures identified in section 6.2. Two-dimensional kink solutions with rotational symmetry have been found, and are reported on in [3]. However, to our knowledge, an equivalent two-dimensional kink-gas phenomenology to that presented in appendix D does not exist.

The next step was to identify the level of anisotropy that would produce the dynamics required for the validity of the mean field approximation. The choice of values for lattice spacing also had to be considered carefully. Obviously, using fine lattice spacings would result in a high resolution study. In contrast, coarse lattice spacings would result in a lattice with a large physical area. With a lattice consisting 800×800 points, a balance between accuracy versus physical size had

to be determined.

With the optimal set of parameters identified, attempts to extract correlation lengths are presented section 6.3. Initially, poor results were obtained. This prompted an investigation into alternative computational methods in order to get the most out of the computing hardware available. With insufficient accuracy in the extracted correlation length values, the initial behaviour of the ensemble field average value was studied. This study yielded results from which conclusions could be made.

6.1 Ising Methods

The anisotropic $(2+1)$-dimensional ϕ^4 field theory may be thought of as a system of N linear anharmonic oscillators coupled by springs. In this section, an equivalent Ising model formulation of this system [15][39] is discussed in which chain states are represented by the presence (or absence) of a fermion. Modeling the lattice system of chapter 2 with a spin-1/2 Ising system might seem a drastic oversimplification. Appropriate parameter restrictions, in which this method becomes valid, are discussed in detail in the next section.

As with the one-dimensional kink-gas phenomenology, the Ising treatment assumes an equilibrium consisting of only the two lowest eigenstates. The Hamiltonian of the Schrödinger-type equation in eq.(3.88) is diagonalized in the truncated basis of states, $\{|0,a\rangle, |0,s\rangle\}$ where the a and s labels are for the minimums at ϕ_1 and ϕ_2, respectively. The two lowest energy eigenstates are nearly degenerate, split only by tunneling between the two wells. Bishop and Krumhansl [23] have investigated the validity of the two state basis in detail by numerically

determining the expectation values,

$$\begin{aligned}\langle 0,a|\phi^2|0,a\rangle &= \langle 0,a|\phi^2|0,s\rangle + \mathcal{O}\left(\langle 0,a|\phi^2|1,a\rangle\right)\\ \langle 0,s|\phi^2|0,s\rangle &= \langle 0,a|\phi^2|0,s\rangle + \mathcal{O}\left(\langle 0,s|\phi^2|1,s\rangle\right).\end{aligned} \tag{6.1}$$

If the two-state basis was complete, the two quantities above should equal $\langle 0,a|\phi^2|0,s\rangle$ exactly. It was shown in [23] that below some critical temperature the two lowest eigenvalues of the coupled oscillators are close together, and all other eigenvalues are much larger. In this regime, the two lowest eigenstates lie well below the potential barrier. A simple method for identifying this regime in simulations is discussed in the next section.

The two-state basis, in effect, restricts each of the N oscillators to be *entirely* within one of the two lowest states. This calls to mind the level of anisotropy required by the mean-field approximation in chapter 3. Recall that it was necessary to have order-disorder patterns in the weak-coupling direction and displacive patterns in the strong-coupling direction. A chain displaying displacive patterns would occupy a ground-state given the temperature was low enough. Thus, Ising methods are applicable in the parameter range required by the mean field approximation with added condition of the system being at a low temperature. Parameter choices are discussed further in the next section.

With each oscillator restricted to its two lowest eigenstates, (given a lower enough temperature and high enough anisotropy), they may be represented by the presence or absence of a fermion. Fermion creation and annihilation operators acting on the ith chain are denoted by follows, $c_i^\dagger$ and c_i. Scalapino and Stoeckly in [39][40], constructed an effective Hamiltonian which has all the same matrix elements as the original Hamiltonian eq.(3.88) in the truncated basis,

$$\mathrm{H}_{eff} = \sum_{i=1}^{M}\{\epsilon c_i^\dagger c_i + \Delta[1-(c_i^\dagger - c_i)(c_{i+1}^\dagger + c_{i+1})]\}. \tag{6.2}$$

ϵ is the tunnel splitting between the two eigenstates and Δ is given by,

$$\Delta = \frac{2\beta}{\Delta y^2}|\langle 1|\varphi|0\rangle|^2 = \frac{2\beta}{\Delta y^2}\langle 0|\varphi^2|0\rangle, \tag{6.3}$$

Implementing periodic boundary conditions required some care. Because the commuting quantities $(\varphi_i, \varphi_{i+1})$ are replaced by the anti-commuting operators $(c_i, c_i^\dagger)$, minus signs require careful attention. The operators, $c_{M+1}^\dagger$ and c_M, are defined

$$c_{M+1} = (-1)^{1+\sum_i^M n_i} c_1, \tag{6.4}$$

and

$$c_{M+1}^\dagger = (-1)^{1+\sum_i^M n_i} c_1^\dagger, \tag{6.5}$$

Thus, the Hamiltonian has two different forms. H^{even}, which acts on an even number of particles; the other H^{odd} acting on states with an odd number of particles.

Fourier transformation of the operators gives,

$$b_k = \frac{e^{\mathrm{i}\pi/4}}{M}\sum_i^M e^{-\mathrm{i}ki} c_i \tag{6.6}$$

and,

$$b_k^\dagger = \frac{e^{-\mathrm{i}\pi/4}}{M}\sum_i^M e^{\mathrm{i}ki} c_i^\dagger \tag{6.7}$$

The exponetial factors, $e^{\pm\mathrm{i}\pi/4}$, have been introduced to keep coefficients in the Hamiltonian real. Allowed k values for states with an even number of particle states are,

$$k = \pm\frac{\pi}{M}, \pm\frac{3\pi}{M}, \ldots, \pm\frac{(M-1)\pi}{M}, \tag{6.8}$$

Likewise, for states consisting of an odd number of particles

$$k = 0, \pm\frac{2\pi}{M}, \pm\frac{4\pi}{M}, \ldots, \pm\frac{(M-2)\pi}{M}, \pi. \tag{6.9}$$

The even and odd Hamiltonians are given by,

$$\begin{aligned} H^{even} = \sum_{k>0}[&(\epsilon - 2\Delta\cos k)(b_k^\dagger b_k + b_{-k}^\dagger b_{-k}) \\ &+2\Delta + 2\Delta\cos k + 2\Delta\sin k(b_k^\dagger b_{-k}^\dagger - b_k b_{-k})] \end{aligned} \tag{6.10}$$

to act on states with an even number of particles, and

$$\begin{aligned} H^{odd} = &(\epsilon - 2\Delta) b_o^\dagger b_o + 2\Delta + (\epsilon + 2\Delta) b_\pi^\dagger b_\pi \\ &+ \sum_{0<k<\pi} [(\epsilon - 2\Delta\cos k)(b_k^\dagger b_k + b_{-k}^\dagger b_{-k}) \\ &\qquad +2\Delta + 2\Delta\cos k + 2\Delta \sin k (b_k^\dagger b_{-k}^\dagger - b_k b_{-k})] \end{aligned} \tag{6.11}$$

to act on states with an odd number of particles. The Hamiltonians diagonalize for each $(k, -k)$ subspace. The energy of the system is the sum of the energies of each subspace,

$$E^{even} = \sum_k \epsilon(k). \tag{6.12}$$

When all the contributions have been worked out the result is

$$E^{even} = ME_o + \frac{M}{2}\epsilon + M\Delta - \frac{M}{\pi}(\epsilon + 2\Delta) \int_0^{\frac{\pi}{2}} \mathrm{d}y \left(1 - \frac{8\epsilon\Delta}{(\epsilon + 2\Delta)^2} \sin^2 y\right)^{\frac{1}{2}} \tag{6.13}$$

where E_o is the ground-state energy of the single oscillator.

$$E^{odd} = E^{even} + \epsilon - 2\Delta \tag{6.14}$$

The solution of the Hamiltonian is well documented in literature. It follows closely the solution of Shultz, Mattis and Lieb [41] for the two-dimensional Ising model.

The solution outlined above was used in [16] and [42] to determine various thermodynamic quantities including the spin correlation functions. Correlation lengths were also obtained for spin couplings in both the strong and weak directions. In the study presented in section 6.3, only the weak coupling ($\hat{y}$-directional) correlation length was calculated from simulations. For the correlation length in the weakly coupled direction one finds [16]

$$\lambda_y = \frac{1}{2}\Delta y e^{\left(\frac{2\beta}{\Delta y^2}\right)}. \tag{6.15}$$

We expect this expression to have a medium level of precision, given the parameter restrictions are satisfied.

6.2 Identifying Parameter Ranges

The temperature regime for which the two-state basis is applicable was determined by studying kink behaviour. With the field initially situated at the minimum, ϕ_1, kink formation corresponds to barrier-crossings of the field. However, at higher temperatures there are also barrier crossings due to thermal noise i.e. nonlinear phonons. At intermediate temperatures, kinks still exist. However, mixing with higher states is significant. The Ising approximation undoubtedly fails at this temperature. Kinks are expected to vanish at temperatures where the ground state energy is higher than the barrier at ϕ_m. Characteristic probability distribution functions (PDF's) for the these three temperature regimes are plotted in fig.(6.1).

For temperatures which satisfy the Ising approximation, the simulated field rests in the vicinity of the minimum ϕ_1 for a very long time. The field will continue to thermalize about this minimum until large enough fluctuations drive a potion of the field over the barrier situated at, ϕ_m. This marks the formation of the first kink-antikink pair. Thermal equilibrium is reached when the equilibrium kink-antikink density is obtained. In terms of the field configuration, one looks for a mean field value, $\langle\phi\rangle$, close to ϕ_m with a standard deviation close to $|\phi_1| = |\phi_2| = 1$. From fig.(6.1), the PDF obtained for $\beta = 6$ satisfies these requirements. Lower temperatures could be used, however this would mean slower lattice dynamics. As a consequence, longer evolution times would be required to reach thermal equilibrium.

Once β was set, it was straightfoward to determine the level of anisotropy required by the mean-field and Ising approximations. It was a simple matter of fixing one lattice spacing (chosen to be Δx) while varying the other spacing (Δy). The equilibrium field configuration was then observed. One looked for coherance within each "chain" along the $\hat{x}$-direction and order-disorder in the $\hat{y}$-direction. The plots below illustrate the equilibrium field configuration obtained

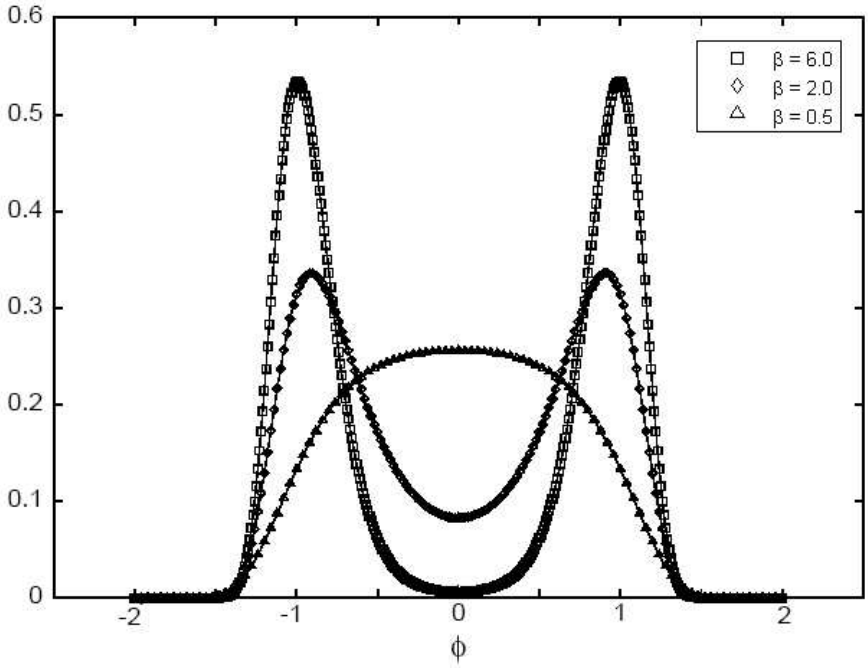

Figure 6.1: PDF's obtained from equilibrium field configurations for three different values of β.

using varying amounts of anisotropy. The first snapshot corresponds to the isotropic case where the coupling ratio, $\Delta x^{-2} : \Delta y^{-2}$, is $1 : 1$. As expected, kinks with rotational symmetry are observed. As the coupling ratio is increased, the kink form begins to show directional dependence. When the ratio reaches a value between 16 and 100, the desired dynamics are obtained. After further investigation, the value $\Delta y^2/\Delta x^2 \sim 25$ was identified. Larger anisotropies require a larger difference in lattice spacing. So, a study of lattice spacing dependence using a coupling ratio of 100 could be affected by the extreme lattice spacing values involved. For this reason, we chose a coupling ratio of 25 to obtain the results that follow. The limits on the choice of lattice spacing values will be discussed further in the following section.

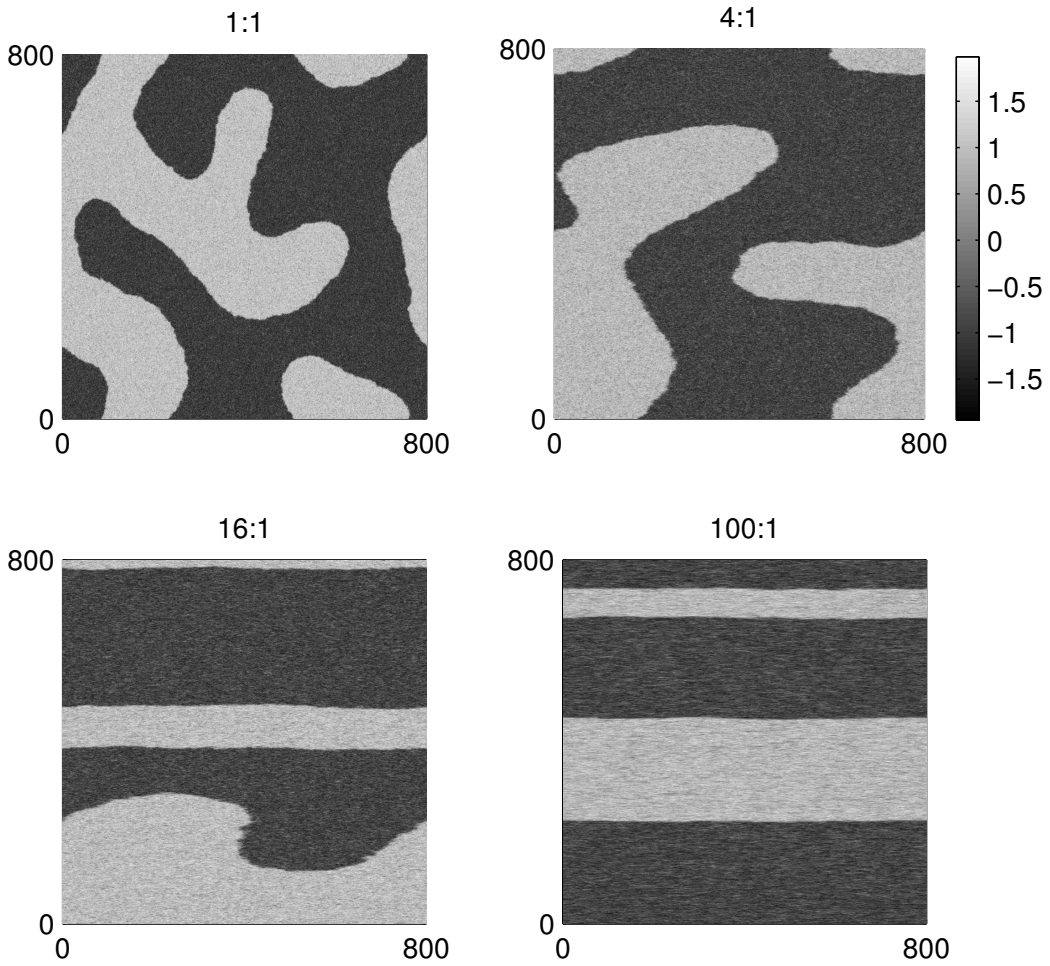

Figure 6.2: Equilibrium field configurations for different $\Delta x^{-2} : \Delta y^{-2}$ ratios.

6.3 Correlation Length Calculations

The anisotropic two-dimensional system has two relevant correlation lengths to consider, one in each spatial direction. In effect, one deals with a correlation "area" illustrated in fig.(6.3). This area is traced out by an ellipse with major and minor axis given by the correlation lengths λ_x and λ_y. The method for extracting correlations lengths from one-dimensional field configurations was discussed in section 5.5 of the previous chapter. This methodology was used to extract correlation lengths along the weakly-coupled direction of the two-dimensional

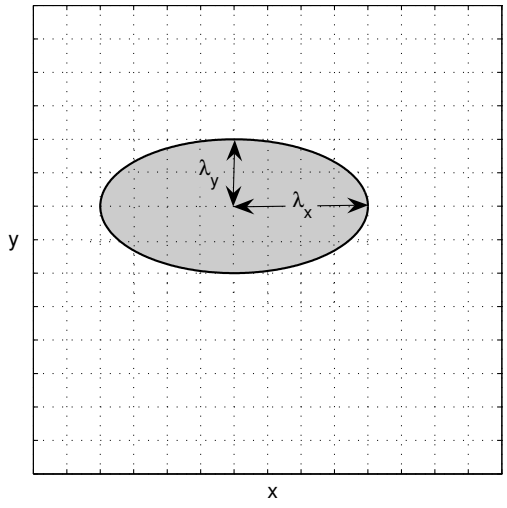

Figure 6.3: The correlation area on a two-dimensional lattice.

configuration.

To achieve thermal equilibrium with the condition, eq.(5.21), simulations generally required $\sim 2 \times 10^5$ iterations. Due to the complexity of the update involved in the modified Euler method, this corresponds to about 24 hours of computing time. As stated in the previous chapter the maximum lattice size available consisted of 800×800 sites. To identify thermal equilibrium, the same mean-field check as mentioned previously was used. Fig.(6.4) is a series of snapshots illustrating the evolution of the field configuration towards equilibrium.

Using a coupling ratio of 25, a series of equilibrium field configurations were obtained using different effective lattice spacings (i.e. the coupling ratio $\Delta y^2/\Delta x^2$ was maintained while varying the lattice spacings). Configurations obtained using the potential of eq.(2.8) are plotted in fig.(6.5). The numbers above each configuration are Δx and Δy values, respectively. With $\Delta x < 0.065$ it was found that the field configuration went to $-\infty$. This indicated a breakdown in the numerical method. With $\Delta y > 2.5$, the level of accuracy was considered too low to extract correlation lengths.

The field averages with their standard deviations, corresponding to each of

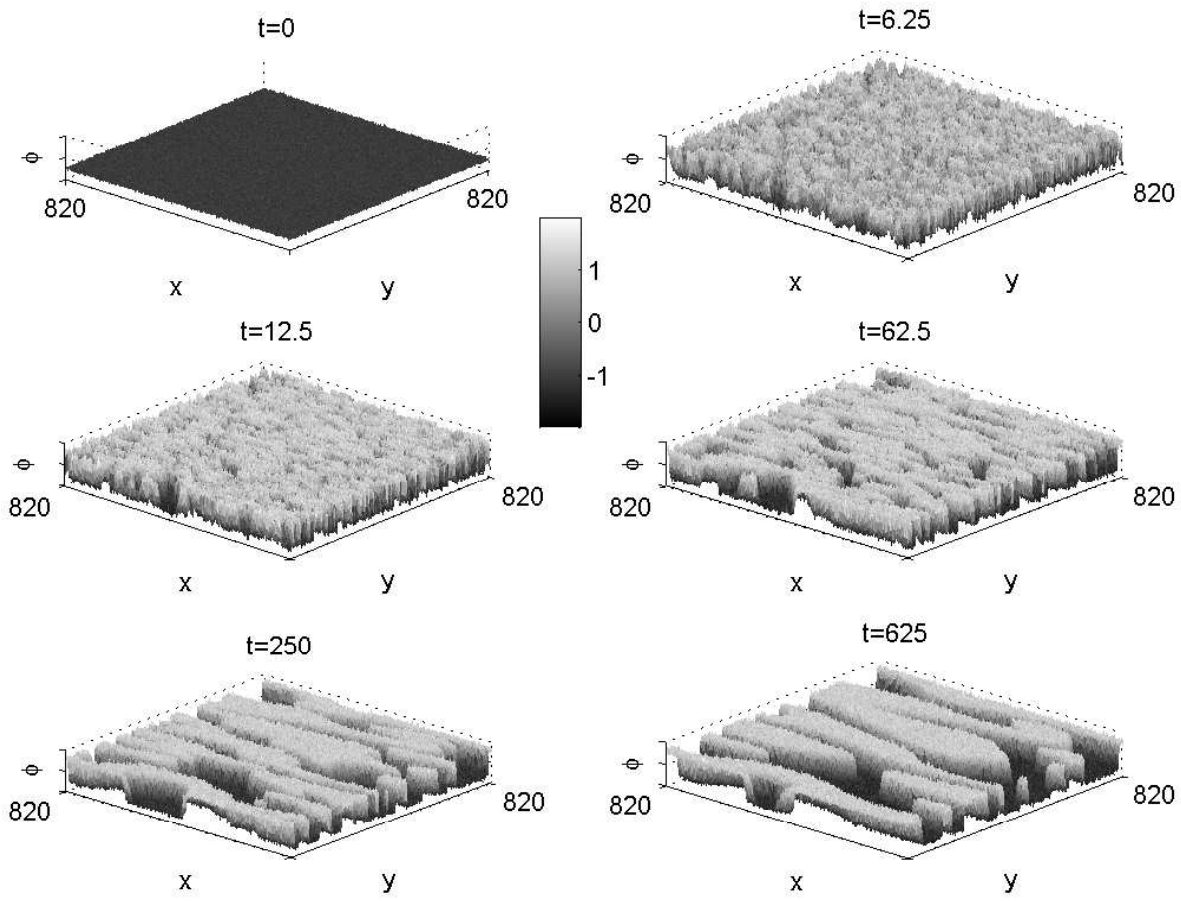

Figure 6.4: Snapshots of the lattice field configuration at differents times. The final configuration at t=625, shows the field at thermal equilibrium.

the configurations plotted in fig.(6.5), are presented in fig.(6.6). It is clear from fig.(6.6) that the higher accuracy simulations never achieve thermal equilibrium. The reason for this is evident from the corresponding field configurations in fig.(6.5). Only one or two kink/antikink pairs have formed on the lattice. The kink/antikink density in this case is $1/L$ - a very poor estimation of the exact value. It is clear that results with $\Delta x < 0.1$ cannot be used.

Likewise, configurations for $\Delta x > 1.0$ show a breakdown of displacive patterns in the strongly-coupled direction. This is partly due to the lower accuracy

of these simulations. By increasing the coupling ratio displacive patterns could be recovered. However, doing this would restrict the range of effective lattice spacings available for studying.

Attempts were made to extract a correlations length from the field configuration with $\Delta x = 0.15$, $\Delta y = 0.75$ of fig.(6.5). A plot of $\lambda(y)$ versus y did not show the intermediate "plateau" that was observed in the one-dimensional studies of the previous chapter. To obtain a correlation length, the $\lambda(y)$ data was averaged over the range $7.5 < y < 37.5$. This gave a value of $\lambda_\infty \sim 40$ with a percentage uncertainty of 14.7%. In comparison, Eq.(6.15) gives the value $\lambda_\infty = 28.2$. The poor quality of the extracted correlation lengths means a comparison with other values is not useful.

Its is clear why the inaccuracies arise. The two-dimensional lattice used above consists of the same number of data points that made up the one-dimensional lattice of the previous chapter. The important quantity, however, is the number of kink/antikink structures on the lattice. With only several kinks present at thermal equilibrium, the field configurations above yield low quality data. Compare this to the one-dimensional field configuration obtained in the previous chapter, which contained up to 1000 kink/antikink pairs.

Attempts were made to increase the lattice size using the computing hardware available. In principle, it is possible to perform lattice simulations of a size limited only by hard-disk space. Areas of $\phi(t), \pi(t), \psi(t)$ values are printed to files of a size equal to that of the random access memory (RAM) available. Data from these files are reread into arrays when updating to the next time level. By doing this over the entire lattice, one can achieve a virtual memory equal up to the hard disk space available. Consequently, with large, relatively inexpensive amounts of hard disk space readily available, very large lattice sizes can be realised. Unfortunately, printing data to a file then reading data into arrays is a very time consuming process. For a lattice consisting of 820×820 lattice

sites, simulations using RAM were 25 to 30 times faster than this "print-to-file" procedure. Therefore, using large lattices to get sufficient data will drastically increase the time for each iteration. Considering the time span of this study, such a procedure was not feasible.

Algorithms were also written which simulate different "segments" of a larger lattice simultaneously. Each segment is assigned to a different central processing unit (CPU), and relevant boundary values required by calculations in neighbouring segments are printed to file. This acts as a means of communication between CPU's. Here the computing limits were the number of CPU's on the computer cluster and the RAM of each CPU. Using three CPU's, it was possible to increase the maximum lattice size by 300%, from 820×820 to 1420×1420. With no noticible improvement to the accuracy of extracted correlation lengths ($\sim 13\%$), different techniques for testing the counterterms were used.

6.4 Ensemble Averages of the Field

A direct comparison between the correlation lengths was not achievable with the low quality data obtained. However, it is still possible to test whether lattice spacing dependence is suppressed. This involves a qualitative investigation into the initial behaviour of the average field value $\langle\phi\rangle$ [14]. It would be expected that if such a dependence had been successfully countered by a control method, one should observe little variance between ensemble field averages obtained from simulations which use different effective lattice spacings. $\langle\phi\rangle$ values that do not appear to vary with the lattice spacing indicate that the control method has been successful.

This procedure has the advantage that simulations do not need to run till thermal equilibrium is achieved. Only a small set of $\langle\phi\rangle$ values are required to observe the ensemble field average behaviour relative to other data sets. Due to its level of simplicity, it does have disadvantages however. A successful correla-

tion length study would not only allow one to determine which control method suppresses lattice spacing dependence, but also whether the correct continuum theory is being studied. Conclusions about matching the continuum result cannot be made in an average field value study unless, of course, exact average field values are available from analytic methods. Finding exact values would require the exact solution of the nonlinear Schrödinger-type equation, eq.(3.88). One could find analytic solutions using the Ising methods discussed previously. However, such solutions are for thermal equilibrium field configurations. It has been determined already that an adaquate description of the field theory at thermal equilibrium cannot be achieved using the lattice size available in this study.

The series of plots of ensemble field averages that follow were obtained for three different values of anisotropy. From the discussion above, the level of anisotropy identified for which the mean field approximation is valid was when the coupling ratio, $\Delta y^2/\Delta x^2 \sim 25$ or greater. The Langevin simulation ran as before. Field averages over the lattice were calculated after every iteration and then plotted. Only values from the first 500 iterations were considered, as this data was sufficient to observe the qualitative behaviour.

Figures eq.(6.7) through to eq.(6.15) show the field average $\langle\phi\rangle$ plotted against physical time t. Each plot has the same initial dynamics. The field begins in the minimum, $\phi_1 = -1$ with values Gaussian distributed with a mean $\langle\phi\rangle = -1$ and small divergence. This small divergence has the effect of correlating the field slightly. Stochastic evolution causes the initially correlated field to oscillate about ϕ_1 until thermal noise disrupts the correlation and kink/antikink pairs form. For labelling purposes, an area containing all five plots has been magnified in the inset of each figure. The values labelling each plot correspond to Δy values used in each simulation.

A coupling ratio of $\Delta y^2/\Delta x^2 = 25$ was first considered. The following pairs

of lattice spacing values were used,

$$\{(\Delta x, \Delta y)\} = \{(0.1, 0.5), (0.125, 0.625), (0.15, 0.75), (0.175, 0.875), (0.2, 1.0)\}.$$

Fig.(6.7) shows the average field behaviour in simulations using no control method. That is to say, the bare potential of eq.(2.8) was used. The lattice spacing dependence is clearly illustrated. Fig.(6.8) shows average field values obtained using the potential of eq.(4.60) in the simulation. From fig.(6.8) it is clear that the one-loop renormalization (1LR) method fails to supress discretization effects at tis level of anisotropy. In fact, field average plots calculated using the 1LR method deviate from each other more so than the bare potential results. In contrast, the results presented in fig.(6.9) using the TIO control method (eq.(3.92)) show a successful supression of lattice spacing dependence. We return to this significant result at a later point.

A full understanding of the mean field approximation's parameter range of validity could be obtained by slowly decreasing the coupling ratio towards unity. Such a study was felt unneccesary given the aims of this study. When the coupling ratio is low (< 20), the mean field approximation is expected to break-down. Consequently, so too would the effectiveness of the TIO control method. It was important to check this. A coupling ratio of 9 was considered with the expectation that only the 1-loop counterterm might have some success. The following pairs of lattice spacing values were used,

$$\{(\Delta x, \Delta y)\} = \{(0.1, 0.3), (0.125, 0.375), (0.15, 0.45), (0.175, 0.525), (0.2, 0.6)\}.$$

The results are presented in fig.(6.10) through to fig.(6.12). As expected, the TIO method fails. However, it is still improvement to using no control method. The results obtained using the 1LR method, again, appear more lattice spacing dependent than the bare potential results.

A coupling ratio of 49 was also studied for completeness. The following

pairs of lattice spacing values were used,

$$\{(\Delta x, \Delta y)\} = \{(0.1, 0.7), (0.125, 0.875), (0.15, 1.05), (0.175, 1.225), (0.2, 1.4)\}.$$

The behaviour seen in fig.(6.13) through to fig.(6.15) differs little from the $\Delta y^2/\Delta x^2 = 25$ results. The only difference is that the ensemble field averages are generally lower. This is due to the stronger coupling in the system. Larger fluctuations are required for barrier-crossing to occur.

From these results, two conclusions can be made. In the parameter range where the mean field approximation is valid, the TIO control method successfully suppresses lattice spacing dependence. For all three coupling ratios studied, the 1LR method failed to suppress lattice spacing dependence. Unfortunately, due to the nature of this ensemble average study, it is not clear if the TIO method reproduces the continuum result.

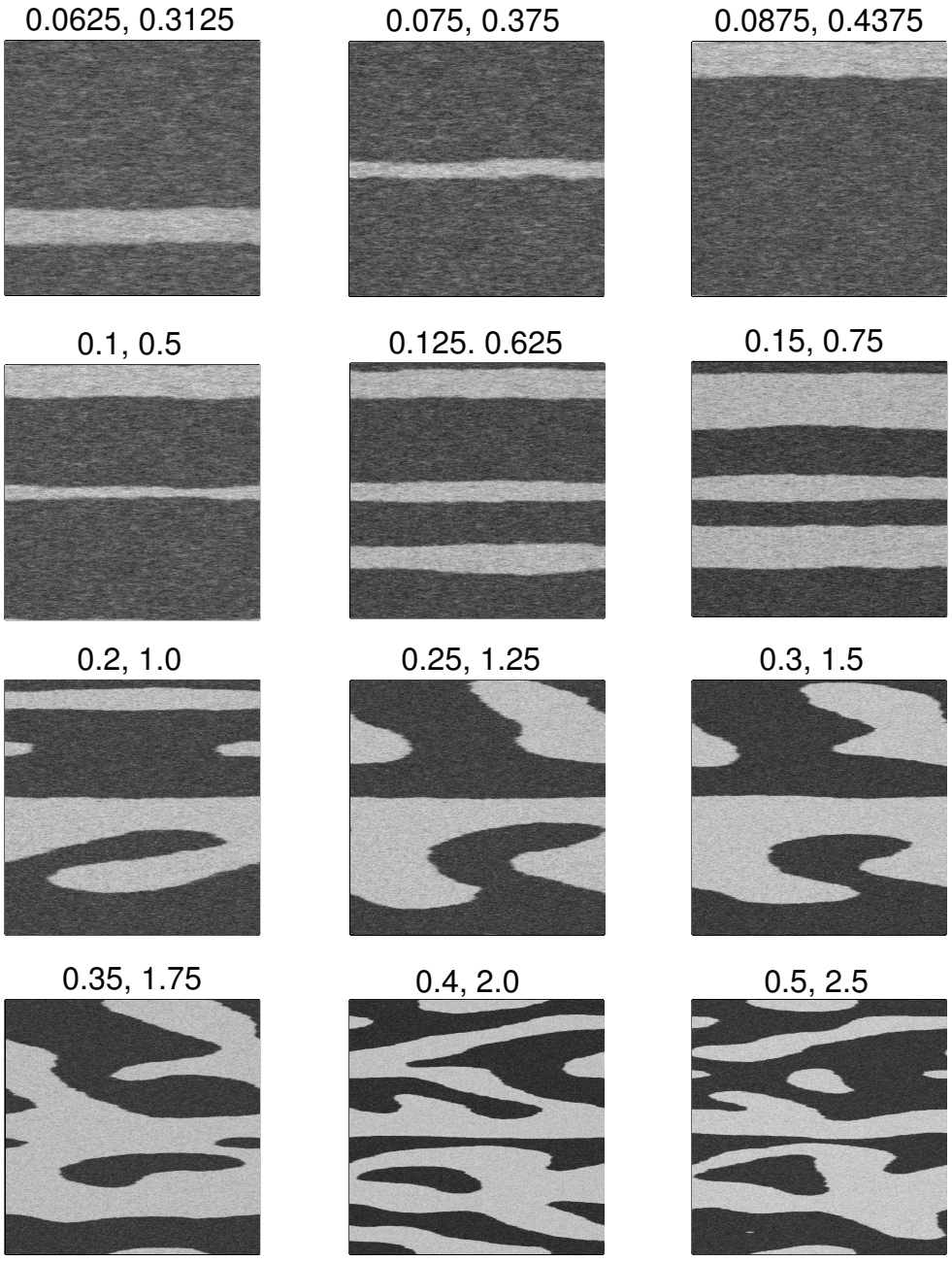

Figure 6.5: Field configurations after long stochastic evolution for different effective lattice spacings. The same colormap has used as in previous field configuration plots. The numbers above each configuration are Δx and Δy values, respectively.

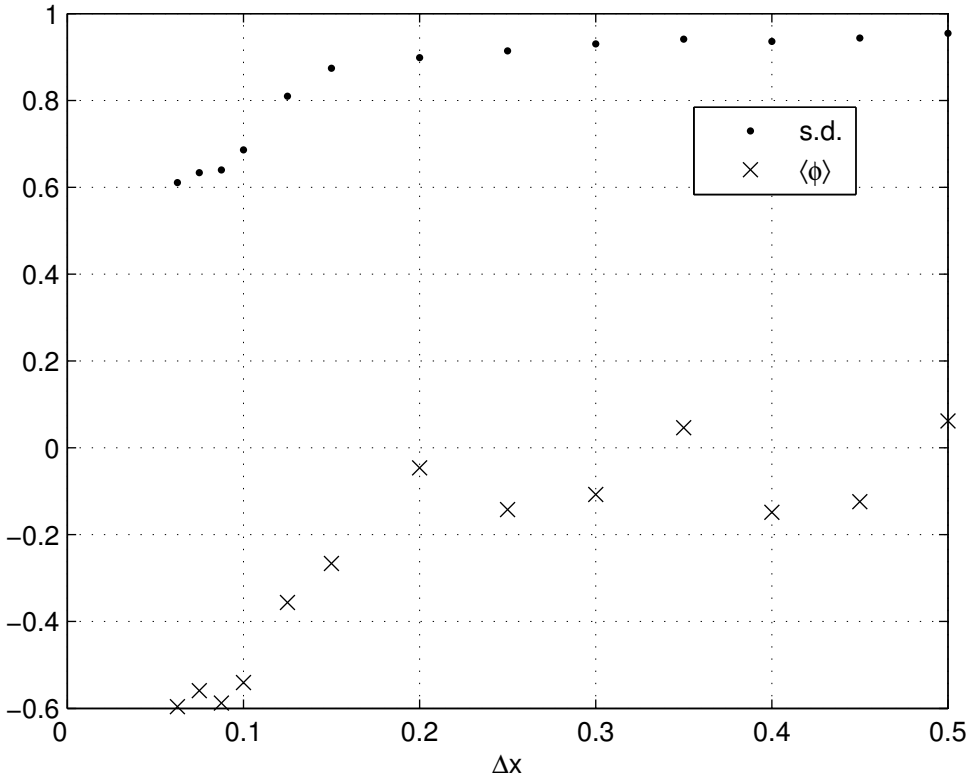

Figure 6.6: Mean field values × and standard deviations • obtained from the field configurations in fig.(6.5) are plotted against Δx.

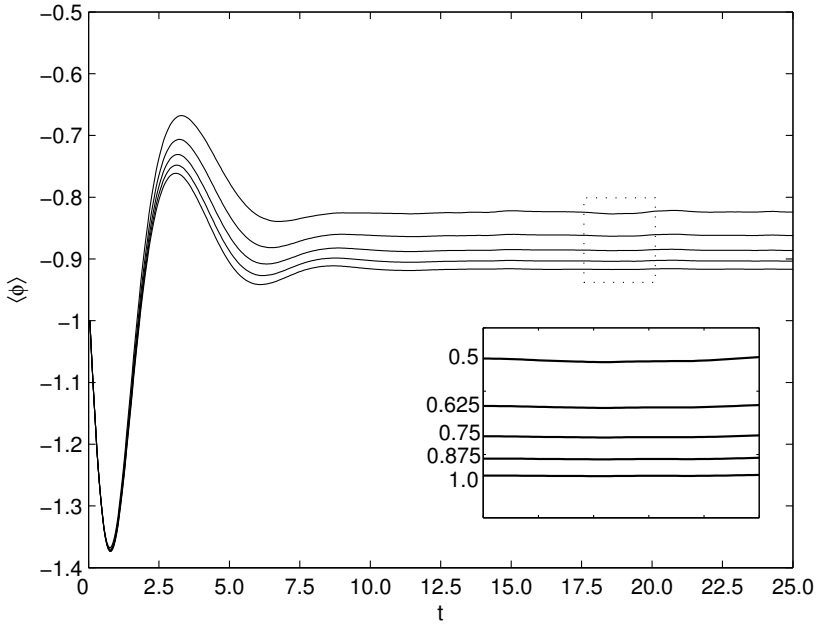

Figure 6.7: Field averages obtained for a coupling ratio of 25 using no control method.

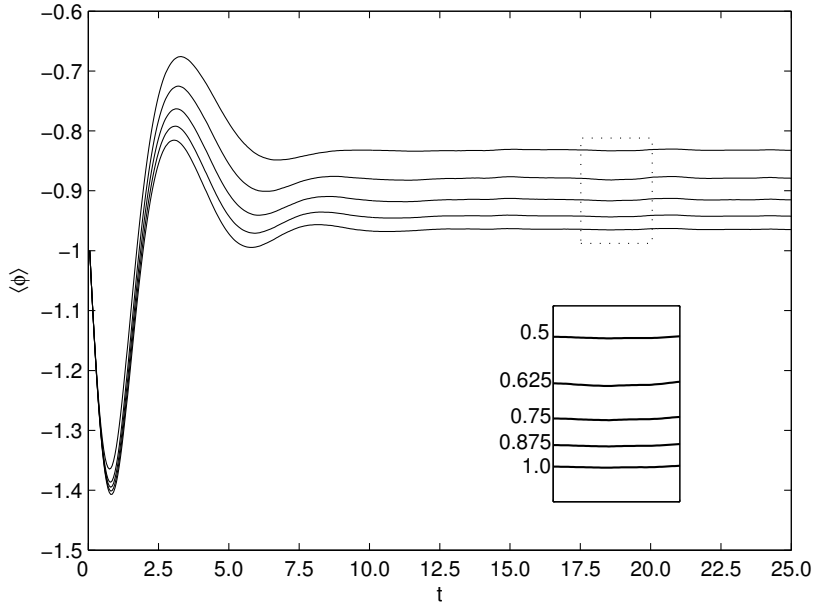

Figure 6.8: Field averages obtained for a coupling ratio of 25 using the 1LR control method.

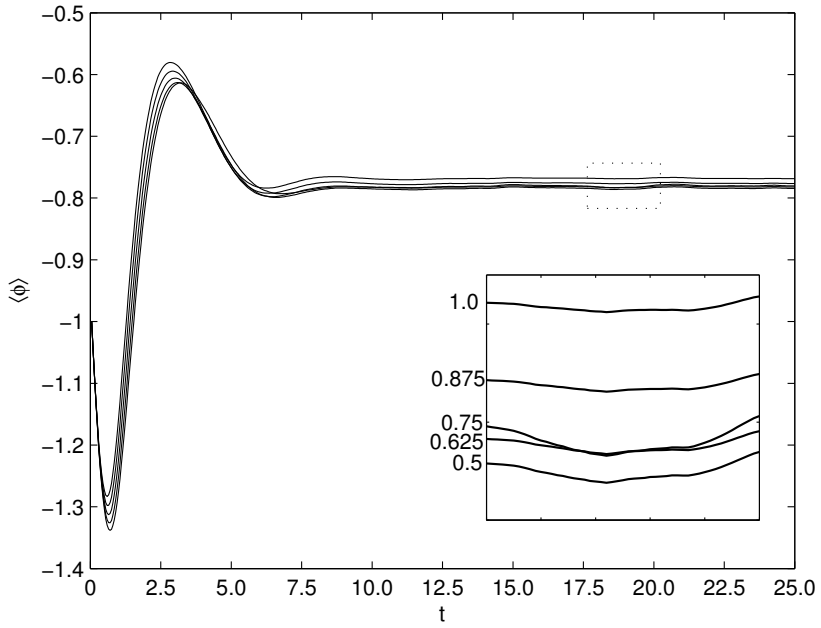

Figure 6.9: Field averages obtained for a coupling ratio of 25 using the TIO control method.

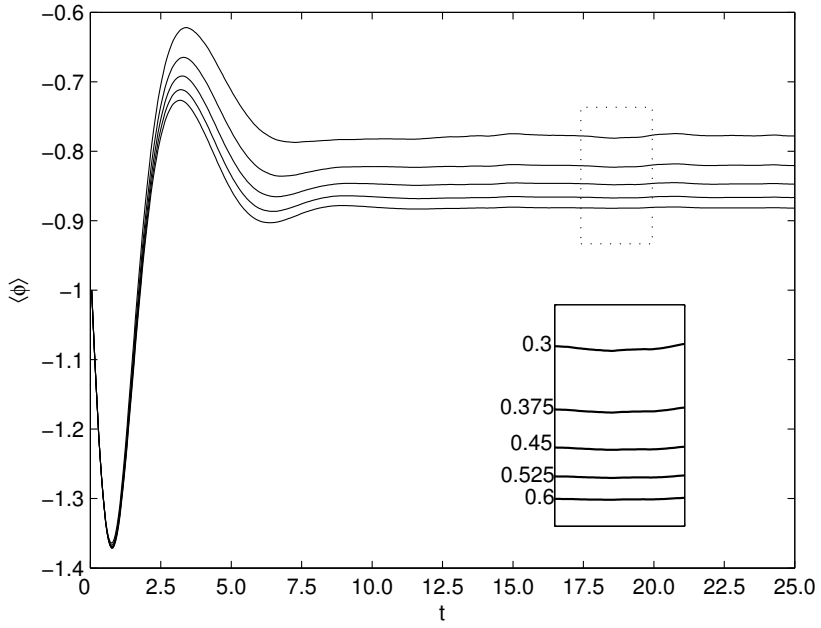

Figure 6.10: Field averages obtained for a coupling ratio of 9 using no control method.

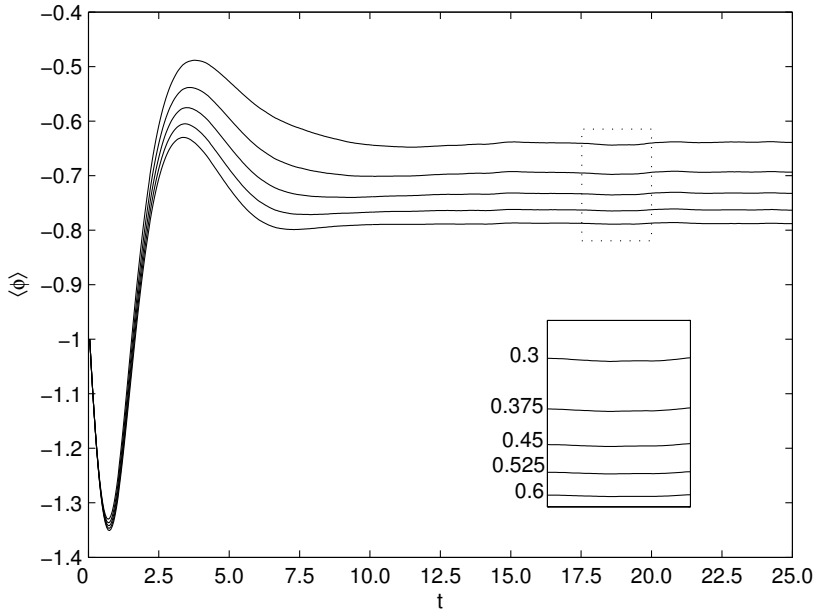

Figure 6.11: Field averages obtained for a coupling ratio of 9 using the 1LR control method.

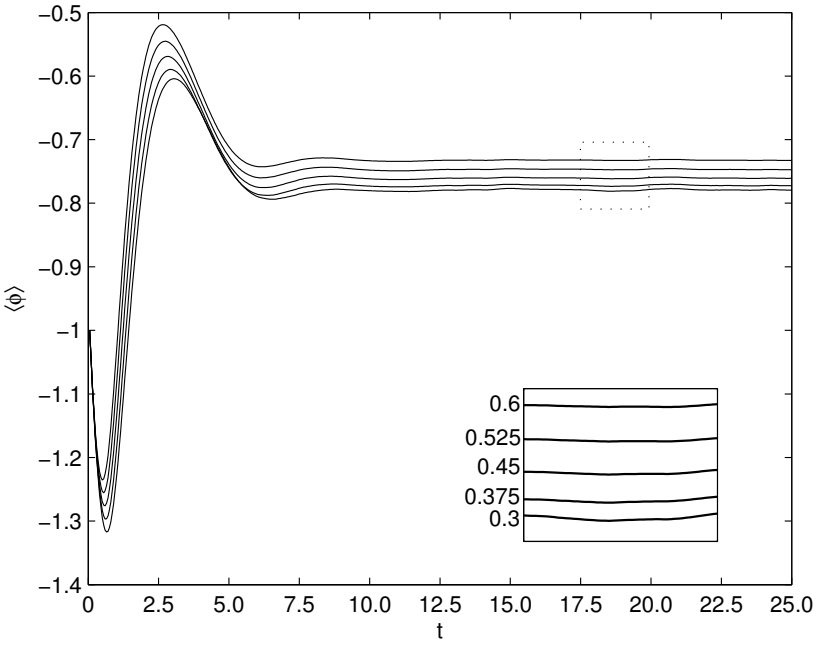

Figure 6.12: Field averages obtained for a coupling ratio of 9 using the TIO control method.

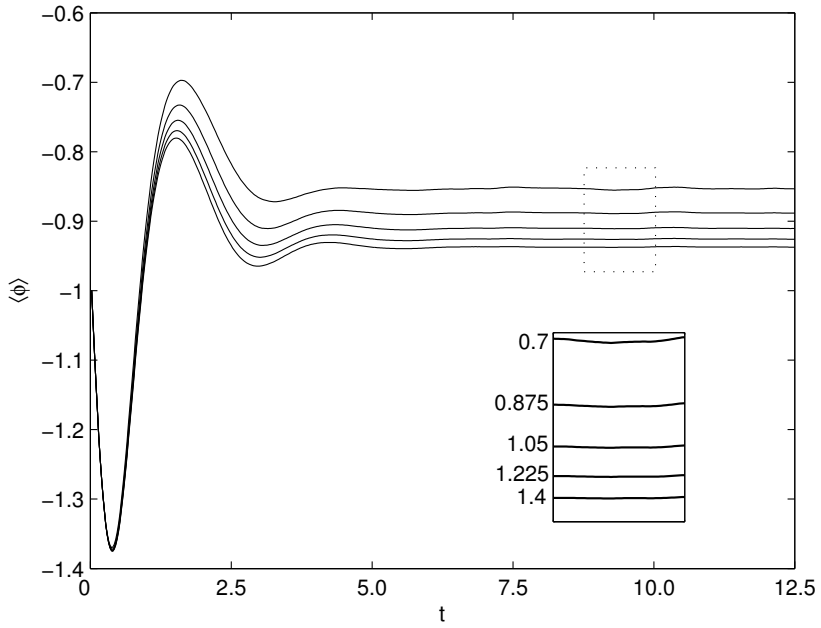

Figure 6.13: Field averages obtained for a coupling ratio of 49 using no control method.

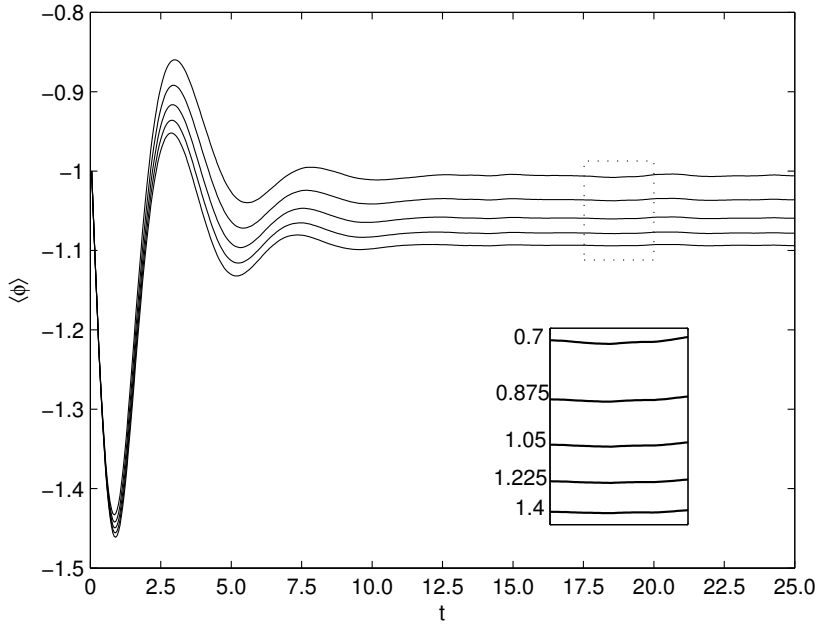

Figure 6.14: Field averages obtained for a coupling ratio of 49 using the 1LR control method.

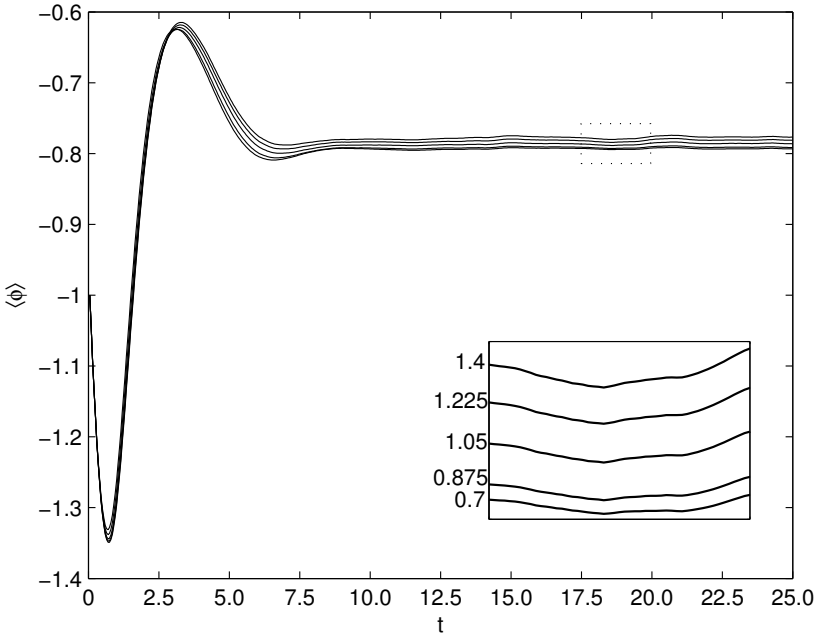

Figure 6.15: Field averages obtained for a coupling ratio of 49 using the TIO control method.

Chapter 7

Conclusion

The aim of this study was to suppress lattice spacing dependence in (2+1)-dimensional Langevin simulations. To implement a transfer integral operator (TIO) method it was necessary to specialize this study to field-systems with anisotropy. Two control methods were utilized for such a system. The TIO method showed considerable success at suppressing lattice spacing dependence in the mean-field limit. The 1LR method failed to suppress lattice spacing dependence for all coupling values studied.

A TIO method was employed, consistent with previous one-dimensional studies [17][37]. The result was the lattice potential, eq.(3.92) which contains counterterms that eliminate lattice spacing dependence to order, Δx^2. During the implementation of this procedure a mean field approximation was made for the weakly coupled interaction. To perform a particular Taylor expansion, it was required that one of the directions have strong-coupling ($\Delta x \to 0$). Continuity of the orthonormal eigenbasis $\{\Psi_n(\varphi)\}$ was also assumed.

A one-loop renormalization (1LR) procedure was also used to find a lattice potential with counterterms that cancel lattice spacing dependence. Our calculation was consistent with the methodology used in previous isotropic two-dimensional studies [13][14]. A number of approximations were made during the calculation. Most notably, an effective potential was truncated at one-loop order, neglecting finite, higher order loop corrections. The one-loop effective potential

was evaluated by regularizing a constituent divergent integral with the lattice ultraviolet cutoffs, Λ_x and Λ_y. To perform a renormalization procedure, a series expansion of the one-loop effective potential to first order in V'' was necessary.

The second part of this study involved the numerical testing of the two control methods by means of Langevin simulation. Due to the complicated nature of the control methods, it was important to ensure our numerical method was accurate. Time-step dependence and truncation error were treated such that they became subdominant to the lattice spacing dependence in Langevin simulations. We were able to reproduce the correlation length results of [12] to a comparable level of accuracy.

A similar correlation length study was attempted using the control methods derived for the anisotropic two-dimensional model. Ising methods were used to simplify the model such that a continuum exact correlation length could be calculated. This calculation was valid in the moderately anisotropic, low temperature limit. Low temperatures were required for the two-state basis assumption to be valid. Correlation lengths obtained using the extraction methods presented in chapter 5 were of insufficient accuracy with percentage uncertainties $\sim 15\%$.

The poor quality of the correlation length results was attributed to having a small data set. In this study, equilibrium field configurations contained only several kink/antikinks. Larger systems are necessary to get acceptable statistics at the low temperatures considered. Different methods of implementing the algorithm on the computing hardware were explored. A study on a 1420×1420 lattice yielded a correlation length with a percentage uncertainty $\sim 13\%$. This was of little improvement to the results obtained on the 820×820 lattice.

It was possible to make some conclusions on the effectiveness of the control methods by studying the initial behaviour of the ensemble field average. From this study, it was clear that the TIO method is successful at suppressing lattice spacing dependence given certain anisotropy conditions are satisfied. An extensive study

of the limits in which this method was applicable was not performed. Ensemble averages obtained using a coupling ratio of $\Delta y^2/\Delta x^2 = 9$ did show lattice spacing dependence. Work towards an isotropic two-dimensional TIO method would require replacing the mean-field approximation with some alternative method for treating the $\hat{y}$-directional interaction term.

It was also clear from the study of ensemble field average behaviour, that the 1LR method failed to suppress lattice spacing dependence. This was true for all three of the coupling ratio values studied. In fact, the study showed this method gave results more lattice spacing dependent than results using no control method.

Success of the isotropic 1LR method in two dimensions was reported in [14] by studying ensemble field average behaviour. Care was taken to show that the isotropic 1LR method of [14] was recovered from our anisotropic method in the isotropic limit. It is not understood why the method should work in the isotropic limit only. The 1LR method derived in this study needs to be tested over the full range of anisotropies including the isotropic limit to address this question. One should note that the findings in this study are consistent with what was found in the one-dimensional correlation length study.

It was successfully shown that the TIO method suppressed lattice spacing dependence in anisotropic (2+1)-dimensional Langevin studies. It was not shown whether the continuum result was produced. To determine this would require a continuum exact quantity for comparison, such as the correlation length obtained using Ising methods. An accurate correlation length study would provide the ultimate validation of the TIO method presented in this work.

The computing resources available for this study were exhausted. The largest lattice size achievable using RAM was a 820×820 lattice. Other algorithm methods allowing for larger lattice studies, were devised with the penalty of long computing times. Relatively accurate correlation lengths have been extracted

from one-dimensional field configurations on lattice sizes as small as $M = 16384$ [43]. This lattice dimension could be achieved using the techniques described in chapter 6, given the long computing time is not of concern. One tool that would be of use is Fourier acceleration. The idea is to accelerate the dynamics of slow modes. Langevin propagation is studied in momentum space rather than coordinate space. Fast Fourier transforms (FFT's) are used to relate the two descriptions. In [44], it shown that this technique can considerably decrease computer run-time. Each mode is dealt with seperately. This is accomplished by updating the field configuration in momentum space, using different Δtś for different momenta in such a way as to accelerate the evolution of low momenta without comprimising the the high momenta. Consequently, the number iterations for a simulation is reduced considerably. Unfortunately, Fourier acceleration only came to our attention during the write-up stage of this work.

The alternative would be to use more powerful computing resources. With Moore's law still in effect, the correlation length study presented in this work could be carried out to a high level of accuracy in the near future.

Appendix A

The Commutator of Eq.(3.65)

In Eq.(3.65) of chapter 3, a commutator was expanded with little explanation. Because its final form is of extreme importance to this study, full details have been included here. With expansion, the commutator term reads

$$\begin{aligned}
&\left[\frac{1}{\beta^2}\frac{\partial^2}{\partial\varphi^2} - U, \left[\frac{\partial^2}{\partial\varphi^2}, U\right]\right] \\
&\qquad = \left(\frac{1}{\beta^2}\frac{\partial^2}{\partial\varphi^2} - U\right)\left(\frac{\partial^2}{\partial\varphi^2}\left(U\Psi_n\right) - U\frac{\partial^2\Psi_n}{\partial\varphi^2}\right) \\
&\qquad\quad + \left(\frac{\partial^2}{\partial\varphi^2}U - U\frac{\partial^2}{\partial\varphi^2}\right)\left(\frac{1}{\beta^2}\frac{\partial^2\Psi_n}{\partial\varphi^2} - U\Psi_n\right) \\
&\qquad = \left(\frac{1}{\beta^2}\frac{\partial^2}{\partial\varphi^2} - U\right)\left(2\frac{\partial U}{\partial\varphi}\frac{\partial\Psi_n}{\partial\varphi} + \frac{\partial^2 U}{\partial\varphi^2}\Psi_n\right) \\
&\qquad\quad + \left(\frac{\partial^2}{\partial\varphi^2}U - U\frac{\partial^2}{\partial\varphi^2}\right)\left(\frac{1}{\beta^2}\frac{\partial^2\Psi_n}{\partial\varphi^2} - U\Psi_n\right)
\end{aligned} \tag{A.1}$$

Expanding out the brackets and letting operators act, the commutator has the completely decomposed form,

$$\begin{aligned}
&\frac{2}{\beta^2}\frac{\partial^2}{\partial\varphi^2}\left(\frac{\partial U}{\partial\varphi}\frac{\partial\Psi_n}{\partial\varphi}\right)+\frac{1}{\beta^2}\frac{\partial^2}{\partial\varphi^2}\left(\frac{\partial^2 U}{\partial\varphi^2}\Psi_n\right)-U\frac{\partial^2 U}{\partial\varphi^2}\Psi_n-2U\frac{\partial U}{\partial\varphi}\frac{\partial\Psi_n}{\partial\varphi}\\
&-\frac{1}{\beta^2}\frac{\partial^2}{\partial\varphi^2}\left(U\frac{\partial^2\Psi_n}{\partial\varphi^2}\right)+\frac{1}{\beta^2}U\frac{\partial^4\Psi_n}{\partial\varphi^4}+\frac{\partial^2}{\partial\varphi^2}\left(U^2\Psi_n\right)-U\frac{\partial^2}{\partial\varphi^2}\left(U\Psi_n\right)\\
&\quad=\frac{2}{\beta^2}\left(\frac{\partial U}{\partial\varphi}\frac{\partial^3\Psi_n}{\partial\varphi^3}+2\frac{\partial^2 U}{\partial\varphi^2}\frac{\partial^2\Psi_n}{\partial\varphi^2}+\frac{\partial^3 U}{\partial\varphi^3}\frac{\partial\Psi_n}{\partial\varphi}\right)\\
&\quad+\frac{1}{\beta^2}\left(\frac{\partial^2 U}{\partial\varphi^2}\frac{\partial^2\Psi_n}{\partial\varphi^2}+2\frac{\partial^3 U}{\partial\varphi^3}\frac{\partial\Psi_n}{\partial\varphi}+\frac{\partial^4 U}{\partial\varphi^4}\Psi_n\right)-U\frac{\partial^2 U}{\partial\varphi^2}\Psi_n-2U\frac{\partial U}{\partial\varphi}\frac{\partial\Psi_n}{\partial\varphi}\\
&\quad-\frac{1}{\beta^2}\left(U\frac{\partial^4\Psi_n}{\partial\varphi^4}+2\frac{\partial U}{\partial\varphi}\frac{\partial^3\Psi_n}{\partial\varphi^3}+\frac{\partial^2 U}{\partial\varphi^2}\frac{\partial^2\Psi_n}{\partial\varphi^2}\right)+\frac{1}{\beta^2}U\frac{\partial^4\Psi_n}{\partial\varphi^4}+U^2\frac{\partial^2\Psi_n}{\partial\varphi^2}\\
&\quad+2\left(\frac{\partial U^2}{\partial\varphi}\right)\frac{\partial\Psi_n}{\partial\varphi}+\left(\frac{\partial^2 U^2}{\partial\varphi^2}\right)\Psi_n-U^2\frac{\partial^2\Psi_n}{\partial\varphi^2}-2U\frac{\partial U}{\partial\varphi}\frac{\partial\Psi_n}{\partial\varphi}-U\frac{\partial^2 U}{\partial\varphi^2}\Psi_n
\end{aligned}\tag{A.2}$$

Certain terms can be seen to cancel one another, giving

$$\begin{aligned}
&\frac{1}{\beta^2}\left\{\frac{\partial^4 U}{\partial\varphi^4}\Psi_n+4\frac{\partial^3 U}{\partial\varphi^3}\frac{\partial\Psi_n}{\partial\varphi}+4\frac{\partial^2 U}{\partial\varphi^2}\frac{\partial^2\Psi_n}{\partial\varphi^2}\right\}-2U\frac{\partial^2 U}{\partial\varphi^2}-4U\frac{\partial U}{\partial\varphi}\frac{\partial\Psi_n}{\partial\varphi}\\
&\qquad+2\left(2U\frac{\partial U}{\partial\varphi}\right)\frac{\partial\Psi_n}{\partial\varphi}+\left(2U\frac{\partial^2 U}{\partial\varphi^2}+2\left(\frac{\partial U}{\partial\varphi}\right)^2\right)\Psi_n\\
&\qquad=\frac{1}{\beta^2}\left(\frac{\partial^4 U}{\partial\varphi^4}\Psi_n+4\frac{\partial^3 U}{\partial\varphi^3}\frac{\partial\Psi_n}{\partial\varphi}+4\frac{\partial^2 U}{\partial\varphi^2}\frac{\partial^2\Psi_n}{\partial\varphi^2}\right)+2\left(\frac{\partial U}{\partial\varphi}\right)^2\Psi_n
\end{aligned}\tag{A.3}$$

Appendix B

Gaussian Integrals

Through out this work, Gaussian integrals (or probability integrals) were solved without proof. Here, a brief outline of their solutions are presented. The first Gaussian integral encountered was in eq.(3.8). A similar, yet more complicated, Gaussian integral appears in eq.(3.45). These are 1-D Gaussian integrals over $(-\infty, \infty)$ and which have a simple solution

$$\int_{-\infty}^{\infty} \mathrm{d}x e^{-(ax^2+bx+c)} = \sqrt{\frac{\pi}{a}} e^{(b^2-4ac)/4a} \tag{B.1}$$

where erfc is the complementary error function.

In eq.(4.14), a k-dimensional integral of the form

$$F = \int \mathrm{d}^k\phi \exp\left(\frac{1}{2}(\phi, A\phi)\right) \tag{B.2}$$

was solved, where

$$(\phi, A\phi) = \phi_j A_{ij} \phi_j \tag{B.3}$$

The matrix A can be diagonalized,

$$SAS^T = D = \mathrm{diag}(\lambda_1, \ldots, \lambda_k), \qquad \forall \lambda_i > 0 \tag{B.4}$$

A change of variables can be performed as follows,

$$u = S\phi,$$
$$\mathrm{d}^k\phi = |\mathrm{det}S|^{-1}\mathrm{d}^k u = \mathrm{d}^k u. \tag{B.5}$$

Eq.(B.2) is now of the form,

$$\begin{aligned}\int \mathrm{d}^k\phi \exp\left(\frac{1}{2}(\phi, A\phi)\right) &= \int \mathrm{d}^k u \exp\left(-\frac{1}{2}\sum_i^k \lambda_i u_i^2\right) \\ &= \prod_i^k \left(\frac{2\pi}{\lambda_i}\right)^{1/2} \\ &= (2\pi)^{k/2}(\mathrm{det}A)^{-1/2} \qquad \text{(B.6)}\end{aligned}$$

Appendix C

The One-Dimensional One-loop Effective Potential

$(1+1)$-dimensional scalar field theories turn out to be free of ultraviolet divergences, such that the one-loop momentum integral in the effective potential can be evaluated without the introduction of a cutoff.

$$\begin{aligned}
V_{1LP} &= \frac{T}{2}\int_0^\infty \frac{\mathrm{d}k}{2\pi}\ln\left(1+\frac{V''(\phi)}{k^2}\right) \\
&= -\frac{T}{2}\frac{1}{2\pi}\frac{\partial}{\partial\alpha}\int_0^\infty \mathrm{d}k\frac{1}{\left(1+\frac{V''(\phi)}{k^2}\right)^\alpha}\bigg|_{\alpha=0} \\
&= -\frac{T}{2}\frac{1}{2\pi}\frac{\partial}{\partial\alpha}\int_0^\infty \mathrm{d}k\, k^{2\alpha}\frac{1}{\left(k^2+V''(\phi)\right)^\alpha}\bigg|_{\alpha=0} \\
&= -\frac{T}{2}\frac{1}{2\pi}\frac{\partial}{\partial\alpha}\left[\frac{(-1)^{\alpha-1}\pi\sqrt{V''}^{2\alpha+1-2\alpha}\Gamma[(2\alpha+1)/2]}{2\sin(\frac{\pi}{2}(2\alpha+1))(\alpha-1)!\Gamma[(2\alpha+1)/2-\alpha+1]}\right]\bigg|_{\alpha=0} \\
&= -\frac{T}{8}\frac{V''}{d}\left[\frac{(-1)^{\alpha-1}\Gamma[\alpha+\frac{1}{2}]}{\Gamma[\frac{3}{2}]}\right]\bigg|_{\alpha=0} \\
&= \frac{T}{4}\sqrt{V''}
\end{aligned} \tag{C.1}$$

Regardless, the one-dimensional lattice will still impose an artificial momentum cutoff, Λ, so the momentum integral above must integrated from 0 to Λ.

$$\begin{aligned}
V_{1LP} &= \int_0^\Lambda \frac{\mathrm{d}p}{2\pi}\ln\left(1+\frac{V''(\phi)}{k^2}\right) \\
&= \frac{T}{2}\left(\Lambda\ln\left(\frac{\Lambda^2+V''}{\Lambda^2}\right)+2\sqrt{(V'')}\tan^{-1}\left(\frac{\Lambda}{\sqrt{V''}}\right)\right)
\end{aligned} \tag{C.2}$$

With the condition $V'' \ll \Lambda$ satisfied, the result above may expanded about V''. To order $\mathcal{O}(V'')$, the effective potential to one-loop order is

$$V_{eff} = V + \frac{T}{4}\sqrt{V''} - \frac{T}{4\pi}\frac{V''}{\Lambda} \tag{C.3}$$

Appendix D

Kink-Gas Phenomenology

In Section 5.6 of Chapter 5, a value for the continuum exact correlation length was compared to numerical results. It was obtained from kink-gas phenomenology conceived originally by Krumhansl and Schrieffer [45] to calculate the density of thermally excited kinks on a one-dimensional particle chain of non-linear Klein-Gordan type. The idea was to treat a low-temperature one-dimensional kink-bearing ensemble as an ideal gas of noninteracting particle-like kinks and phonons. Currie, Krumhansl, Bishop and Trullinger [1] later improved this treatment by considering the influence of kinks on the density of states. The exactness of this phenomenology at low temperatures has been well demonstrated [46].

Originally, it was thought the phenomenology required explicit knowledge of the phase shifts of extended small oscillations in the presence of kinks as well as the frequencies of any internal modes of the kinks. It was later realised [47] that such detailed knowledge was not needed. In [47], the authors express the kink-gas phenomenology in its simplest form applicable to the entire class of non-linear, $(1+1)$-dimensional kink-bearing systems. They present a general formula for the low-temperature kink/anti-kink densities. Quantities entering this formula are obtained from the local potential, $V(\phi)$, only. We followed their formalism in the calculation of the correlation length.

The formalism begins with the expression for the kink-energy [3]

$$E_K = \int_{\phi_1}^{\phi_2} \mathrm{d}\phi \, [2V(\phi)]^{1/2} \,, \tag{D.1}$$

(see fig.(2.1) for the ϕ^4 case). The correlation length can be found by considering the two-point correlation function,

$$\langle\phi(0)\phi(x)\rangle = \sum_n e^{-\beta(\epsilon_n-\epsilon_o)x}\left|\langle 0|\phi|n\rangle\right|^2. \tag{D.2}$$

At low T, the sum is dominated by the lowest pair of eigenstates. Namely, the ground states of each well of the double-well potential, $\epsilon_{o,a}$ and $\epsilon_{o,s}$ for the wells at ϕ_1 and ϕ_2 respectively. Therefore, in the limit $T \to 0$

$$\langle\phi(0)\phi(x)\rangle = e^{-\beta(\epsilon_{0,a}-\epsilon_{0,s})x}\left|\langle 0,s|\phi|0,a\rangle\right|^2. \tag{D.3}$$

The correlation length, λ, is, by definition, the denominator in the exponent of eq.(D.3). That is, in the limit $T \to 0$,

$$\lambda = \frac{1}{\beta(\epsilon_{0,a}-\epsilon_{0,s})} = \frac{1}{2\beta t_o}. \tag{D.4}$$

The kink density is,

$$n = \frac{1}{4\lambda}. \tag{D.5}$$

The quantity t_o, is termed the "tunnel-splitting" contribution to the lowest eigenvalue ϵ_o. This may be evaluated at the low-temperature limit for general $V(\phi)$ using an improved Wentzel-Kramers-Brillouin (WKB) method [48]. For potentials having a single barrier (Sinh-Gordon, double-quartic, ϕ^4 etc.), it can be shown

$$t_o = \frac{\phi_2-\phi_1}{\sqrt{\pi}B}e^{\eta}\frac{1}{\sqrt{\beta}}e^{-E_K\beta}, \tag{D.6}$$

where the temperature-independent quantity η is given by,

$$\eta = \int_{\phi m}^{\phi_2} \mathrm{d}\phi\left(\frac{1}{\sqrt{2V(\phi)}} - \frac{1}{\phi_2-\phi}\right), \tag{D.7}$$

and B is a topological factor (B=2 for double-well potentials) and $\phi_m = (\phi_2 + \phi_1)/2$. Note importantly that eq.(D.6) contains no reference to the kink solutions of the equation of motion [3] which are usually accompany such a treatment.

To be able to solve the integral of eq.(D.7) in the ϕ^4 case, we begin with a bare ϕ^4 potential of the dimensionless form,

$$V(\phi) = \frac{1}{4}(\phi^2-1)^2. \tag{D.8}$$

In its expanded form, eq.(D.7) is just the potential eq.(2.8) shifted by the amount 1/4 and so the dynamics are equivalent. It is useful to scale the effective potential, V_{eff}, of eq.(5.48) such that it has unit curvature at its minima,

$$\widetilde{V}(\phi)_{eff} = \left[2 - \frac{\Delta x^2}{3}\right]^{-1} V_{eff}, \tag{D.9}$$

$$\widetilde{V}''_{eff}(\phi)|_{\phi_1,\phi_2} = 1. \tag{D.10}$$

The scaling factor is absorbed by rescaling β^2 and ϵ_n,

$$\tilde{\beta}^2 = \left[2 - \frac{\Delta x^2}{3}\right] \beta^2, \tag{D.11}$$

$$\tilde{\epsilon}_n = \left[1 - \frac{\Delta x^2}{12}\right]^{-1} \epsilon_n. \tag{D.12}$$

With the considerations above, the effective potential is of the form,

$$\widetilde{V}(\phi)_{eff} = \frac{1}{4}\left[2 - \frac{\Delta x^2}{3}\right]^{-1} (\phi^2 - 1)^2 \left(1 - \frac{\Delta x^2}{6}\phi^2\right) \tag{D.13}$$

Substituting eq.(D.13) into eq.(D.7) and noting that $(\phi^2 - 1)^2 = (1 - \phi^2)^2$, one finds

$$\eta = \ln\left[2\left(2 - \frac{\Delta x^2}{3}\right)\right] \tag{D.14}$$

Similarly, inserting eq.(D.13) into eq.(D.1) we have

$$E_K = \sqrt{\frac{9}{8}}\left(2 - \frac{\Delta x^2}{45}\right) \tag{D.15}$$

With these results for E_k and η, and the values $\beta = 5$ and $\Delta x = 0.5$, eq.(D.4) gives the value $\lambda = 17.81$.

Bibliography

[1] J.F. Currie, J.A. Krumhansl, A.R. Bishop, and S.E. Trullinger. *Phys. Rev. B*, 22:477–496, 1980.

[2] S. Habib, A. Khare, and A Saxena. *Physica D*, pages 341–356, 1998.

[3] R. Rajaraman. *Solitons and Instantons*. North-Holland, Amsterdam, 1982.

[4] R. Dalven. *Introduction to Applied Solid State Physics*. Plenum, New York, 1990.

[5] E.W. Kolb and M.S. Turner. *The Early Universe*. Addison-Wesley, 1990.

[6] A. M. Green, editor. *Hadronic Physics from Lattice QCD*. World Scientific, 2004.

[7] A. Griffin, D.W. Snoke, and S. Stringari, editors. *Bose-Einstein Condensation*. Cambridge, 1995.

[8] M. Sher. *Phys. Rept.*, 179:273–418, 1989.

[9] A.D. Linde. *Particle Physics and Inflationary Cosmology*. e-Print Archive: hep-th/0503203, 2005.

[10] G.W. Anderson and L.J. Hall. *Phys. Rev. D*, 45:2685, 1992.

[11] K. Heitmann, P.M. Ricker, M.S. Warren, and S. Habib. *Astrophys.J.Suppl*, 160:28–58, 2005.

[12] L.M.A. Bettencourt, S. Habib, and G. Lythe. *Phys. Rev. D*, 60(105039), 1999.

[13] M. Alford and M. Gleiser. *Phys. Rev. D*, 48:2838, 1993.

[14] J. Borill and M. Gleiser. *Nucl. Phys. B*, 483(1):416–428, 1997.

[15] T.R. Koehler and N.S. Gillis. *Phys. Rev. B*, 7:4980–4999, 1973.

[16] D.J. Scalapino, Y. Imry, and P. Pincus. *Phys. Rev. B*, 11:2042–2048, 1975.

[17] S.E. Trullinger and K. Sasaki. *Physica D*, 28:181–188, 1987.

[18] D.J. Scalapino, M. Sears, and R.A. Ferrell. *Phys. Rev. B*, 6:3409–3416, 1972.

[19] G. Arfken. *Mathematical Methods for Physicists*. Academic press, Inc., 1970.

[20] H.A. Kramers and G.H. Wannier. *Phys. Rev.*, 60:252, 1941.

[21] L. Onsager. *Phys. Rev.*, 65:117, 1944.

[22] P.M. Morse and H. Feshbach. *Methods of Theoretical Physics*. McGraw-Hill Book company, Inc., New York, 1953.

[23] A.R. Bishop and J.A. Krumhansl. *Phys. Rev. B*, 12:2824–2831, 1975.

[24] G. Parisi. *Statistical Field Theory*. Addison-Wesley, New York, 1988.

[25] A. Das. *Finite Temperature Field Theory*. World Scientific Publishing Co. Pte. Ltd., Singapore, 1997.

[26] P. Ramond. *Field Theory: A Modern Primer*. Addison-Wesley, 1989.

[27] B.M. McCoy. Prepared for the 7th Physics Summer School on Statistical Mechanics and Field Theory, Canberra, Australia, 10-28 Jan 1994. arXiv:hep-th/9403084.

[28] I.S. Gradshteyn and I.M. Ryzhik. *Tables of Integrals, Series and Products*. Academic Press, Inc., 1980.

[29] P. Langevin. *Comptes Rendes*, 146:530, 1908.

[30] S. Seunarine and D.W. McKay. *Phys. Rev. D*, 64(105015), 2001.

[31] S. Rajarshi, R.and Sengupta. *Phys. Rev. D*, 65(063521), 2002.

[32] M. Gleiser and R. Ramos. *Phys. Rev. D*, 50:2441, 1994.

[33] H.J. Lee and W.E. Scheisser. *Ordinary and Partial Differential Equation Routines in C, C++, Fortran, Java, Maple and Matlab.* Chapman and Hall/CRC, 2004.

[34] A. Greiner, W. Strittmatter, and J. Honerkamp. *J. Stat. Phys.*, 51:95–108, 1988.

[35] S. Coleman. *Phys. Rev. D*, 15:2929, 1977.

[36] C. Callan Jr. and S. Coleman. *Phys. Rev. D*, 16:1762, 1977.

[37] M. Croitoru, D. Grecu, and A. Visinescu. *unpublished*, 1989.

[38] M. Gleiser and H.R. Müller. *Phys. Lett. B*, 422(1):69–75, 1998.

[39] R. Stoeckly and D.J. Scalapino. *Phys. Rev. B*, 11:205–210, 1975.

[40] D.J. Scalapino and B. Stoeckly. *Phys. Rev. D*, 14:3376–3380, 1976.

[41] T.D. Schultz, D.C. Mattis, and E.H. Lieb. *Ann. Phys.*, 16:856–871, 1961.

[42] J. Lajzerowicz and P. Pfeuty. *Phys. Rev. B*, 11:4560–4562, 1975.

[43] F.J Alexander, S. Habib, and A. Kovner. *Phys. Rev. E*, 48:4284–4296, 1993.

[44] G.G. Batrouni, G.R. Katz, A.S. Kronfield, G.P. Lepage, B. Svetitsky, and K.G. Wilson. *Phys. Rev. D*, 32:2736, 1985.

[45] J.A. Krumhansl and J.R. Schrieffer. *Phys. Rev. B*, 11:3535–3545, 1975.

[46] K. Sasaki. *Prog. Theo. Phys.*, 67:464–474, 1982.

[47] R.M. DeLeonardis and S.E. Trullinger. *Phys. Rev. B*, 22:4558–4561, 1980.

[48] S. Goldstein. *Proc. R. Soc. Edinburgh*, 49:210, 1929.